Schweizerische Eidgenossenschaft
Confédération suisse
Confederazione Svizzera
Confederaziun svizra

Eidgenössisches Departement für Umwelt, Verkehr, Energie und Kommunikation UVEK
Département fédéral de l'environnement, des transports, de l'énergie et de la communication DETEC
Dipartimento federale dell'ambiente, dei trasporti, dell'energia e delle comunicazioni DATEC

Bundesamt für Strassen
Office fédéral des routes
Ufficio federale delle Strade

Sekundärer Feinstaub vom Verkehr

Aérosol secondaire produit à partir des émissions véhiculaires

Secondary aerosol from road vehicles

Laboratory of Atmospheric Chemistry,
Paul Scherrer Institute (PSI),
Villigen,
CH-5232
Switzerland

Stephen Platt
Dr Imad El-Haddad
Simone Pieber
Dr Jay Slowik
Dr Ru-jin Huang
Dr Urs Baltensperger
Dr Andre Prévôt

Forschungsprojekt ASTRA 2010/21 auf Antrag des Bundesamts für Strassen (ASTRA)

April 2014 **1467**

Schweizerische Eidgenossenschaft
Confédération suisse
Confederazione Svizzera
Confederaziun svizra

Eidgenössisches Departement für Umwelt, Verkehr, Energie und Kommunikation UVEK
Département fédéral de l'environnement, des transports, de l'énergie et de la communication DETEC
Dipartimento federale dell'ambiente, dei trasporti, dell'energia e delle comunicazioni DATEC

Bundesamt für Strassen
Office fédéral des routes
Ufficio federale delle Strade

Sekundärer Feinstaub vom Verkehr

Aérosol secondaire produit à partir des émissions véhiculaires

Secondary aerosol from road vehicles

Laboratory of Atmospheric Chemistry,
Paul Scherrer Institute (PSI),
Villigen,
CH-5232
Switzerland

Stephen Platt
Dr Imad El-Haddad
Simone Pieber
Dr Jay Slowik
Dr Ru-jin Huang
Dr Urs Baltensperger
Dr Andre Prévôt

Forschungsprojekt ASTRA 2010/21 auf Antrag des Bundesamts für Strassen (ASTRA)

April 2014 **1467**

Impressum

Forschungsstelle und Projektteam

Projektleitung
Andre Prévôt

Mitglieder
Stephen Platt
Imad El-Haddad
Simone Pieber
Jay Slowik
Urs Baltensperger

Begleitkommission

Präsident
Martin Schiess

Mitglieder
Anthi Liati
Martin Weilenmann
Jan Czerwinski
Dirk Bergmann
Thomas Gasser
Sascha Grunder
Meinrad Signer
Peter Maly
Brigitte Gaelli

KO-Finanzierung des Forschungsprojekts

Bundesamt für Umwelt (BAFU)

Antragsteller

Bundesamt für Strassen (ASTRA).

Bezugsquelle

Das Dokument kann kostenlos von http://www.mobilityplatform.ch heruntergeladen werden.

Inhaltsverzeichnis

Zusammenfassung

In der Schweiz werden die Immissionsgrenzwerte für Feinstaub vielerorts überschritten, mit beträchtlichen Auswirkungen auf die Gesundheit und Umwelt. Feinstaub besteht aus einer Vielzahl chemischer Komponenten, wobei organische Verbindungen einen beträchtlichen Teil der Feinstaubmasse darstellen. Der organische Teil des Feinstaubs kann weiter unterteilt werden in direkt emittiertes „primäres“ organisches Aerosol (POA) (Aerosol: Synonym für Feinstaubpartikel) und in „sekundäres“ organisches Aerosol (SOA). SOA wird in der Atmosphäre durch Oxidations- und Alterungsprozesse aus gasförmigen organischen Vorläuferschadstoffen (VOC; volatile organic compounds) gebildet. Jede Quelle von VOC oder primärem, direkt emittiertem, organischem Aerosol (POA) kann auch zur Bildung von sekundärem organischem Aerosol (SOA) führen. In diesem Kontext ist der Verkehr als wichtige Quelle von VOC und primärem organischem Feinstaub deshalb möglicherweise auch eine substantielle Quelle von SOA - vor allem in städtischen Gebieten, wo die Gesundheitsauswirkungen gross sind wegen der höheren Emissions- und Bevölkerungsdichte und der schlechteren Ausbreitungsbedingungen (geringeren Verdünnung der Schadstoffe). Die Emissionen und die SOA-Bildungspotentiale von verschiedenen Strassenfahrzeugen (2-Takt- und 4-Takt-Mopeds (<50ccm), Benzin- und Diesel-Personenwagen, sowie Diesel-Lastwagen) wurden in einer neuen mobilen Smogkammer untersucht. Die Smogkammer simuliert die Prozesse, die in der Atmosphäre ablaufen. Der Hauptfokus dieser Studie liegt auf der Quantifizierung der SOA-Bildung aus den Emissionen der Strassenfahrzeuge sowie ersten Einblicken in die Bildungsprozesse. In diesem Projekt wurde eine neue mobile atmosphärische Reaktionskammer (oder Smogkammer) entwickelt und charakterisiert und an den Motorfahrzeug-Prüfständen des europäischen Gemeinschaftsforschungszentrums (JRC: Joint Research Center) in Ispra, Italien eingesetzt (Fig. 1). In dieser Studie werden aufgewirbelte Partikel, Bremsabrieb, Bildung von sekundären inorganischen Feinstaubanteilen, welche auch durch den Verkehr verursacht werden können, nicht untersucht. Die Arbeit beschränkt sich auf die toxischen kohlenstoffhaltigen Bestandteile.

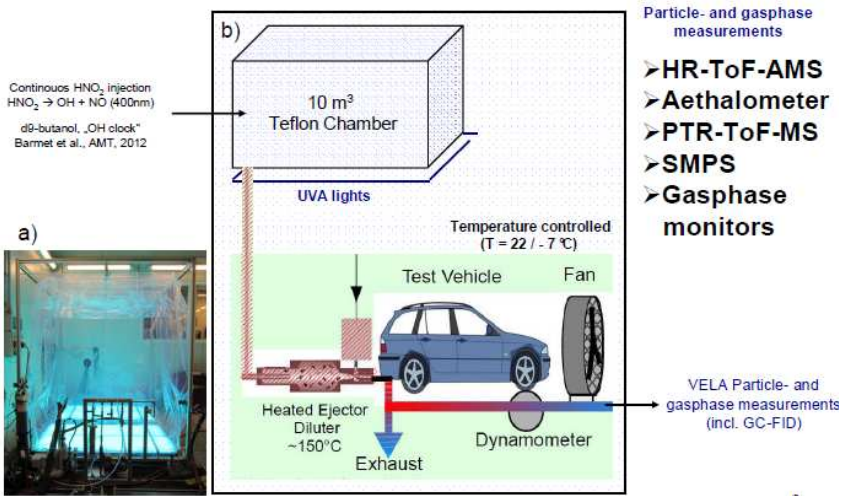

Figur 1: *a) Die mobile Smogkammer mit angezündetem UV-Licht während eines Experimentes. b)Schema der Smogkammer-Experimente von einem Personenwagen. Das Fahrzeug wird auf einem Rollenprüfstand (Dynamometer) in den Emissionslabors des JRC Ispra getestet. Die Emissionen werden durch geheizte Leitungen und Verdünnungssysteme (sogenannte Injektionsverdünner) in die Smogkammer geleitet, wo die Emissionen mit schadstofffreier Luft (Nullluft) weiter verdünnt werden. Online-Emissionsmessungen werden durch das JRC durchgeführt. Nach Abschluss des Emissionszyklus werden die Lichter der Smogkammer angezündet, um die atmosphärische Photochemie und Alterung zu simulieren. Während der Alterung werden verschiedenste Parameter gemessen, u.a. mit einem Aerosolmassenspektrometer (HR-ToF-AMS) zur Messung chemischer Feinstaubbestandteile, einem Aethalometer für*

schwarzen Russ (englisch: black carbon; BC), einem Proton-Transfer-Reaktions-Massenspektrometer (PTR-ToF-MS) für (gasförmige) VOCs und ein physikalisches Messsystem (SMPS) für Aerosolgrössenverteilungen. Als Marker (Tracer) wurde neunfach deuteriertes Butanol (d9-Butanol) am Anfang des Experimentes injiziert, um die OH-Radikalkonzentrationen zu bestimmen: Die Abnahmerate von d9-Butanol, welches mit dem PTR-ToF-MS gemessen wird, ist proportional zur OH-Konzentration und damit ein Mass für die Alterungszeit des Schadstoffgemisches in der Atmosphäre.

Die mobile Smogkammer wurde mehrere Monate lang in den Emissionslabors des europäischen Forschungszentrums in Ispra eingesetzt, wo die Expertise zur Messung von Fahrzeugemissionen und zur Durchführung von Alterungsexperimenten ideal kombiniert werden konnte. Die Emissionen von modernen Fahrzeugen (Euro 5 für Personenwagen, Euro V für Lastwagen, Euro 2 für Mopeds) wurden während der EU-konformen Fahrzyklen (siehe Figur 2) in die Smogkammer geleitet. Jeweils ein Alterungsexperiment pro Tag konnte durchgeführt werden, wobei auch der Einfluss der Temperatur und der relativen Feuchte auf die Emissionen und die Alterung in der Smogkammer in verschiedenen Tests untersucht wurde. Spezifische Experimente wurden auch für alternative (aromatenfreie, alkylierte) Treibstoffe bei den Mopeds durchgeführt.

Figur 2 fasst die Emissionsfaktoren (EF) in Gramm Kohlenstoff pro Kilogramm Treibstoff (gC kg^{-1}) für die verschiedenen Fahrzeugkategorien mit Standardtreibstoff zusammen. Bei der Beurteilung der Relevanz der hier gewonnen Resultate muss hervorgehoben werden, dass nur 2-3 Fahrzeuge pro Fahrzeugkategorie untersucht wurden und diese erste begrenzte Stichprobe deshalb mit entsprechenden Unsicherheiten behaftet ist. Wesentliche Teile der Resultate werden durch ähnliche meist noch unveröffentlichte Untersuchungen in den USA bestätigt (z.B. höherer Beitrag von kohlenstoffhaltigem Feinstaub durch Benzin- als Diesel-Personenfahrzeuge).

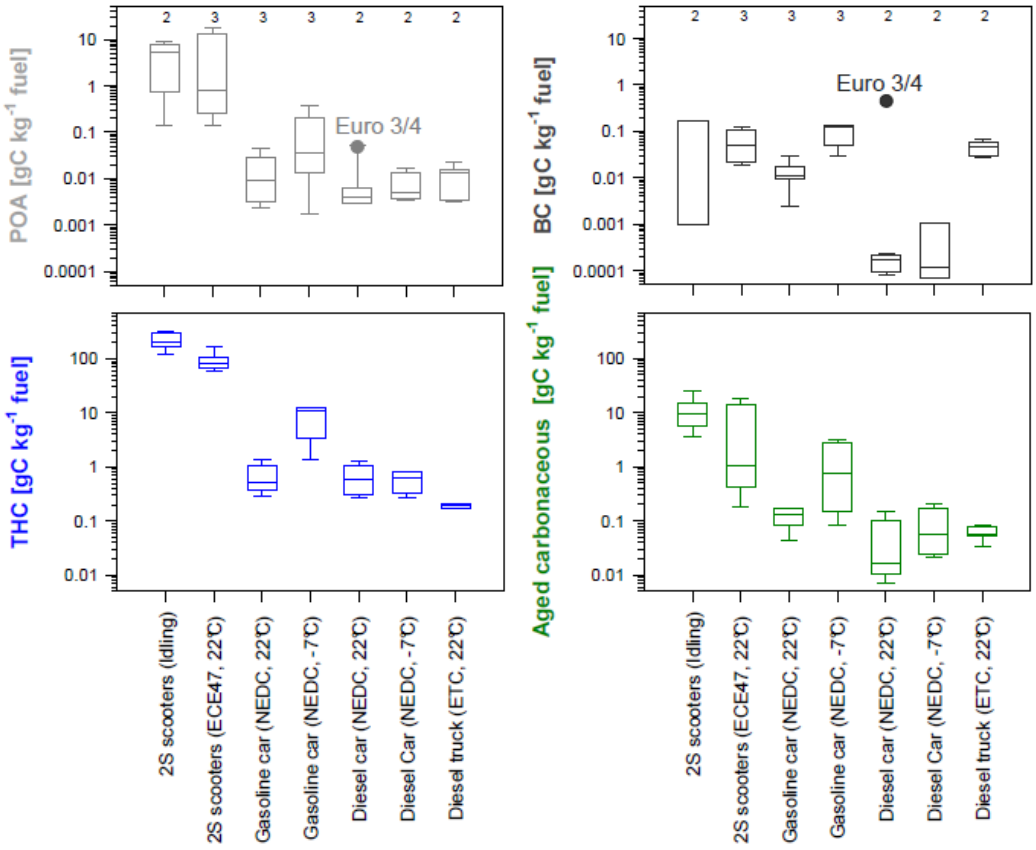

Figur 2: *Box-Whisker-Diagramme (mittlere Linie: Median, Box-Begrenzung: 25- und 75-Perzentile , äusserste Linien: 5- und 95-Perzentile) zeigen die Emissionsfaktoren von schwarzem Russ (BC), primärem organischem Aerosol (POA), totalen gasförmigen Kohlenwasserstoffen (THC) und totaler gealterter kohlenstoffhaltiger Aerosolmasse (BC+POA+SOA, "aged carbonaceous") für alle Fahrzeugkategorien dieser Studie. Als Einzelpunkte sind zusätzlich auch die Emissionen von Euro-3- und Euro-4-Dieselfahrzeugen ohne Partikelfilter dargestellt (ETH-Dissertation Roberto Chirico). Die Experimente mit den Mopeds wurden im Leerlauf (mit aufgewärmtem Motor) oder mit dem europäischen Fahrzyklus ECE47 bei 22℃ durchgeführt. Die Personenwagen wurden im europäischen Fahrzyklus NEDC bei 22℃ oder -7℃, die Lastwagen im Fahrzyklus ETC bei 22℃ getestet. Die Kaltstartphasen wurden bei allen Experimenten mitberücksichtigt. Die Zahl der getesteten Fahrzeuge in jeder Fahrzeugkategorie ist am oberen Rand der Figur angegeben.*

Figur 2 stellt die wichtigsten Resultate dar:

- Alle Fahrzeuge (unabhängig von der Treibstoffart) produzieren bei allen Umgebungsbedingungen SOA. Deshalb genügt die Kenntnis der primären Emissionen nicht, um den Einfluss von Fahrzeugen auf atmosphärischen Feinstaub zu schätzen, zu verstehen und schliesslich zu regulieren.
- Die Anwendung von Diesel-Partikelfiltern (DPF) reduziert den primären organischen Feinstaub (POA) und den schwarzen Russ (BC) beträchtlich. Im Vergleich zu einer früheren Studie mit älteren Personenwagen (Euro 3 und 4 ohne DPF) wurden in der jetzigen Studie mit modernen Fahrzeugen (Euro 5 mit DPF) bis zu 100-fach tiefere POA- und 10'000-fach tiefere BC-Emissionen beobachtet.
- Bei Diesel- und Benzin-Personenwagen übertrifft die Produktion von sekundärem organischem Aerosol (nach wenigen Stunden atmosphärischer Oxidation) die direkten Emissionen von primärem Aerosol.
- Moderne (Euro 5) Personenwagen mit Benzin produzieren im Durchschnitt mehr SOA und emittieren auch mehr primäres organisches Aerosol (im Durchschnitt sechsmal mehr) als Euro-5-Personenwagen mit Diesel, welche wie üblich mit Partikelfilter ausgerüstet sind. Der überwiegende Anteil der SOA-Vorläuferstoffe wird bei den Benzinfahrzeugen während des Kaltstarts emittiert, also solange der Katalysator seine Funktion noch nicht erfüllen kann.
- Kalte Umgebungstemperaturen (-7℃ versus 22℃) haben bei Benzinfahrzeugen dramatische Effekte auf die Kaltstartemissionen und die SOA-Bildung. Die Abgasemissionen von VOC und von kohlenstoffhaltigem Feinstaub (inklusive SOA) steigen um mehrfaches an, während bei Personenwagen mit Diesel kein Temperatureffekt feststellbar ist. Der Beitrag von Benzinfahrzeugen an die Belastung mit kohlenstoffhaltigem Aerosol ist somit im Winter wegen den hohen Emissionen während des verlängerten Kaltstarts deutlich erhöht.
- Zweitakt-Mopeds sind extreme Emittenten. Bezogen auf den verbrauchten Treibstoff emittieren sie höchste Mengen an primärem Feinstaub und toxischen gasförmigen Aromaten. Zudem bilden sie beträchtliche Mengen von SOA. Die gesamte kohlenstoffhaltige Feinstaubmasse (POA+BC+SOA) ist etwa 100-mal (Median) höher als bei einem Benzinfahrzeug. Selbst wenn nur ein kleiner Teil der Fahrzeugflotte aus Mopeds besteht und diese nur einen geringen Anteil des gesamten Treibstoffs verbrauchen, können sie zum dominanten verkehrsbedingten Feinstaub-Produzenten werden. Dies trifft insbesondere in Teilen von Süd-Ost-Asien, Afrika und Südeuropa zu. Auch in Europa und der Schweiz ist ihr Beitrag an den verkehrsbedingten Feinstaub relevant - trotz ihres sehr kleinen Anteils am Treibstoffverbrauch.
- Die Produktion von sekundärem organischem Aerosol (SOA) durch Lastwagen ist im Vergleich zu ihren direkten Emissionen (POA) gering.

Eingehende Analysen und Auswertungen zeigen, dass SOA von den Zweitakt-Mopeds fast ausschliesslich aus den Emissionen aromatischer gasförmiger Kohlenwasserstoffe (Benzol, Toluol, Xylole, etc.) gebildet wird. Bei Kleinmaschinen wie Motorsägen werden zur Verminderung der Benzolbelastung teilweise aromatenfreie Treibstoffe (Aspen)

eingesetzt. Um den Effekt solcher Treibstoffe auf die SOA-Bildung zu testen, wurden in Smogkammerexperimenten Mopeds mit konventionellem Treibstoff und mit aromatenfreiem Treibstoff verglichen. Figur 3 zeigt eine sehr deutliche Reduktion der SOA-Produktion bei Anwendung von alkylierten, aromatenfreien Treibstoffen. Dies ist in Übereinstimmung mit dem oben beschriebenen Resultat, dass SOA bei 2-Taktern durch chemische Umwandlung von flüchtigen aromatischen Kohlenwasserstoffen entsteht. Die Emissionen von 4-Takt-Motorrädern sind wesentlich geringer als von 2-Taktern. Die SOA-Bildung lässt sich aber auch hier durch Verwendung von aromatenfreiem Treibstoff stark vermindern.

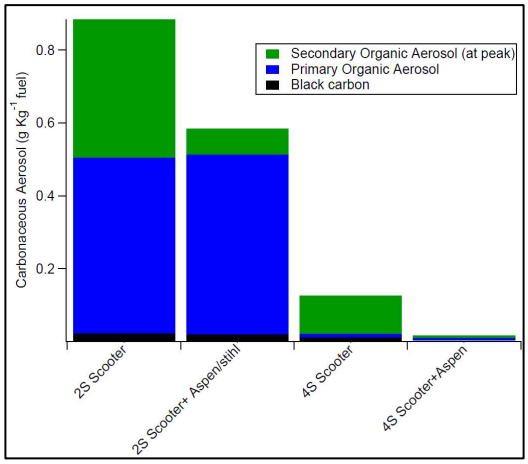

Figur 3: *Emissionsfaktoren von primärem organischem Aerosol, schwarzem Russ (BC) und sekundärem organischen Aerosol (SOA) von 2-Takt und 4-Takt-Mopeds mit konventionellem und mit aromatenfreiem (Aspen) Treibstoff mit jeweils konventionellem Öl und synthetischem reinen Schmieröl (Stihl HP Ultra).*

Bei Euro-5 Benzin- und Diesel-Personenwagen lässt sich nur ein kleiner Teil der SOA-Masse auf die Emissionen von aromatischen gasförmigen Kohlenwasserstoffen zurückführen. Hier müssen weitere VOC zur SOA-Bildung beitragen.

Résumé

Le dépassement régulier des valeurs limites de particules fines (PM) dans plusieurs zones en Suisse peut avoir de graves conséquences sur la santé et l'environnement. PM renferme de nombreux composés, parmi lesquels les espèces organiques constituent une fraction majeure. L'aérosol organique (OA) peut être émis directement (aérosols organiques primaires, POA) ou formé in-situ dans l'atmosphère (aérosols organiques secondaires, SOA) via la réaction de composés organiques volatils (VOC). Toute source de VOC ou POA peut être associée à la production de SOA. Dans ce contexte, les émissions véhiculaires, une source importante de particules primaires et de VOC, peut également être une source importante de précurseurs de SOA, particulièrement dans les milieux urbains ou l'impact de la pollution atmosphérique est un enjeu de santé publique. Durant cette étude, les émissions de plusieurs types de véhicules (deux-roues équipés de moteurs à 2 ou 4 temps (<50cc), voitures diesel et gazoline, et poids lourds) ont été quantifiées dans la nouvelle chambre de simulation mobile. L'un des objectifs principaux de l'étude était d'estimer le potentiel de formation de SOA à partir des différentes sources d'émissions et d'appréhender les mécanismes par lesquels cet aérosol est produit. Dans le cadre de cette étude, une nouvelle chambre de simulation mobile (Fig.1) a été développer et caractériser.

La chambre mobile a été employée au laboratoire des émissions véhiculaires (VELA) du centre de recherche de la Commission Européenne (Ispra, Italie). Les émissions véhiculaires ont été échantillonnées dans la chambre au cours des nouveaux cycles de conduite réglementaires conçues pour imiter de façon reproductible les conditions rencontrées sur les routes européennes. L'effet de la température ambiante et de l'humidité relative sur les profils d'émission et leurs vieillissements ont été étudiés. Des tests ont également été réalisés afin d'évaluer l'effet de l'utilisation de combustibles alternatifs (Alkylate fuel) sur les profils d'émissions des deux roues. Une batterie d'instrumentations en ligne a été déployée a fin de quantifier les facteurs d'émission des polluants gazeux et particulaires.

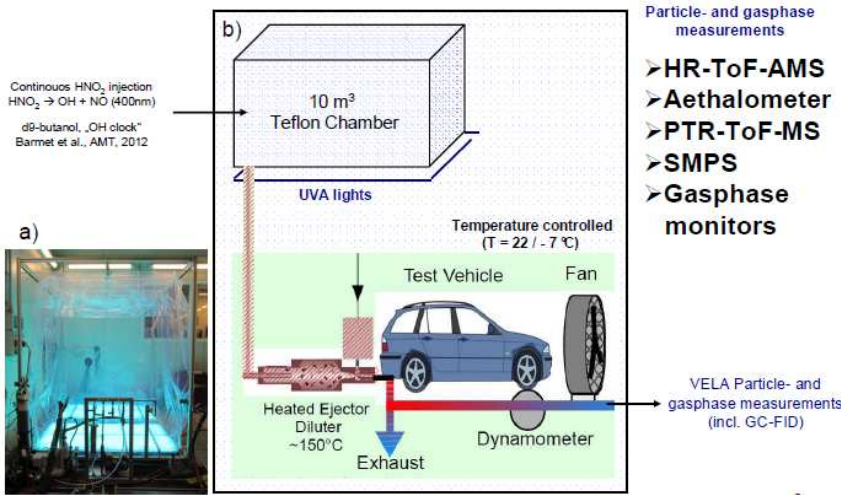

Figure 1: *La chambre de simulation mobile en opération. Le véhicule est placé sur un banc de test à rouleaux au laboratoire des émissions véhiculaires (VELA) du centre de recherche de la Commission Européenne (Ispra, Italie). Les émissions sont échantillonnées dans la chambre au cours des cycles de conduite par l'intermédiaire d'un système de prélèvement chauffé, muni d'un système de dilution à jet. Pendant le cycle, des mesures en temps réel sont effectuées en utilisant les instrumentations du VELA. Après le prélèvement, les lampes UV sont allumées pour initier la photochimie et le vieillissement. Le vieillissement des émissions est suivi dans la chambre, en utilisant une batterie d'instrumentations, dont un spectromètre de masse haute résolution à temps de vol pour la caractérisation en temps réel des composés chimiques particulaires non-*

réfractaires (HR-ToF-AMS), des aethalometers pour la mesure du carbone suie, un spectromètre de masse haute résolution à temps de vol pour la caractérisation en temps réel des composés organiques volatiles (PTR-ToF-MS) pour les mesures de phases de gaz et d'un SMPS (Scanning Mobility Particle Sizer) pour la mesure du nombre total des particules submicroniques et de leur distribution granulométrique. La mesure du vieillissement du d9-butanol (butanol neuf-fois deutéré), injecté au début de l'expérience permet la détermination de la concentration moyenne de OH dans la chambre au cours de la réaction.

Figure 2 montre les facteurs d'émission (EF), en g de carbone par kg de carburant consommé, pour les véhicules étudiés. Notons que ces données se basent sur un nombre restreint de véhicules et ne peuvent pas être généralisées sur l'ensemble du parc automobile en Europe. Cependant, nos résultats sont en accord avec les données d'un groupe de recherche américain. Figure 2 met en évidence plusieurs points clés :

- Les émissions des véhicules à moteur diesel ou essence produisent des quantités significatives d'aérosol organique secondaire, qui sont pour la plupart des systèmes supérieures aux émissions primaires. Par conséquent, la connaissance des émissions primaires est insuffisante pour l'établissement de réglementations sur les émissions particulaires par les véhicules.
- L'utilisation d'un filtre à particules sur les véhicules légères à moteurs diesel (DPF) réduit considérablement les émissions primaires d'aérosols organiques (POA) et de carbone suie (BC). Ainsi, Les émissions de POA et de BC par les véhicules équipés d'un DPF sont de plusieurs ordres de grandeur inférieures à celles des véhicules sans DPF.

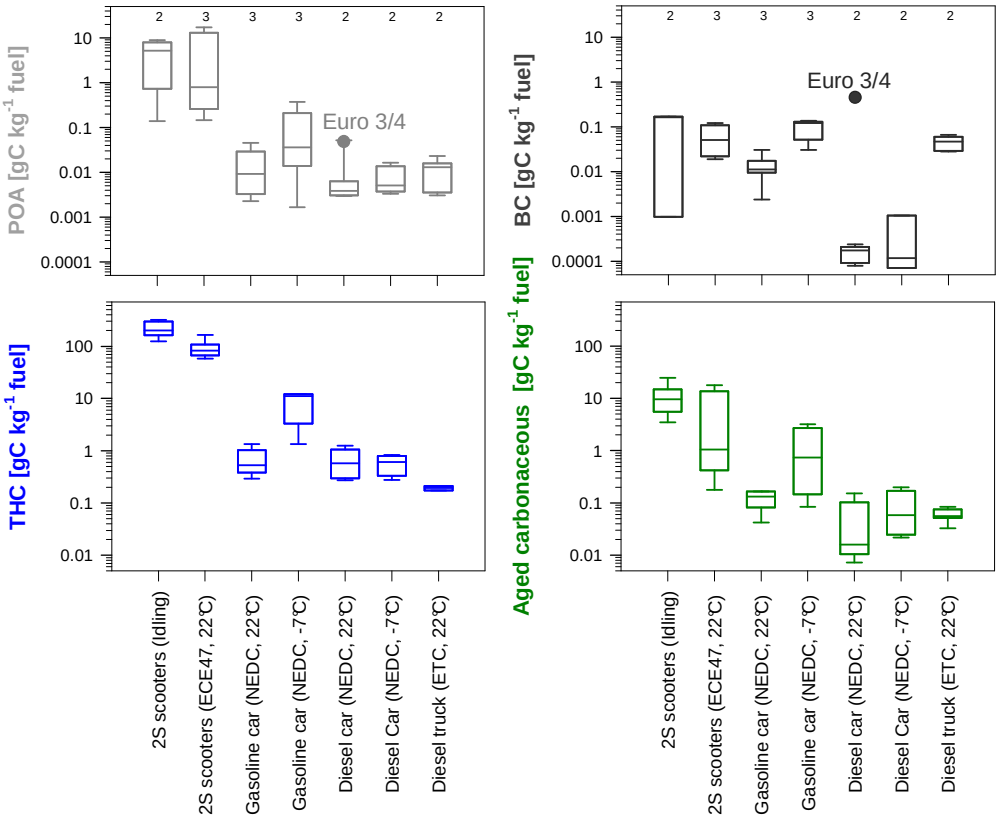

Figure 2: *Facteurs d'émission de carbone suie (BC), aérosol organique primaire (POA), hydrocarbures totaux (THC), et aérosol carboné total après vieillissement, pour les véhicules testés courant cette étude. Les émissions moyennes de BC et de POA à partir de véhicules soumis à la norme Euro 3 et Euro 4 sont également indiquées. Le nombre de véhicules testés est représenté pour chaque type de moteurs par les chiffres de dessus.*

- Les véhicules à moteur essence produisent en moyenne plus de SOA et de PM primaires que les véhicules à moteur diesel.
- Nos résultats montrent clairement que la température a un effet dramatique sur les émissions des véhicules à essence, qui augmente d'un ordre de grandeur quand la température diminue de 22℃ à -7° C. Cet effet n'e st pas observé pour les véhicules à moteur diesel.
- Les deux-roues équipés de moteurs à 2 temps peuvent être considérés comme des « super-pollueurs », émettant des quantités considérables d'aérosols primaires et d'hydrocarbures aromatiques nocifs, qui excèdent par plusieurs ordres de grandeur celles émises par tous autres véhicules testés. Nous montrons également que les composés aromatiques constituent des précurseurs majeurs d'aérosol organique secondaire dans le cas des deux-roues. Nous concluons que ce type de véhicules, bien qu'il constitue une fraction négligeable du parc automobile Européen, peut dominer les émissions véhiculaires, surtout en Europe du Sud.
- L'aérosol organique secondaire ne constitue qu'une fraction relativement limitée des émissions particulaires totales des véhicules lourds à moteur diesel.

L'analyse chimique des aérosols a pu montrer que, bien que la production de SOA à partir des émissions des deux-roues soit majoritairement expliquée par l'oxydation des composés aromatiques, le SOA à partir des émissions des moteurs diesel et gazoline ne l'est pas. Par conséquent, pour déterminer si la production de SOA à partir des émissions des deux-roues pourrait être réduite, nous avons examiné l'effet de carburants sans composés aromatiques, généralement utilisés dans les machines de construction. Figure 3 montre que une réduction considérable de SOA pourrait être atteinte suite à l'utilisation de carburant sans composés aromatiques.

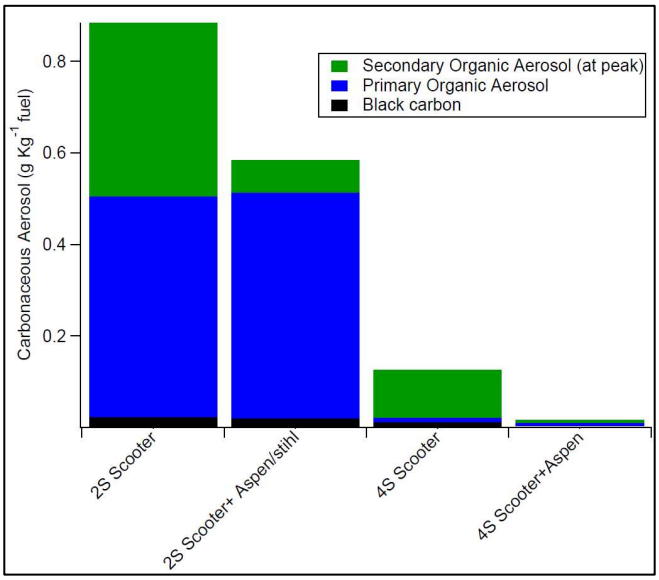

Figure 3: *Facteurs d'émission de carbone suie (BC), aérosol organique primaire (POA), et aérosol organique secondaire (SOA), à partir des émissions des deux-roues équipés de moteurs à 2 temps et 4 temps. Les moteurs fonctionnaient avec de l'essence standard ou sans composés aromatiques et d'huile de lubrification ultra-propre dans le cas des moteurs à 2 temps.*

Summary

In Switzerland, legislative limits for particulate matter (PM) are regularly exceeded at many locations with significant, negative, consequences for health and the environment. PM consists of many compounds, with organic species a major constituent. Organic aerosol (OA) may be directly emitted (primary organic aerosol, POA) or formed from the reactions of volatail organic compounds (VOC) precursors (secondary organic aerosol, SOA). Any source of VOCs or POA may be associated with the production of SOA. In this context vehicular exhaust, as an important source of primary PM and VOCs, may also be an important source of SOA precursors, particularly in urban areas where the health implications of pollutants are greater due to higher population density. Emissions of several road vehicle types (2- and 4-stroke scooters (2S and 4S), gasoline and diesel passenger cars, diesel heavy duty vehicles) were studied in a newly developed mobile smog chamber (Fig .1).

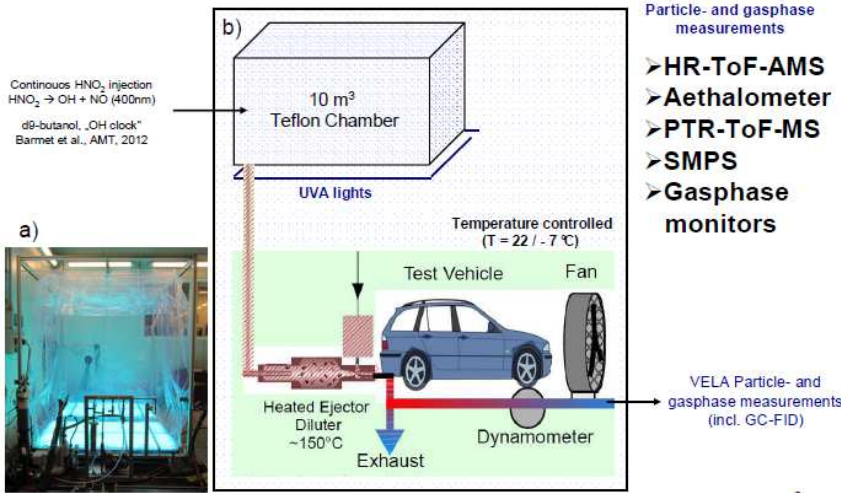

***Figure 1**: a) The mobile smog chamber in operation with UV lights switched on. b) Schematic of the chamber during testing of a light duty vehicle. The vehicle is operated on a chassis dynamometer in a vehicle emissions laboratory (VELA) test cell. Emissions are sampled during driving cycles through a heated sampling system powered by an ejector diluter and injected into the chamber. During the cycle online measurements are taken using VELA instrumentation. After sampling into the chamber UV lights are switched on to simulate atmospheric photochemistry and aging. Measurements from the smog chamber during aging of the emissions are performed using a suite of instruments including a high resolution time-of-flight aerosol mass spectrometer (HR-ToF-AMS) for online characterisation of aerosol particles, aethalometers for black carbon (soot), a proton transfer reaction time-of-flight mass spectrometer (PTR-ToF-MS) for gas phase measurements and a scanning mobility particle sizer (SMPS) for aerosol size distributions. Nine times desuterated butanol (d9-butanol) is injected at the start of experiments as a tracer to determine OH radical concentrations: its decay rate as measured by the PTR-ToF-MS is proportional to OH.*

In this study, a scooter is defined here as a small powered two wheeled vehicle with engine displacement <50cc. The key focus was on the quantification of secondary organic aerosols (SOA) from vehicles and understanding the mechanisms by which such aerosol may be produced. For this project a mobile environmental reaction chamber or *smog chamber* (Fig.1) was developed and characterised. The mobile smog chamber was deployed at the Vehicle emissions laboratory of the European Commission Joint Research Centre (Ispra, Italy) for many experiments, thus combining the techniques of smog chamber experiments with vehicle emissions testing expertise. Emissions were sampled during regulatory driving cycles. The effect of ambient temperature and relative

humidity on emission profiles and emissions aging inside the chamber were investigated. Tests were also performed to evaluate the use of alternative (alkylate) fuels in scooters.

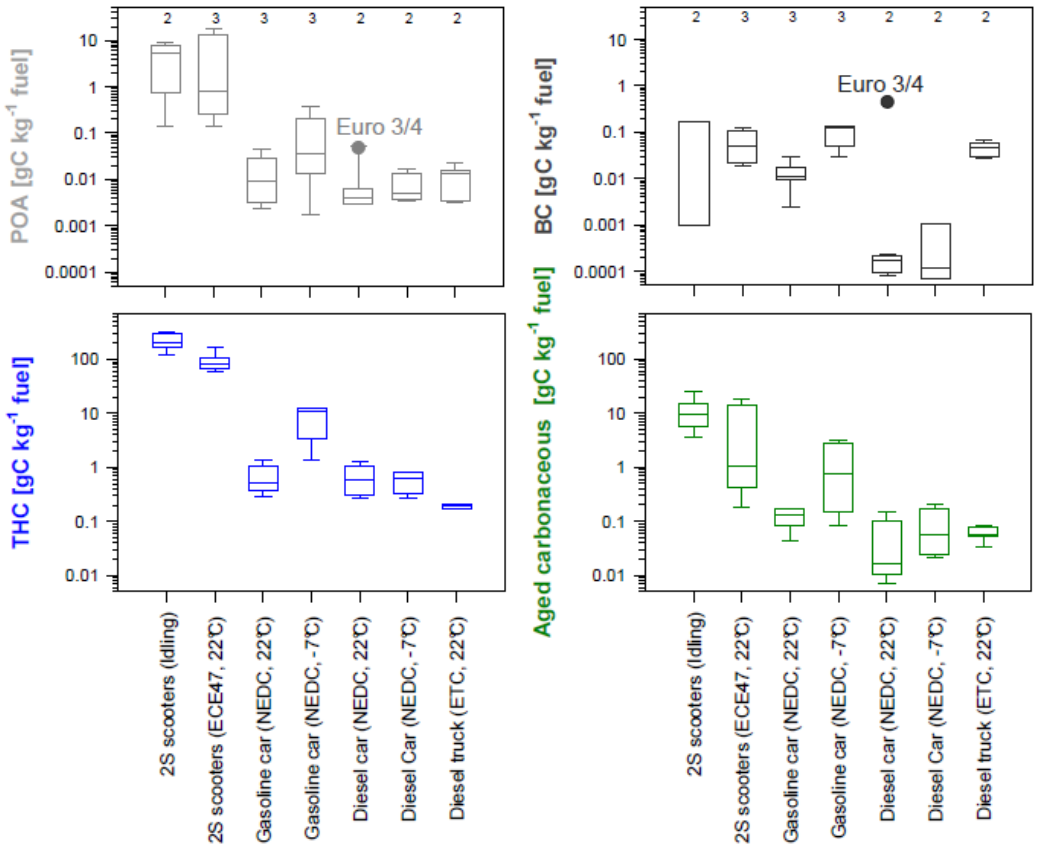

Figure 2: *Box-whisker diagram showing emission factors of black carbon (BC), primary organic aerosol (POA), total hydrocarbon (THC), and total aged carbonaceous aerosol (sum of POA, BC, and secondary organic aerosol) for the vehicles tested in this study. Also indicated as a single point are average values from Euro 3 and 4 diesel vehicles (not eqioeed with particle filters). Hot refers to tests at 22℃ while cold refers to tests at -7℃. The number of vehicles studied as shown at the top of each of the top panels.*

Figure 2 shows emission factors (EFs) in g carbon per kg fuel (g C kg^{-1} fuel) for the vehicles studied, run on standard fuels. EFs are plotted as box and whisker points, indicating the median EF (solid line), 50^{th} percentile (box lines) and 95^{th} percentile (whiskers). It should be emphasised that the data shown are based on a relatively small sample size (few vehicles). However, our results agree well with as yet unpublished data from a US research group.

Figure 2 highlights several key points:

-
- All vehicle types tested, operated with every fuel type, and under every ambient condition produced at least some SOA. Therefore knowledge of primary emissions is insufficient to fully regulate, estimate, and understand vehicular particulate matter (PM) pollution.
- The use of a diesel particle filter (DPF) in diesel passenger cars significantly cuts organic aerosol and black carbon (soot) emissions compared to older vehicles without DPFs (e.g. Euro 3 and 4, from Chirico et al., *in Prep*). A reduction of up to 100 times for POA, and a significant 10000 times for BC was observed for vehicles equipped with a DPF compared to earlier results on older vehicles.

- Both diesel and gasoline passenger cars produce more SOA than they emit primary
- Modern (Euro 5) gasoline cars produce on average more SOA, and emit more primary PM (average six times higher) than DPF-equipped Euro 5 diesel cars
- The effect of cold conditions (-7℃ vs. 22℃) is s evere for gasoline vehicles, increasing emissions of PM and hydrocarbons by up to 15 times. No such low temperature effect was observed for diesel passenger cars.
- Two-stroke scooters may be viewed as 'asymmetric polluters': since they emit more primary aerosol and toxic aromatic hydrocarbons per kg fuel combusted and form considerable secondary organic aerosol than any other vehicle type tested (median value around 100 times higher than a gasoline car for aged total carbonaceous aerosol), we conclude that they need only make up a small fraction of fleet before dominating vehicular PM in some regions, e.g. East Asia, or southern Europe. Even where they do not dominate they likely produce a relatively large proportion of vehicular PM (see also Fig. 4)
- SOA production was observed to be only a small fraction of the total aerosol from heavy duty diesel vehicles

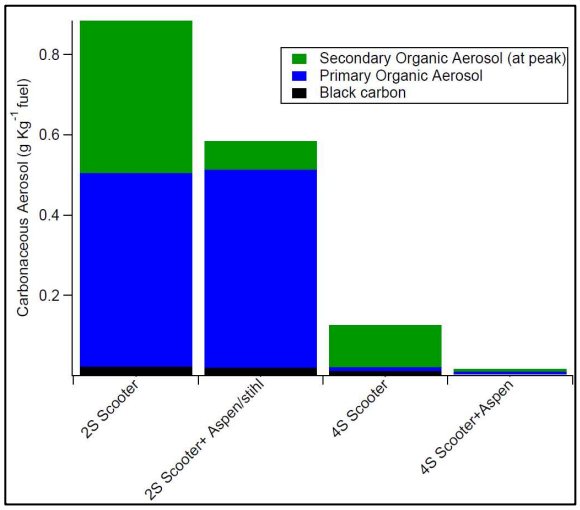

Figure 3: *Emission factors of primary organic aerosol, black carbon and secondary organic aerosol from 2- and 4- stroke scooters measured in the mobile smog chamber from emissions generated during driving cycle. Vehicles were run on standard fuel, or an alkylated fue (Aspen)l, with ultra clean lube oil (Stihl) in the case of the 2S scooters.*

Chemical analysis of the aerosols showed that while SOA from 2S scooters can be explained from the oxidation of aromatic hydrocarbons in the exhaust, SOA from Euro 5 gasoline and diesel vehicles could not. Therefore to test whether SOA production from scooters could be mitigated we examined the effect of aromatic free fuels, typically only used in hand held construction machinery on aerosol formation. Figure 3 shows that consistent with the observation that SOA in 2S scooter is predominantly from the oxidation of aromatic precursors, a considerable reduction in SOA formation could be attained.

1 Introduction

1.1 Primary and secondary aerosols

An *aerosol* is a colloidal system of liquid or solid particles in a gas, where a *particle* is defined as a cluster of molecules [1]. The effects of airborne particulate matter (PM) include damaging health altering the climate [2], influencing transport of pollutants, and reduced visibility.

The atmospheric aerosol comprises a complex mixture of inorganic species e.g. nitrate, sulfate, chloride, crustal material etc.; black carbon (soot, BC); and millions of organic compounds. Aerosols may be classified as primary or secondary. Primary aerosol is freshly emitted (this definition includes the emission of high temperature gases which subsequently cool and condense), while secondary aerosol is formed in the atmosphere by chemical transformation of precursor gases. The atmospheric aerosol typically contains a significant secondary organic aerosol component, Fig. 1, formed in the atmosphere by gas to particle conversion processes such as nucleation, condensation and the reactions of gaseous volatile organic compounds (VOCs) with atmospheric oxidisers: mainly hydroxyl radicals (OH) on the global scale, and, especially in urban regions ozone (O_3), and nitrate radicals (NO_3). Oxidation can produce species with lower vapour pressure, since addition the of oxygen or nitrogen groups increases molecular weight, resulting in new particle formation. Furthermore, recent studies conducted at atmospherically relevant concentrations have shown that SOA can be produced via the oxidation of primary material partly partitioned into the gas phase, which undergoes oxidation resulting in further condensation of organic species [3].

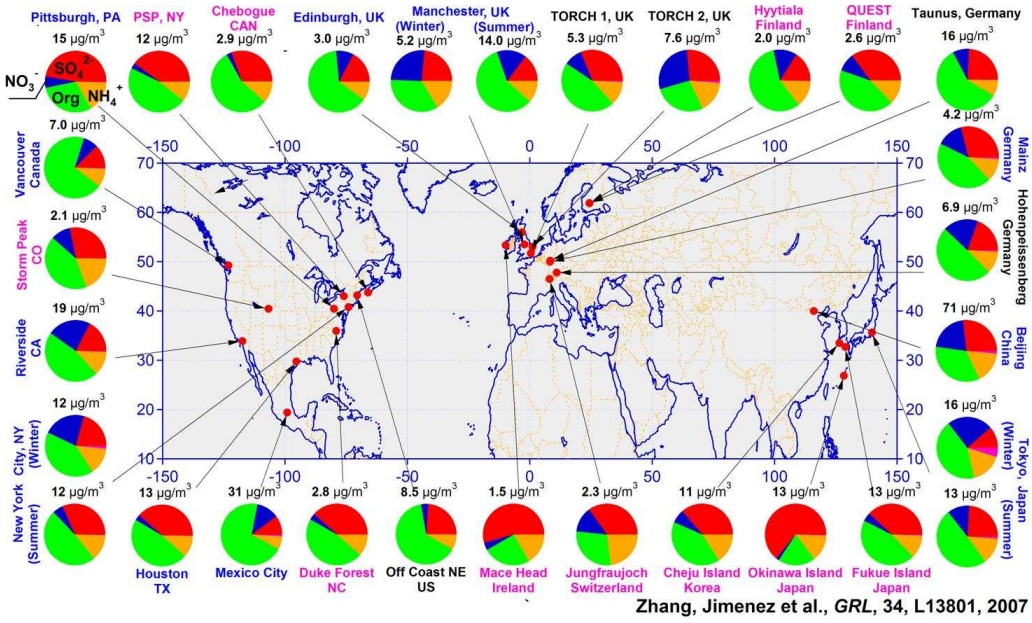

Figure 1: *Atmospheric aerosol composition at different locations/ seasons. Sub – micron atmospheric aerosol comprises a mix of inorganics: nitrate (blue), sulfate (red), ammonium (orange), and organic species (green). Black carbon, also ubiquitous is not shown. From Zhang et al., 2007 [4].*

1.2 Secondary aerosol from road vehicles

Any source of VOCs or primary, directly emitted, organic aerosol (POA) may be associated with the production of SOA. In this context vehicular exhaust, as an important source of primary PM and VOCs, may also be an important source of SOA precursors, particularly in urban areas where the health implications of pollutants are greater due to higher population density and higher pollutant concentrations [5]. Emissions controls technologies in vehicles (such as the “Euro” regulations in Europe), based on limiting primary emissions, have been introduced. The level of adoption of new regulations varies by vehicle type: while passenger cars are now being produced to meet Euro 6 regulations, powered two wheelers (PTW) such as mopeds must only meet Euro 2 regulations (hereunder no limits on particulate matter). There exist no direct limitations for secondary aerosol production and little or no information on SOA formation from vehicle emissions exists in the literature. Furthermore, how SOA production varies by vehicle type (e.g. diesel or gasoline, vehicle legislative standard etc.) and thus the relative contribution of different vehicle classes to ambient PM, remains poorly constrained. For example, top-down estimations of SOA production from vehicle exhaust have yielded contradictory results. Recent ambient aerosol mass spectrometer measurements in the L.A. Basin concluded that secondary organic aerosol (SOA) from gasoline vehicle emissions can dominate background urban organic aerosol [6]. Conversely, another recent study has suggested, using raw diesel fuel combined with tunnel measurements, that diesel vehicles produce more SOA than gasoline vehicles [7]. Bottom-up estimations of SOA production from real tailpipe vehicular emissions, and the facilities required to perform such studies, are therefore needed.

1.3 Purpose of this report

This report describes the facilities developed and experiments performed to investigate secondary aerosol from road vehicles. The development of a mobile *smog chamber* is presented first, while following chapters include the results of experiments on two-stroke scooters, passenger vehicles and heavy duty trucks. The effect of fuel type on emissions as well as ambient conditions is presented. Note that PM data presented in this report refers to tailpipe emissions of OA (2< µm in diameter), inorganics, and BC, and does not include other possible vehicular PM sources such as brake wear and tyre dust. Furthermore legislative limits for ambient PM refer only to PM_{10} (PM with diameter less than 10 µm), a specific parameter not measured here.

2 Development of a new mobile smog chamber and methodology

Environmental reaction chambers or *smog chambers* are of considerable utility in the study of SOA formation [8]. However, the generation of realistic emissions from many combustion sources (including vehicle engines) under controlled, highly repeatable, conditions typically requires specialist testing facilities (e.g. chassis dynamometers) not generally accessible to large, stationary, smog chambers. For ambient studies a further limitation is that only air in the immediate vicinity of the smog chamber may be sampled. Here, we present the new Paul Scherrer Institute (PSI) mobile smog chamber constructed for this project, to overcome these limitations. Some features of this chamber are similar to those of the mobile chamber used by Carnegie Mellon University (CMU), see e.g. [9]. As part of this project, we demonstrated the utility of the mobile smog chamber by investigating and quantifying SOA formation from a modern (Euro 5) gasoline light duty vehicle (from here on in GLDV1) from the New European Driving Cycle [10] and other vehicles on a chassis dynamometer. These experiments required the transport to, installation, and operation of the chamber at a second facility, the European Commission Joint Research Center (JRC), Italy.

2.1 The mobile smog chamber and integrated systems

The mobile chamber set up during the vehicle emissions aging experiments is illustrated in Fig. 2, which also highlights the modular design of the mobile smog chamber. Instrumentation used during this project, is listed in Table 1. The design offers significant flexibility in terms of installation and operation at host facilities. For example during the gasoline vehicle emissions aging experiments, the chamber and sampling system was placed inside a testing cell with the vehicle, while the instruments and injection system were operated from outside of the cell. This allowed access to instrumentation during testing as well as a precise control of the chamber temperature. Photographs illustrating this set up are shown in Fig. 3. The mobile smog chamber (Fig. 2, purple) is an approximately 12 m^3 (when full), nominally 9 m^3 (2.5×1.8×1.9 m, L×W×H), 125 µm thick collapsible Teflon bag (DuPont Teflon fluorocarbon film (FEP), type 500A, Foiltec GmbH, Germany) suspended from a mobile aluminium frame (2.3×2×2.5 m, L×W×H) with a battery of 40×100 W UV lights (Cleo Performance solarium lamps, Phillips).

Controlling concentrations of gas phase species (e.g. NO_X) inside smog chambers is necessary in order to simulate atmospheric processes. Therefore as illustrated in Fig. 3, the chamber is connected to an injection system, allowing the input of gases or liquids under controlled conditions. The injection system consists of a pure air generator (Atlas Copco SF 1 Oil-free scroll compressor with 270 L container, Atlas Copco AG, Switzerland) with an air purifier (AADCO 250 series, AADCO Instruments, Inc., USA) coupled to an injection system. Pure air can be injected directly into the chamber through the main injection line, an extendable, insulated 12 mm stainless steel tube, which can be heated up to 150 °C (Fig. 3, red hatching, To Chamber). The maximum operational flow rate from the pure air generation system is 120 l min^{-1}. Since the Teflon bag is not fixed onto the frame, but rather suspended from rollers, the volume of the chamber may be adjusted by filling with pure air or withdrawing air through a pump. Rapid cleaning of the chamber is therefore possible by sequentially reducing the bag volume to around 1 m^3 and flushing with O_3 and humidified, pure air. The pure air stream may be diverted through different sections of the injection system using a series of two- and three-way valves. The ratio direct air into the main line to air through the injection system is controlled using rota meters. Gaseous components e.g. NO, NO_2, or propene (C_3H_6) are injected from gas bottles through one of two mass flow controllers: a low flow 1-1000 mL min^{-1} or a high flow 1-10 L min^{-1}. Air inside the chamber can be humidified by diverting part of the pure air at ~20 L min^{-1} through a glass flask containing heated MilliQ water. To prevent condensation, heated (~80 °C) stainless steel tubing (red hatching, Fig. 4) is used after the flask and the humidified stream is re-combined with dry air in the main line, also heated to ~80 °C. O_3 is generated by passing pure air over a UV light source housed

inside a stainless steel cylinder. Using this system O_3 concentrations in the range ppb – ppm can be generated inside the chamber. Liquid volatile organic compounds (VOCs) can be injected through a septum into the main injection line. Nitrous acid (HONO), used as a source of OH radicals, may be injected into the chamber using the continuous HONO generation system described by Taira and Kanda (1990) [11]. Briefly, constant flows of sodium nitrite and sulfuric acid, regulated by a programmable peristaltic pump (REGLO Digital MS-4/8, IDEX Health & Science GmbH, Germany), are reacted in a custom-built glass vessel to produce HONO. Pure air passes through the vessel to purge the HONO and then through a polytetrafluoroethylene (PTFE) filter before injection into the chamber. Waste chemical solution is removed from the vessel by the peristaltic pump.

Emissions sampling into the chamber is performed using a modified ejector dilutor (DI-1000, Dekati Ltd, Finland), equipped with a pressurized air heater (DH-1723, Dekati Ltd, Finland). The Dekati is placed inside a stainless steel housing, which can be heated up to 200 °C, to reduce VOC and particle losses. The sampling lines are constructed from separable 2 m segments of insulated 12 mm silica steel tubing (outer diameter), also heatable up to 150 °C. Using separable segments allows the distance between the chamber and emissions source to be varied as required, providing maximum flexibility in terms of installation at different facilities. Sampling lines to the instrumentation are of variable length and constructed from stainless steel or copper for aerosol sampling, and Teflon for gas phase sampling. Temperature probes are placed at the top and the bottom surface of the bag (Fig. 2, T1 and T2). Relative humidity (RH) and a third temperature reading, are measured in the sampling lines directly adjacent to the chamber (Fig. 2, RH/T3).

Data from the gas phase instruments (NO_X, CO_2, THC, O_3, Table 1) and the RH sensor are recorded and saved in real time using a data acquisition (DAQ) system (NI 9201 8 channel analogue input module and cDAQ-9178 8 slot USB chassis, National Instruments). Temperature at T1 and T2 is also recorded using the same DAQ system (NI 9214 16 channel module for high accuracy thermocouple measurements, National Instruments).

Table 1: *Overview of instrumentation used to study the aging of emissions in the mobile smog chamber*

Measured Parameter	**Instrument**	**Manufacturer**	**Lower limit/Range**
Size resolved non-refractory particulate matter (mainly organics (OA), nitrates, sulfates, ammonium, chloride)	High Resolution Time-of-Flight Aerosol Mass Spectrometer (HR-ToF-AMS) with high pressure lens	Aerodyne	<1 µg m^{-3} / D_P 0.1-2.5 µm
Number-weighted aerosol size distribution	Scanning Mobility Particle Sizer (SMPS)	Home built, with TSI long DMA, TSI 3022 CPC	0.01 cm^{-3}, D_P 15-850 nm
Black carbon (BC)	Aethalometer AE33 (beta)	Aerosol d.o.o.	30 ng m^{-3} 10 ng m^{-3} > 100 ng m^{-3}
Particle number	Condensation particle counter CPC 3776	TSI	4 nm, 0.01-10^7 particles cm^{-3}
NO+NO_Y (Trace	NO_X Monitor 42C	Thermo	0-200 ppb

level)		environmental	
$NO+NO_Y$	NO_X Monitor 9841A	Monitor Labs	0-2000 ppb
O_3	UV Photometric O3 Analyzer Model 49C	Monitor Labs	0.05-1.0 ppm
$CO_2+CO+CH_4+H_2O$	Picarro Cavity Ring-Down Spectrometer G2401	Picarro	0-1000 ppm (CO2) 0-5 ppm (CO) 0-20 ppm (CH_4) 0-7 % (H_2O)
Total Hydrocarbon (THC)	THC Monitor APHA-370	Horiba	0.02-100 ppmC
Trace volatile organic compounds (VOCs)	Proton Time-of-Flight Mass Spectrometer (PTR-ToF-MS)	Ionicon Analytik	10 ppt -1 ppm
Relative Humidity and temperature	Dew point hygrometer SC-05	Rotronic	RH 0-100 %, -40-100 °C
Temperature	Thermocouple type K	Messelemente	0-1200 °C

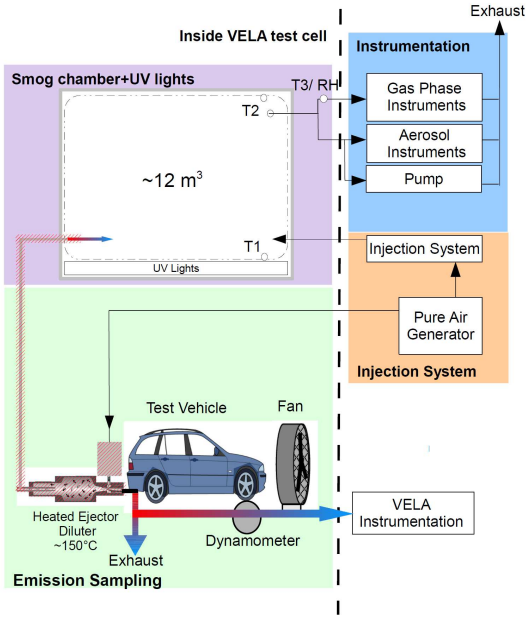

Figure 2: *Schematic (not to scale) of the mobile chamber as set up during experiments on a Euro 5 gasoline light duty vehicle at the vehicle emissions laboratory (VELA) of the European Commission Joint Research Center (JRC) , Ispra, Italy. Highlighted are different sections of the setup. Green: emissions sampling is performed using a modified Dekati ejector equipped with a pressurized air heater. Purple: the smog chamber, an approximately 12.5 m^3 (when full), nominally 9 m^3 (2.5×1.8×1.9 m, L×W×H), 125 µm thick collapsible Teflon bag (suspended from a mobile aluminium frame (2.3×2×2.5 m, L×W×H) with a battery of 40 100 W UV lights. Orange: Injection system and pure air generator. Blue: instrumentation, which was located outside of the test cell. Gas phase instruments are connected to the chamber via Teflon tubing, while steel or copper tubing is used to connect aerosol instruments.*

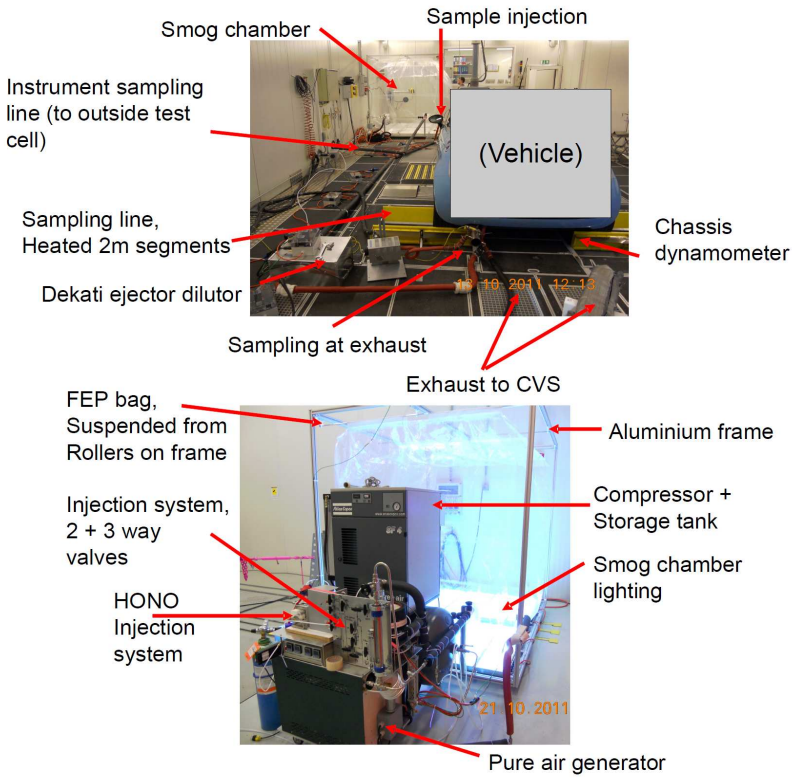

***Figure 3**: A) Illustrated photograph of the smog chamber and sampling system as set up during sampling of emissions from a gasoline light duty vehicle at the vehicle emissions laboratory (VELA). B) Illustrated photograph of the mobile smog chamber and injection system*

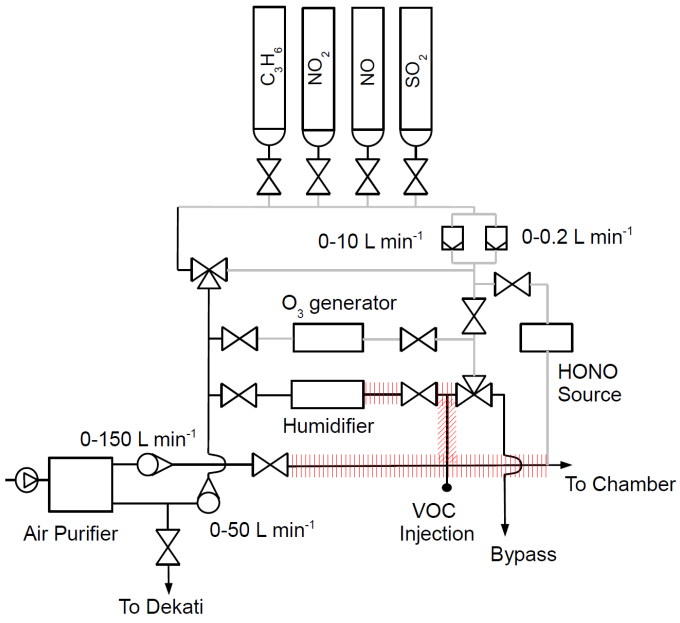

Figure 4: *Schematic (not to scale) of the primary component injection system of the mobile chamber. Pure air may be injected directly into the chamber through the main injection line, an insulated 12mm (outer diameter) stainless steel tube which can be heated up to a maximum of 150 ℃ (red hatching, To Chamber). All or part of the pure air stream may be diverted through different sections of the primary injection system using a series of two- and three-way valves.*

2.2 Light characterisation experiments

Actinometry experiments to determine the photolysis rate of NO_2 (J_{NO2}) were performed to characterise the smog chamber lighting. 80 ppbv of nitrogen monoxide (NO, 1000 ppmv, 5.0, in N_2, Carbagas) was injected into the chamber followed by injection of ozone (O_3). After allowing several minutes for equilibration the lights were switched on. NO_X and O_3 concentrations were monitored throughout. The spectrum of the lights was measured using a photometer (USB2000 UVVIS, Ocean Optics, Inc., USA). The effect of varying temperature on light emission, and accordingly photochemistry, was determined by placing a small number of UV lights inside a refrigeration unit and measuring the spectrum over the range -7 to 25 ℃.

2.3 Vehicle exhaust aging experiments

In this chapter we report some results from two emissions aging experiments performed at the vehicle emission laboratory (VELA) of the European Commission Joint Research Centre (JRC), on exhaust emissions from one EURO 5 gasoline light duty vehicle (GLDV1). The experiments were conducted on 13.10.2011 (here, Exp. 1) and 14.10.2011 (here, Exp. 2). The emissions were studied after injection into the smog chamber and directly at the tail pipe. The emissions measurements from the smog chamber allowed an assessment of the performance of the smog chamber during typical operating conditions, including wall losses, leak rates and sampling efficiencies. The testing procedures

outlined were also applied to the other passenger cars, scooters, and heavy duty trucks presented in subsequent chapters. Further results from the aging of emissions from GLDV1 are presented in Chapter 6.

2.3.1 Vehicle testing procedure

Emission tests are performed on chassis dynamometers in climatic test cells (temperature range -10 to 35 ℃) equipped with a co nstant volume samplers (CVS) with a critical flow venturi (Horiba, Germany).The temperature inside the test cell was 22 ℃ during warm (standard) experiments, but was also maintained at -7 ℃ for some experiments. GLDV1 is equipped with a three-way-catalyst (TWC) and stop-start system; an overview of all vehicles tested and experiments performed is given in Table 2. Emissions for passenger cars were generated during the New European Driving Cycle (NEDC, Fig. 5, grey) used for type approval of light duty vehicles in Europe. For tests with scooters, the ECE15 cycle was used while for heavy duty vehicles the ETC cycle was used. The tests started after a mandatory minimum ambient temperature (22 or -7 ℃) soaking time of 6 hours. The NEDC used for passenger cars is made up of a first urban phase of 780 s followed by an extra-urban phase of 400 s, following EU Regulation 692/2008 (EC, 2008), as highlighted in Fig. 5. Regulated emissions (THC, NMHC, CO, NO_X, and PM) are sampled from the CVS and measured offline onto heated filters (Heated Particulate Filter Module, Horiba HFU-4770) in accordance with Directive 70/220/EEC (EEC, 1970), and its following amendments by means of non-dispersive infrared (regulated CO and unregulated CO_2), chemiluminiscence (NO_X) and flame ionization detector (THC) (Horiba MEXA 7400 HTRLE). In addition, a time-resolved (1 Hz) tailpipe emission characterisation is performed with the same methods described above (for CO, THC, NO_X and CO_2) and with a High Resolution Fourier Transform Infrared spectrometer (HR-FTIR, MKS Multigas analyzer 2030, Wilmington, MA, USA), used to monitor alkanes and alkenes (e.g., methane, ethylene and toluene), nitrogen species (NO_X and ammonia), and oxygenated compounds such as formaldehyde, acetaldehyde, and ethanol (see Clairotte et al., (2011) [12] for details). Finally, gaseous emissions are sampled from the CVS and analysed offline by dedicated gas chromatography (Agilent, model 6890 with dual column and FID) allowing measurement of gas phase species such as alkanes, alkenes and aromatic hydrocarbons. Prior to, and immediately after, each test the CVS is flushed for 30 minutes with dilution air. Particle number, as well as total hydrocarbon measurements, CO, and CO_2 are all below detection at the start of any test.

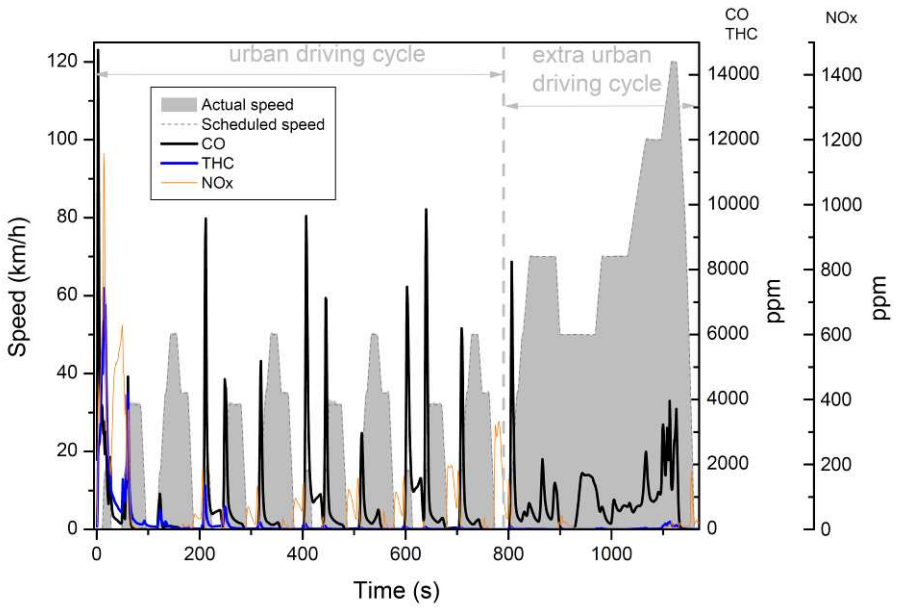

Figure 5: *Vehicle speed during the New European Driving Cycle (NEDC, grey, left axis) and average exhaust concentrations of the regulated compounds carbon monoxide (CO, black) and total hydrocarbon (THC, blue), both on the first right axis, and oxides of nitrogen (NO_X, orange) second right axis, for Exp. 2 during the driving cycle. The NEDC is split into two phases representing urban driving and a second phase representing extra urban driving.*

Table 2: An overview of vehicles tested and experiments performed during this project

Campaign	Vehicle	Designation	Standard /Technology	Driving mode				Ambient condition				Alternative Fuel
				Idle	Full Cycle	Hot	Cold	Temperature		Chamber humidity		
								22C	-7C	30-50%	80-90%	
Mopeds 2010	2S Scooter A	E1	Euro 1/ OC	3				3		3		
	2S Scooter B	E2a	Euro 2/ OC	3				3		3		
	4S Scooter A	(-)	Euro 2/ OC	2				2		2		
			Total	8								
Ispra 2011	2S Scooter C	E2b	Euro 2/ OC		5	3	1	9		9		6 (Aspen)
	4S Scooter B	(-)	Euro 2/ OC		2	2		4		4		2 (Aspen)
	Gas. car A	GLDV1	Euro 5/ TWC, MPI		4			2	2	4		
	Truck A	HDDV1	Euro V/ SCR		6			4	2	6		3 (LPG)
			Total		23							
Ispra 2013	Gas. car B	GLDV2	Euro 5/ TWC, DI		9			6	3	7	2	
	Gas. car C	GLDV3	Euro 5/ TWC, DI		4			2	2			
	Diesel car A	DLDV1	Euro 5/ DPF, SCR		6			4	2	6		
	Diesel car B	DLDV2	Euro 5/ DPF, SCR		6			5	1	4	2	
	Truck B	HDDV2	Euro V/ DPF, SCR		6	2		4	2	6		
	Flexi car E85	EtOH	Euro 5/ TWC(?)		6			4	2	4	2	6 (EtOH)
			Total		39							

OC=Oxidation catalyst, TWC=Three-way catalyst, MPI=Multi-point injection, DI=Direct injection, DPF=Diesel particle filter
SCR=Selective catalytic reduction, LPG=Liquid petroleum gas

2.3.2 Smog chamber procedure

Prior to all experiments the mobile chamber is cleaned by reducing its volume to ~1 m^3 and flushing first with O_3 and humidified air, illuminating the chamber with UV light for a period of around 1 hour and then flushing with pure dry air for several hours, typically overnight. At the start of each experiment the bag is filled to approximately two thirds full with humidified air (i.e. leaving a volume free for sample injection during several minutes). Relative humidity was maintained at either 40% or 90%. Emissions from driving cycles are sampled directly at the vehicle tailpipe and injected into the chamber using the Dekati

ejector dilutor. The Dekati and sampling lines are heated to 150 ℃. Table 3 shows the initial conditions inside the smog chamber, after exhaust injection, for Exp 1 and Exp 2.

Subsequent to exhaust injection, the chamber is filled to close to maximum volume with pure air, ensuring more rapid mixing of the sample and allowing longer experiment times (since sampling from the chamber involves reducing its volume). An ambient relevant 30 to 15 µg m^{-3} of primary aerosol (sum of black carbon and primary organic) is typically injected into the chamber.

A period of several minutes is allowed for the equilibration inside the chamber and for characterisation of the primary emissions. Then, 1 µl (~20 ppbv) nine times deuterated butanol (butanol-D9, 98 % Aldritch) is injected to quantify OH exposure during the experiments [13]. Briefly, butanol-D9 is used as a unique OH tracer and measuring its decay, here with the PTR-ToF-MS, yields time resolved OH concentrations. An OH exposure 10^6 $cm^{-3}h$ corresponds to the average ambient global OH exposure during one hour. During summer-smog situations in the afternoon the OH exposure is typically (5-10) $\cdot 10^6$ $cm^{-3}h$.

Vehicles may emit significant NO_X (e.g. Fig. 5, orange). In the lower troposphere most NO_X is present as NO_2, therefore, in experiments with high NO_X, ozone was injected to oxidise most NO to nitrogen dioxide (NO_2) prior to switching on the lights. Note that only enough ozone was added to convert the NO, and that an excess was not present before lights on. Furthermore, propene (1000 ppm, 5.0, Carbagas) was added after two hours of lights on for Exp. 1 and before lights on for Exp. 2. to adjust the VOC/NO_X ratio to, in the case of these experiments, approximately 6:1 (see Table 3). The oxidation of propene is not likely to produce SOA (due to the high volatility of its oxidation products) and has previously been used to adjust the VOC/NO_X ratio during smog chamber experiments [14, 15]. Previous studies have shown that propene can reduce SOA yields of aromatic hydrocarbons during smog chamber experiments by up to 15 % by acting as an OH scavenger [16], though this effect is quantified using the butanol-D9 tracer. Furthermore propene addition resulted in a significant increase in OH radical production, as shown in Fig. 6. The addition of ozone and propene served therefore to shorten experiment times, while adjusting the conditions in the chamber to match more closely those of the ambient atmosphere.

For some experiments on diesel vehicles, several ppbv of ammonia (NH_3, 200 ppm, 5.0, Carbagas) was added to the chamber either at the start or during experiments. The effect of NH_3 is not presented here, but was added to the chamber to ensure that conditions between gasoline and diesel vehicle exhaust aging were as similar as possible, since the TWC of the gasoline vehicles also emits NH_3.

After adjusting the gases in the chamber and after allowing time for instrument readings of the injected gases to stabilise, the UV lights are switched on to initiate photochemistry. Aging of the emissions and associated SOA production are measured during a period of ~4-5 hours.

The procedure described here can be adapted for the study of other emissions e.g. from ship engines, wood combustion etc. Adjustment of the VOC/NO_X ratio, if at all necessary, may in other studies also be achieved by the addition of NO_X, in cases where the NO_x concentration is low in the chamber.

For this study, and all vehicles presented throughout this report, the emissions were sampled directly at the tailpipe of the vehicle, thereby avoiding potential particle losses in the CVS. The CVS operates with a dynamic dilution system, ensuring that the total flow through the system is constant, even as exhaust flow rate varies during a driving cycle. This offers significant advantages in terms of quantification, and indeed is required for legislative testing, but is likely to incur losses of semi-volatile species as the system is not heated even at relatively low dilution. In this study for example the dilution in the CVS varied between 2 and 200, while the average dilution during the whole NEDC for Exp. 1 and Exp. 2 was 37, less than the dilution inside the chamber during these experiments (average dilution factor 100). The most significant disadvantage with sampling directly at

the tailpipe is that while exhaust flow is variable, the sampled flow is constant. A different fraction of the complete exhaust is sampled as the flow rate varies. In theory this could lead to a sampled composition different to that which is emitted. However, Fig. 7 shows that the relative composition of the total VOC emission is very close, within 20 %, to that of the average tailpipe VOC emission (measured at the tailpipe using the FTIR). I.e. tailpipe sampling offers the advantage of minimising losses while allowing quantification of emissions. For the results presented below it is assumed that the composition of VOC sampled at the tailpipe is the same as that sampled at the CVS (e.g. from GC-FID analysis).

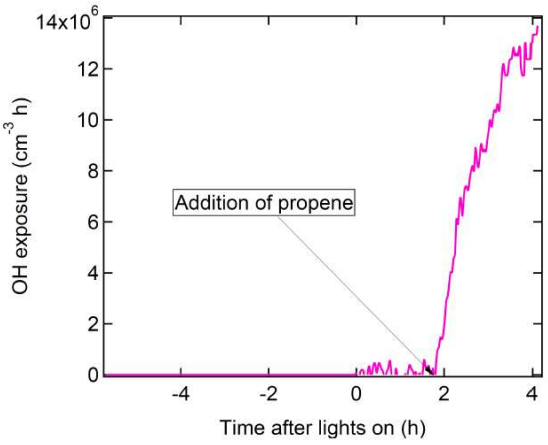

Figure 6: *OH exposure (cm^{-3} h) measured from the smog chamber during the aging of vehicle emissions. The addition of propene can be used to significantly enhance OH.*

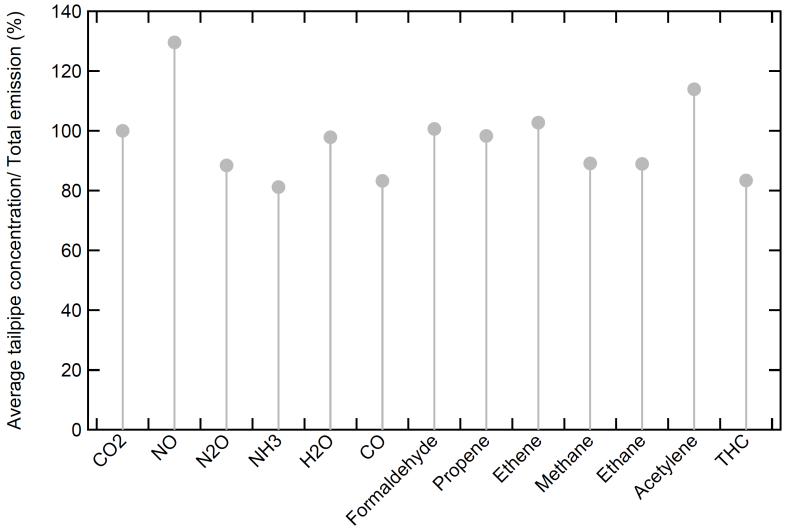

Figure 7: *CO_2 normalised concentrations of gas phase species measured at the tailpipe (i.e. concentration of the constant flow injected into the smog chamber) vs. total mass emitted (i.e. accounting for variable exhaust flow as a function of time), measured using FTIR. Normalised concentrations are within 20 % for most gas phase species, suggesting that sampling a constant flow from the vehicle exhaust yields samples with chemical composition close to those of the total emissions.*

Table 3: Initial and adjusted parameters inside the mobile smog chamber for the gasoline light duty vehicle aging experiments. Addition of propene after 2 hours during Exp .1 and before lights on for Exp. 2 resulted in adjusted VOC/ NO_X ratios to around 6.

Experiment #	**Date**	**Initial Conditions (before lights on and addition of propene)**					**Adjusted THC (ppmv)**	**Adjusted VOC/ NO_X**
		RH %	**T (°C)**	**Ozone (ppbv)**	**THC (ppmv)**	**NO_X (ppmv)**		
	13.10.2011	50	25.1	<10	1.5	0.53	3.2	6.1
	14.10.2011	64	23.6	<10	1.4	0.41	2.3	5.6

2.4 Instrumentation

Table 1 reports a non-exhaustive list of instrumentation typical of that available for measurements from the mobile chamber. These allow the characterisation and quantification of particle and gas phase species.

2.4.1 Particle phase measurements

Time resolved online measurements of particle composition were performed using a high resolution time of flight aerosol mass spectrometer (HR-ToF-AMS) and an aethalometer (Model AE33 prototype). A detailed description of the working principles of the HR-ToF-AMS and associated data analysis may be found in DeCarlo et al., (2006) [17]. The instrument provides quantitative size-resolved mass spectra of non-refractory PM_1 components, empirically defined as vaporisable species over a 1 s time interval, at 600 ℃ and 10^{-7} torr. These include organic aerosol (OA) and ammonium nitrate and sulfate (NH_4^+, NO_3^- and SO_4^{2-}). Data from the high resolution time of flight aerosol mass spectrometer (HR-ToF-AMS) are analysed using high-resolution analysis fitting procedures.

Black carbon (BC) concentrations and aerosol optical absorption spectra were measured using an aethalometer (Model AE33). This new aethalometer incorporates two simultaneous parallel sampling channels from the same inlet stream collected at different rates of accumulation, resulting in different loading of the filter with collected aerosols on the two respective spots. Loading effects can then be extrapolated to zero loading allowing online “loading effect” compensation for all wavelengths used for the measurement.

An important consideration in the quantitative analysis of AMS data is the collection efficiency (CE), related to particle bounce. Correcting scanning mobility particle sizer (SMPS) data from the chamber for density, based on the particles chemical composition measured by the HR-ToF-AMS, and subtracting black carbon (BC) as measured by the aethalometer, provides a second measurement of the total non-refractory PM mass (i.e. those species quantified in the HR-ToF-AMS). This was used to correct for CE, typically 0.5-1.0 throughout experiments, consistent with recent laboratory and ambient measurements of CE [18, 19]. Note that error is possible in the quantification of the primary particles, which have a relatively high content of BC characterised by a non uniform shape, since the SMPS relies on mobility diameter. An overestimation of total primary emissions could be expected where black carbon content is large. However gravimetric analysis of primary emissions yielded similar primary EFs, suggesting only minimal error in this case (Fig. 8). Heavily SOA coated particles are assumed to be spherical therefore not to introduce error in the CE calculation. Data presented below are all corrected for CE.

The HR-ToF-AMS used for these experiments was equipped with a newly developed high pressure lens, which has a lower size limit of 100 nm for 100 % transmission, and can sample aerosol larger than 2.5 µm [20]. Figure 9 shows volume distributions for fresh and aged aerosol during Exp. 2. The volume distribution grows significantly over the experiment. As shown, the primary volume distribution is centred at around 250 nm, while most secondary particles are in the range 350-700 nm. By using the large lens around 40 nm are cut from the lower edge of the volume distribution (<10 % of the mass), while no part of the higher edge is cut. The standard lens would cut a small portion at both sides of the primary aerosol volume distribution. For the secondary aerosol the standard lens would cut a small portion of the larger particles, while none are cut by the large lens. Therefore, while both lenses could reasonably be used to measure the aging of aerosol from this vehicle, the high pressure lens is slightly better suited. Therefore, the large AMS lens was used for all experiments on vehicle aging.

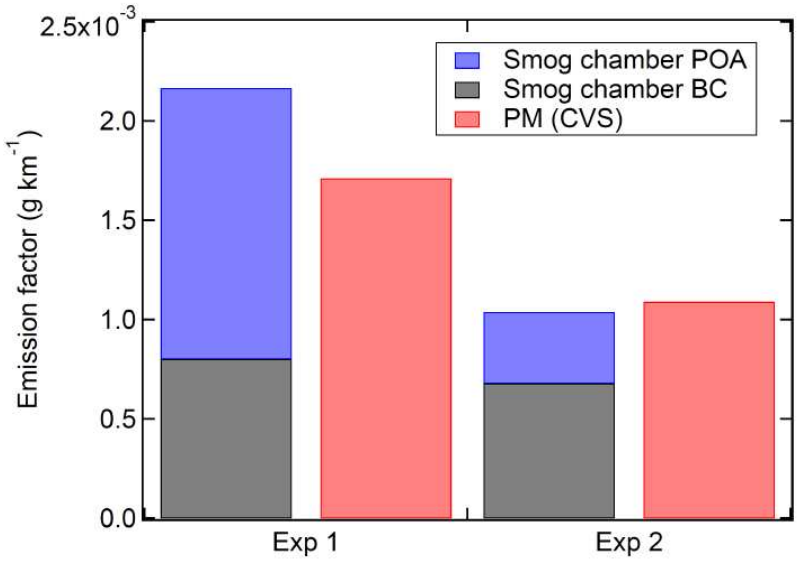

Figure 8: *Primary aerosol emission factors for a Euro 5 gasoline light duty vehicle measured from the CVS and at the mobile smog chamber (sum of black carbon and primary organic aerosol).*

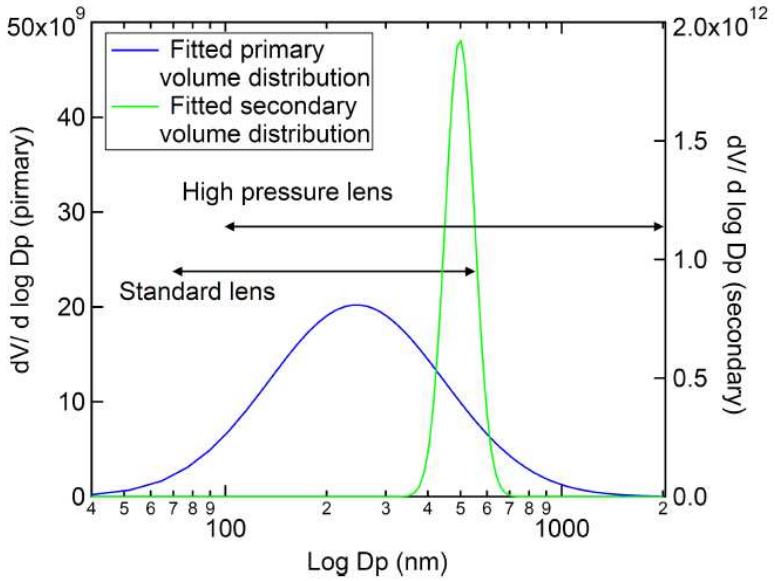

Figure 9: *Example lognormal fitted scanning mobility particle sizer (SMPS) volume distributions of primary (blue) and aged aerosol (green) from a gasoline light duty vehicle measured from the mobile smog chamber. The size cut-offs for the standard AMS lens and for the high pressure lens used in this study are given by the arrows. By using the large lens around 40 nm are cut from the lower edge of the volume distribution (<10%) while no part of the higher edge is cut. The standard lens would cut a small portion at both sides of the primary aerosol volume distribution. For the secondary aerosol the standard lens would cut a small portion of the larger particles, while none are cut by the large lens. Therefore, while both lenses could reasonably be used to measure the aging of aerosol from this vehicle, the high pressure lens is slightly better suited.*

2.4.2 Gas phase measurements

A suite of gas phase instruments was used here and is typically available for studies using the mobile smog chamber. Reactive gases such as O_3 and NO_X are monitored throughout every experiment, while emphasis has been placed on the measurement of combustion products, e.g. CO_2, CO, CH_4 and total hydrocarbon THC (Table 1), allowing establishing the carbon mass balance of the emissions. NO_X is monitored using instrumentation which measures directly NO as well as all nitrogen oxides (NO_Y), with NO_Y assumed to be almost exclusively NO_2 during most experiments.

A proton transfer reaction time-of-flight mass spectrometer (PTR-ToF-MS, Ionicon Analytik) was used to measure concentrations of VOCs inside the chamber, including that of butanol-D9. The instrument performances have already been described in detail previously (Jordan et al., 2009;Graus et al., 2010). The high mass resolution of the PTR-ToF-MS (m/Δm ranging from 3200 to 4500 between m/z 21 and m/z 149) combined with an accuracy below 20 ppm allows separation and formula assignment of most the ions comprising the mass spectra of both primary and secondary vehicle emissions. Based on a 2 minutes integration time, typical limits of detection (LODs) determined as the 3σ uncertainty measured with a Pt catalyst heated at 350 ℃ were below 10 ppt. Data analysis was carried out using TOF Viewer 1.4.3. ToF-to-mass assignment was performed using hydronium ion isotope ($H_3{}^{18}O^+$, 21.022) and protonated acetone ($C_3H_7O^+$, 59.049). Peak fitting and integration was performed using Gaussian functions.

2.5 Characterisation of the mobile smog chamber

The suite of tests conducted (see Sect. 2.2) and emissions experiments (see Sect. 2.3) allowed us a detailed characterisation of the mobile chamber.

2.5.1 Chamber blank and leak rate

Figure 10 illustrates an example of results from Exp. 2, showing time series and concentrations of several gas phase species as well as organic aerosol concentrations measured from the smog chamber and the temperature inside the chamber. In the empty chamber, before sample injection, measured particle number concentration is always below the CPC detection limit (<0.1 cm^{-3}), whereas the CO_2 concentration is around 35 ppmv. By measuring the increase in CO_2 and CH_4 due to diffusion of external air into the empty chamber, an average leak rate of 0.08 % h^{-1} (i.e. ~ 9 L h^{-1}) was calculated. These results show that the chamber has minimal contaminants and that leaks are minor over the course of a typical experiment lasting 5-6 hours (see CO_2, green trace, Fig. 10B).

Two blank experiments were performed, where the chamber was filled with either pure air, or a mix of pure air and ambient air sampled through the heated sampling system and the lights were switched on. In both experiments <1 µg m^{-3} of aerosol were formed.

2.5.2 Temperature control

Since the chamber is not housed in an enclosure, the temperature inside the bag is that of the ambient. For the gasoline aging experiments the ventilation inside the VELA was sufficient to maintain a stable temperature to within 1 ℃, despite the heat generated by the UV lights (see Fig. 5A, grey). The temperature gradient was <1 ℃ as measured using sensors T1 and T2 (Fig. 2).

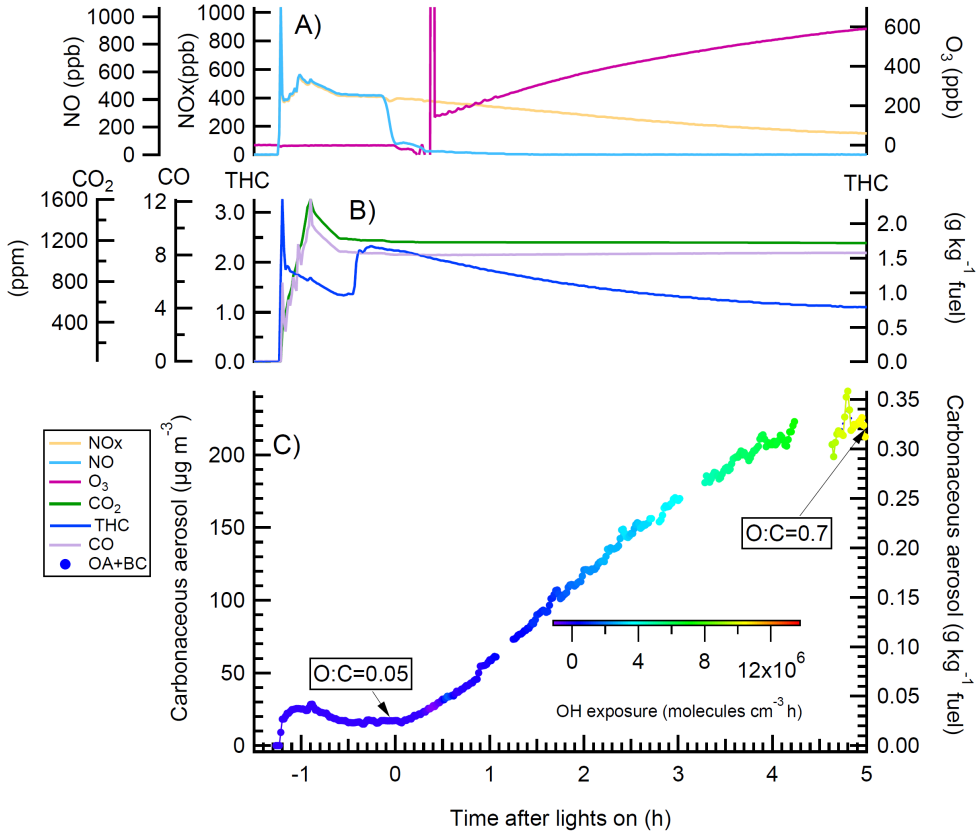

Figure 10: *Measured concentrations and calculated emissions factors (EF) inside the mobile smog chamber of gas and particle phase species after injection of emissions from a Euro 5 gasoline light duty vehicle (GLDV1) (Exp. 2) as a function of time after lights on in the chamber. A) NO_X (yellow), NO (light blue), O_3 (magenta) and chamber temperature (grey). After an initial spike due to sample injection, a small decrease in NO_X before lights on follows the injection of additional air required to completely fill the chamber. O_3 increases after lights on as a consequence of the photochemical processing of emissions occurring inside the chamber. Temperature is stable to within 1 ℃ throughout the*

experiment. B) Carbonaceous gases. After an initial decrease due to the dilution CO_2 (green) and CO (lilac) concentrations are constant indicating that the system is airtight. The increase in total hydrocarbon (blue) before lights on follows the addition of propene required to adjust the VOC/NO_X ratio. C) Wall loss corrected carbonaceous aerosol (black carbon, BC + organic aerosol, OA) increases after lights on due to secondary organic aerosol (SOA) formation. OH exposure is shown by the colour scale. Aging increases the O:C ratio of the emissions from 0.05 for the primary to 0.7 for the secondary, a ratio equivalent to the low volatility oxidised OA observed in highly aged ambient aerosols. The right axis in B) and C) shows the EF calculated for THC and carbonaceous aerosol using Eq. 12.

2.5.3 Particle losses

During smog chamber experiments particles are lost to the walls through deposition following diffusion and gravitational settling. These losses limit the maximum duration of smog chamber experiments by continually removing suspended particle mass until instrument detection limits are reached. The loss rate for a given chamber depends largely on the surface to volume ratio of the chamber, with higher ratios leading to higher loss rates. Other parameters affecting particle loss rates include particle size (small particles have higher diffusion loss rates, while larger particles are more affected by gravitational settling) and turbulence inside the chamber, due to for example temperature gradients.

Aethalometer data, shown in Fig. 11, was used to determine a wall loss corrected suspended organic aerosol concentration ($C_{OA(WLC)}$) during the vehicle aging experiments, assuming that material deposited on the chamber walls does not participate in partitioning:

$$C_{OA(\mathrm{WLC})}(t) = C_{OA(SUSP)}(t) + \int_0 k(t) \cdot C_{OA(SUSP)}(t)dt \quad , \tag{1}$$

Where $C_{OA(SUSP)}$ is the measured organic aerosol concentration, *t* refers to experiment time and k the exponential decay constant of the fitted period. Although BC is expected to be inert, aethalometer measurements are affected by coating of soot particles with SOA, which increases the effective absorption coefficient and hence apparent concentration [21], clearly visible in Fig. 11. Therefore a fitted BC concentration is used. Figure 11 also shows two such fits, one before lights on in the chamber, where no change in absorption from particle coating is expected, and one after 3 hours of lights on where particle growth is negligible. Fitted BC data (Fig. 11) indicate a particle half-life due to wall losses of between 3.3 and 4.0 hours for the period before lights on and the period after lights on, respectively, for Exp. 2. These values indicate that particle losses in the chamber are sufficiently low to conduct experiments over several-hour timescales. Particle half-life in the mobile chamber is shorter than the average 5 hours observed in the 27 m^3 PSI stationary smog chamber [22], an expected consequence of the increased surface to volume ratio of the mobile chamber. Data presented here are all corrected for wall losses. The pre-UV exposure fit before lights on was chosen to correct for losses as the fit after lights is more likely to be influenced by coating. Significant influences due to turbulence during aging as a result of heating from the lights are not expected as only a small change in temperature after UV light exposure was observed and a longer half life is observed during lights on (Fig. 11).

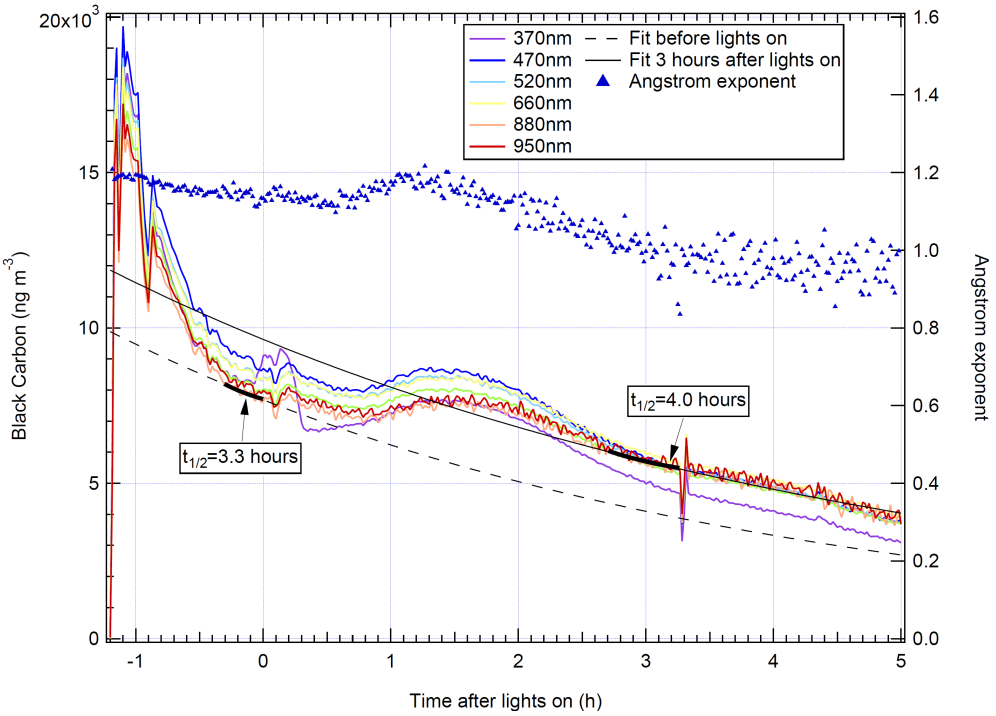

Figure 11: *Smog chamber black carbon (BC) concentration measured at different wavelengths using a prototype AE33 aethalometer as a function of time after lights on in the chamber after sampling emissions from a Euro 5 gasoline car. Also shown: particle half lives ($t_{1/2}$) determined from a fit of BC measured at 880nm before lights on (dashed black line) and 3 hours after lights on (solid black line). The fitted region for each curve during each period is highlighted (thick black line) The Angstrom exponent value calculated for each measurement point is shown on the right axis (blue triangles).*

2.5.4 Smog chamber lighting

Figure 12 shows the light spectrum at 25 ℃ (red) a nd -7 ℃ (blue) of the UV lights of the mobile smog chamber normalised to the peak intensity. The peak in emission is at 368 nm and is in a narrow window between 310-430 nm. The emission fingerprint as a function of wavelength and temperature, ($I(\lambda,T)$), of the smog chamber lighting overlaps with the absorption cross-section ($\sigma(\lambda,T)$) for the photolysis of many important atmospheric trace gases including the OH radical sources O_3, HONO, and HCHO, as well as NO_2 [23]. Therefore although emission intensity may be higher than sunlight over the spectral region at which they emit and much of the solar spectrum is not represented, UV lights are a good substitute for ambient sunlight in smog chambers [23]. An advantage of UV lights over other light sources, such as for example xenon arc lights, is that they do not produce significant heat. Consequently UV black lights are used in many environmental reaction chambers. The photolysis rate of NO_2 (J_{NO2}) can be calculated using the photostationary steady state relation:

$$[O_3] = \frac{J_{NO2}[NO_2]}{k[NO]} \quad , \qquad (2)$$

where the concentrations of O_3, NO_2 and NO as well as the rate constant k between O_3 and NO are known [1], in this case from smog chamber measurements. NO_X was measured with both Thermo and Monitor labs NO_X analysers (Table 1) and an average J_{NO2} of $(8.0\pm0.7)\times10^{-3}$ s^{-1} was calculated from Equation 2, after a correction of 5 % to account for formation of NO_2 in the (dark) sampling lines.

J_{NO2} as a function of wavelength and temperature within a given window $\lambda 2$-$\lambda 1$ is given by

$$J_{NO2}(\lambda,T) = \int_{\lambda 1}^{\lambda 2} \phi_{NO2}(\lambda,T) \cdot \sigma_{NO2}(\lambda,T) \cdot I(\lambda,T)\, d\lambda \tag{3}$$

where $\phi(\lambda,T)$ is the quantum yield of NO_2 photolysis as a function of wavelength and temperature [1]. Thus while *I(λ,T)* in Fig. 12A) is given by the light photometer in arbitrary units only, absolute values for the photolysis rates of a compound *i* (J_i) can be inferred from J_{NO2}:

$$J_i = J_{NO2} \cdot \frac{\int_{\lambda 1}^{\lambda 2} \phi_i(\lambda,T) \cdot \sigma_i(\lambda,T) \cdot I(\lambda,T)\, d\lambda}{\int_{\lambda 1}^{\lambda 2} \phi_{NO2}(\lambda,T) \cdot \sigma_{NO2}(\lambda,T) \cdot I(\lambda,T)\, d\lambda} \,. \tag{4}$$

Inferred photolysis rates at 25 ℃ from Equation 4 are given for several compounds in Table 4, where International Union of Pure and Applied Chemistry (IUPAC) recommended values of $\phi(\lambda,T)$ and $\sigma(\lambda,T)$ [24, 25] were used in Equation 4. The predicted photolysis rates show that the lighting system of the mobile smog chamber can be expected to be particularly effective in generating OH radicals from HONO when in the presence of NO_X) and to a lesser extent from O_3 and formaldehyde.

Figure 12 also shows that the emission fingerprint is largely unchanged over the given temperature range. Theoretical rate constants at -7 ℃, shown in Table 4, were also determined using Equation 4. Minor changes in absorption cross section as a function of temperature ($\sigma(t)$) and quantum yield as a function of temperature ($\Phi(t)$) were accounted for as described in the following sub-sections. For nitrous acid (HONO) and formaldehyde (HCHO), no literature data on how to account for the change in σ and Φ as a function of temperature were found. Therefore the small change in photolysis rates in Table 4 is accounted for by the change in the emission fingerprint between 25℃ and -7℃ (see Fig. 3A, main text).

Nitrogen dioxide (NO_2): The absorption cross section, σ, of NO_2 as a function of temperature (*T*) is given by the following parameterisation [26], which was used to estimate $\sigma(-7℃)$:

$$\sigma(t) = \sigma(0°C) + aT \,, \tag{5}$$

with the parameter *a* tabulated in [26]. $\Phi(t)$ is given in the literature [24]. An estimation of $\Phi(-7℃)$ was calculated by interpolating the values given in the literature at 25℃ and -29℃ [24].

Nitrate (NO_3): $\sigma(-7℃)$ of NO_3 was estimated by interpolating the values given in the literature at 25℃ and -43℃ [24]. For the photolys is reaction

$$NO_3 + h\nu \rightarrow NO + O_2 \,, \tag{6}$$

$\Phi(t)$ is unity below 587 nm [24]. For the photolysis pathway

$$NO_3 + h\nu \rightarrow NO_2 + O \,, \tag{7}$$

and the photolysis pathway in Eq. 2 above 587 nm, $\Phi(t)$ is given at 25℃ and -43℃ in the literature [27] and $\Phi(-7℃)$ was estimated by interpolating $\sigma(\lambda)$ between these values.

Ozone O_3: The effect of temperature *T* on σ of O_3 is only small, decreasing by <1% between 25℃ and -55℃ [28], and was therefore negl ected here. For the reaction

$$O_3 + h\nu \rightarrow O(^1D) + O_2 \,, \tag{8}$$

the main pathway of interest since O(^{1}D) may react with water to produce OH radicals, *Φ(-7℃)* as a function of wavelength *λ* was calculated using the following expression [24]:

$$\Phi(\lambda T) = \left\{\frac{q1}{q1+q2}\right\} \times A1 \times \exp\left\{-\left(\frac{X1-\lambda}{\omega 1}\right)^4\right\} + \left\{\frac{q2}{q1+q2}\right\} \times A2 \times \left\{\frac{T}{300}\right\}^2 \exp\left\{-\left(\frac{X2-\lambda}{\omega 2}\right)^2\right\} + A3 \times \left\{\frac{T}{300}\right\}^{1.5} \exp\left\{-\left(\frac{X3-\lambda}{\omega 3}\right)^2\right\} + c\,, \quad (9)$$

where

$$q(i) = \exp\left(\frac{vi}{RT}\right)\,, \quad (10)$$

where R is the molar gas constant (8.314 J K^{-1} mol^{-1}), and using *A1* = 0.8036, *A2* = 8.9061, *A3* = 0.1192, *X1* = 304.225, *X2* = 314, 957, *X3* = 310.737,*ω1* = 5.576, *ω2* = 6.601, *ω3* = 2.187, *v1* = 0, *v2* = 825.518, and *c* = 0.0765.

For $I_{-7℃}(\lambda)$, measured values (Fig. 12A, blue) were used. Table 4 also shows the ratio of gas phase photolysis rates J_i at -7 ℃ and 25 ℃, $J_{i,-7℃} / J_{i,25℃}$. The ratio is in the range 0.30-0.41, while the ratio in emission intensity at these temperatures, $I_{-7℃}(\lambda)/ I_{-25℃}(\lambda)$, is 0.28 (Fig. 12B). Therefore the decrease in photolysis rates can be largely explained in terms of the decrease in emission intensity of the UV lights. A power fit (dashed lines Fig. 12B) of the measured intensity at different temperatures can therefore be used to predict the relative gas phase photolysis rate of species *i* as a function of temperature ($J_{rel,i}(T)$):

$$J_{rel,i}(T) = J_i(25^\circ C) \cdot \left(-0.064 \cdot \left(\frac{1.080}{1+\exp(-2.466-(T/6.218))}\right)\right)\,. \quad (11)$$

Equation 11 suggests that although significant loss of intensity occurs at low temperatures, the lighting in the mobile chamber will still initiate photochemistry. The mobile chamber can thus be utilised for aerosol aging studies even at zero or sub-zero temperatures. Under such conditions the HONO injection system described in Sect. 2.1 could be used to compensate for the loss in intensity by providing an additional OH source. As Fig. 12 illustrates the mobile chamber may be operated down to ~10 ℃ without large loss in light intensity.

For the gasoline aging experiments the OH exposure was zero before the lights were switched on. The integrated exposure at the end of each experiment, after UV light exposure and aging, was between 5 and 150×10^6 molecules cm^{-3}h (colour scale, Fig. 10). Assuming a global annual mean concentration of 10^6 OH molecules cm^{-3} [29], this corresponds to up to 150 hours in the atmosphere, thereby demonstrating that the lighting of the chamber generates sufficient OH to study atmospheric processes occurring over relevant time scales.

While this study shows that the mobile chamber lighting can be used to simulate atmospheric photochemistry over a range of temperatures, uncertainties remain. The photolysis rates of some compounds, notably ketones and aldehydes, may be enhanced compared to ambient conditions when using UV lights [23]. Furthermore oxidised SOA mass can be lost under UV black lights when OH concentration decreases from 10^7 to 10^6 molecules cm^{-3} s^{-1} [30]. This suggests that photolysis and other OA processing pathways initiated by the UV lights compete with the photooxidation pathways responsible for SOA formation. I.e. the relative importance of SOA decay (due to

photolysis pathways) compared to SOA production via OH oxidation is increased when OH concentration is lowered.

This is consistent with the photolysis rates in Table 4. For example, using k_{OH}=1.1×10^{-11} cm^3 molecule^{-1} s^{-1} for glyoxal and OH=10^6 cm^{-3}, photolysis would account for ~40 % of glyoxal decay in the smog chamber. At OH=10^7 cm^{-3} this drops to ~6 %. Such effects could theoretically lead to an underestimation of the SOA production for the gasoline vehicle in this study relative to ambient conditions. However, the UV light and sunlight spectra overlap, thus the relative importance of the SOA formation/ SOA processing (likely photolysis) pathways will depend both on relative light intensity and OH concentrations, each highly variable in smog chambers and the ambient atmosphere.

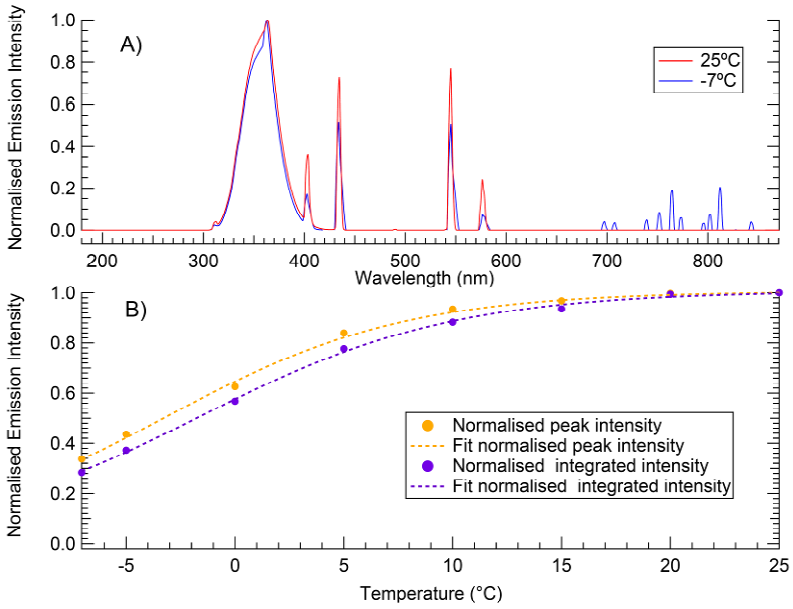

Figure 12: *A) Emission spectrum of the UV black lights of the mobile smog chamber normalised to the peak in emission at 368nm at 25 °C (red) and -7 ℃ (blue). The emission fingerprint does not change significantly over this temperature range. B) The normalised intensity of the smog chamber lighting measured at 368nm and from integrating the full spectrum. The dashed lines show a power fit to the data. Intensity does not vary significantly between 10 ℃ and 25 ℃ (less than ~10 % decrease). At -7 ℃, intensity is decreased significantly (~70 % decrease).*

Table 4: *Predicted gas phase photolysis rates of selected compounds in the mobile smog chamber at 25℃ and -7℃.*

Compound	Reaction	J_i (10^{-5} s^{-1}) 25 ℃	J_i (10^{-5} s^{-1}) -7 ℃	Ratio $J_{i,-7℃}$ / $J_{i,25℃}$
Nitrogen dioxide	NO_2>NO+O(^{3}P)	797	259	0.32
Ozone	O_3>O(^{1}D)	43.1	17.8	0.41
Nitrous acid	HONO>OH+NO	214	68.4	0.32
Nitrate	NO_3>NO+O_2	0.00	0.00	-
	NO_3>NO2+O(^{3}P)	444	135	0.30

Formaldehyde	HCHO>HCO+H	1.50	0.53	0.36
	HCHO>CO+H_2	3.74	1.35	0.36
Acetaldehyde	CH_3CHO>products	0.11	-	-
Methyl hydroperoxide.	CH_3OOH>products	0.43	-	-
Glyoxal	$(CHO)_2$>products	0.71	-	-
Methyl vinyl ketone	$CH_3C(O)CH=CH_2$>products	0.34	-	-
Acetone	$CH_3C(O)CH_3$>products	0.01	-	-
Methyl nitrate	CH_3ONO_2>products	0.29	-	-
Peroxy acetyl nitrate (PAN)	$CH_3C(O)OONO_2$>products	0.04	-	-

3 Emissions from two-stroke scooters

3.1 Introduction

Two-stroke (2S) scooters (powered two-wheeled vehicles with engine displacement <50cc) are popular globally, particularly in Asia and Southern Europe (see Fig. 13). However, regulations for scooters are generally less stringent than for other vehicles, e.g. in Europe having reached Euro 5/V (a fifth tranche of regulations), for passenger cars and trucks, vs. only Euro 2 for small cylinder (<150cm^3) scooters (see Table 5, and EC, (2002)). Accordingly, a scientific report to the European Commission suggests that scooters will emit more volatile organic compounds (VOCs) than all other vehicles combined in Europe by 2020 [31]. Though highly variable, at the global scale, organic aerosol (OA) dominates PM_{10}, with SOA accounting for the largest fraction of OA [8]. Since 2S scooters emit significant VOCs they may also produce significant SOA. This could effectively increase the PM emissions and the health impacts of 2S scooters. High PM levels and toxic aromatic hydrocarbons, important SOA precursors [32], have been observed in many cities, especially in Asia [33]. Passenger cars and trucks, particularly diesel vehicles, are thought to be the main vehicular PM sources [5]. This needs re-thinking, as we show for the first time that elevated PM levels can be a consequence of 'asymmetric pollution' from two-stroke (2S) scooters; vehicles that constitute a small fraction of the fleet, but can dominate urban vehicular pollution through organic aerosol and aromatic emission factors up to 1000s of times higher than from other vehicle classes. Further, we demonstrate that oxidation processes producing SOA from vehicle exhaust also produce potentially toxic 'reactive oxygen species'.

Figure 13: *Scooter 'avalanche' in Taipei, Taiwan, home to millions of scooters. Image from National Geographic.*

***Table 5**: Emission limit values for Euro 1 and Euro 2 powered two wheelers*

Norm	Directive	Effective	CO	$HC+NO_x$
			$mg\ km^{-1}$	$mg\ km^{-1}$
EURO1	97/24/EC	17.06.1999	6000	3000
EURO2	97/24/EC	17.06.2002	1000	1200

3.2 Methodology

We combine the results of two measurement campaigns where 2S scooter exhaust was injected through a heated inlet into smog chambers [22, 34] to produce SOA via photochemistry. Experiments were under high NO_x conditions (several 10s ppb(v)), with average OH~$5 \cdot 10^6$ cm^{-3} and OH~$1\text{-}3 \cdot 10^6$ cm^{-3} (5 and 1-3 hours oxidation at the global average OH concentration of $1 \cdot 10^6$ cm^{-3}) for the first and second campaign, respectively. During the first study 2S scooters Euro 1 (E1) and a Euro 2 (E2a) were run in idle (I) or simulated low power (L, simultaneous application of brakes and power). During the second campaign, emissions from a different Euro 2 2S scooter (E2b) were sampled during ECE47 driving cycles on a chassis dynamometer [10]. Table 6 presents technical specifications of the 2S scooters investigated. OA was monitored using a high resolution time of flight aerosol mass spectrometer (HR-ToF-AMS), and aromatics with a proton transfer reaction mass spectrometer (PTR-MS). CO_2, CO, CH_4 and VOCs were quantified inside the smog chamber and at the tailpipe. OH was quantified using tracers following the "OH clock" methodology of Barmet et al., (2012) [13]. For the driving cycle emissions the mobile smog chamber was deployed at JRC Ispra (see Sect. 2). Methodology for experiments on idling 2S scooters is presented in the following sub-section.

***Table 6**: Technical details of the two-stroke scooters used in this study*

Scooter	**E1**	**E2a**	**E2b**
Registration date	26/10/2007	05/03/2010	2010
km at start of testing	7716	20	1700
Displacement (cm^3)	50	50	50
After-treatment	Oxidation catalyst	Oxidation catalyst	Oxidation catalyst, Carburetor
EC Norm	97/24/CE Euro1	97/27/5/CE Euro 2	97/27/5/CE Euro 2
Fuel	Gasoline+2% lubricant	Gasoline+2% lubricant	Gasoline+ 2% lubricant

3.2.1 Smog chamber experiments on idling two stroke scooters

Emissions from 2-stroke (2S) scooters were sampled directly at the tailpipe and sent through a heated (150°C) ejector dilutor (Dekati Ltd, Tampere, Florida) and introduced

into the 27m^3 Teflon environmental chamber, Fig. 14. The external temperature of the scooter exhaust was monitored (Thermocouple type K, Messelemente) and after an initial warming period of several minutes (consisting of idling or applying low power) the emissions were injected only when the external exhaust temperature was stable at idle or at low power with the brakes applied. Table 7 provides the operating conditions, smog chamber OA concentrations, and aerosol emission factors (see Sect. 3.3).

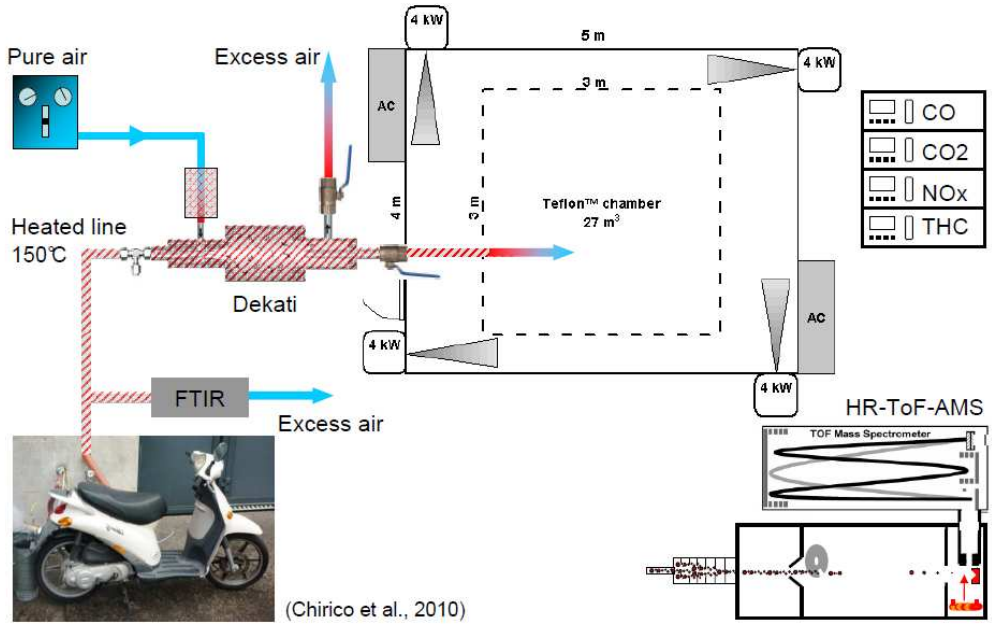

Figure 14: *An illustration of the smog chamber set up used for the study of primary and secondary organic aerosol emissions from 2-stroke mopeds. Heated lines are highlighted by the red hatched lines.*

Table 7: *List of smog chamber tests with driving conditions, smog chamber OA concentrations and calculated primary and secondary organic aerosol in g Carbon (C) kg^{-1} fuel for idling , simulated low power and ECE47 driving cycle (chassis dynamometer, see also Fig. 23) 2S scooter experiments*

Vehicle	Date	Test	OA		Aged OA /POA	Emission Factors	
			POA	Aged OA		POC	SOC(5h)
			µg m^{-3}	µg m^{-3}		g C kg^{-1} Fuel	g C kg^{-1} Fuel
	17.11.10	Idle	11	121.8	11.1	1.02	6.45
E1	19.11.10	Idle	7.5	196.1	26.1	0.72	5.45
	22.11.10	Low Power	70.4	116.4	1.7	5.17	6.59
	15.11.10	Low Power	38.8	114.9	5.0	5.17	6.59
E2a	24.11.10	Low Power	8.3	23.3	3.0	9.18	15.37
	26.11.10	Idle	1.7	157.9	2.8	1.48	2.02
E2b	30.09.11	Full cycle	3.04	4.98	1.6	0.49	0.78
	03.10.11	Phase one only	30.56	71.23	2.3	2.08	3.25

The organic aerosol (OA) concentrations in the chamber were monitored using an Aerodyne high resolution time-of-flight aerosol mass spectrometer (HR-ToF-AMS). Data from the high resolution time of flight aerosol mass spectrometer (HR-ToF-AMS) are analysed using high-resolution analysis fitting procedures. Unity collection efficiency is assumed since emitted particles likely consist of spherical oil-like droplets with low bounce. Figure 15 shows a typical organic concentration time series of one of these experiments. After an initial spike in OA concentration following sample injection, a time of at least twenty minutes was allowed for equilibration of the exhaust in the chamber. The concentration of OA after this point was taken as the initial primary organic aerosol (POA) emission. After background measurements through a filter with the AMS to correct for concentrations of gas phase species, four Xenon arc lamps, used in previous emission studies together with a battery of 80 100W UV black lights (ErgoLine "Cleo Performance", Solarium lights), were switched on to initiate photo-oxidation and secondary organic aerosol (SOA) formation. The first experiment (on 15.11.10) showed that SOA formation was sensitive to the presence of NO_x and subsequent experiments were carried out with a steady injection of NO (<20 ml min^{-1}) whereby NO_x was maintained at around 20 ppb. At the end of each experiment a second background measurement of the gas phase was taken with the AMS. Relative humidity inside the smog chamber was around 50% for all experiments, and temperature was maintained at 25 ℃.

During smog chamber experiments particles are lost to the walls due to diffusion and gravitational settling. Previous experiments have used black carbon (BC) as a tracer to correct for wall losses while assuming that the material on the walls is still able to participate in SOA formation through partitioning [5], using

$$\mathrm{OM}_{\mathrm{WLC}}(t) = \frac{\mathrm{OM}_{\mathrm{Meas}}(\mathrm{t})}{\exp(-kt)}, \qquad (12)$$

where OMWLC(t) and OMMeas(t) are the wall loss corrected and measured organic matter concentrations, respectively, as a function of time t, and k is the first order mass loss rate constant determined from an exponential fit of BC data. However, during these experiments on idling 2S scooters BC concentrations (measured using a Multi Angle Absorption Photometer, MAAP, Model 5012, Thermo) were below detection limits. Therefore we used the mass loss rate of the POA as measured by a scanning mobility particle sizer (SMPS) several minutes after filling in order to determine a first order wall loss correction (WLC). . The main advantage of the SMPS data over the AMS data on the primary aerosol is that the SMPS samples continuously from the chamber during this period whereas the AMS was switched to sampling air through a filter for gas phase corrections. The average particle half life was 4.2±0.5 h. For one experiment (on 17.11.10) a short half life of less than 2 hours was calculated. This short half life may have resulted from e.g. static charge on the chamber walls. For this experiment we apply the average WLC from the other experiments. To check the validity of the assumption that particles do not evaporate before lights on we measured the geometric mean diameter of the particles, also with the SMPS. In all cases there was no observable change.

Volatile organic compounds inside the smog chamber were quantified with a quadrupole proton transfer reaction mass spectrometer (PTR-MS), while carbon monoxide was quantified with a dedicated CO monitor (Aerolaser, CO-Monitor AL5002) and total gas-phase hydrocarbons were measured from the chamber using a flame ionization detector (FID, J.U.M model VE 7). Additional measurements at the tailpipe were performed by transferring emissions through a heated line (191 °C) to a Fourier transformed infrared spectrometer (FTIR, MKS Multigas analyzer 2030) for online measurements (at 1 Hz) of small hydrocarbons, nitrogen containing species (NO, NO_2, N_2O, NH_3 and HCN) and other oxygenated small organics (formaldehyde, acetaldehyde), as well as CO and CO_2.

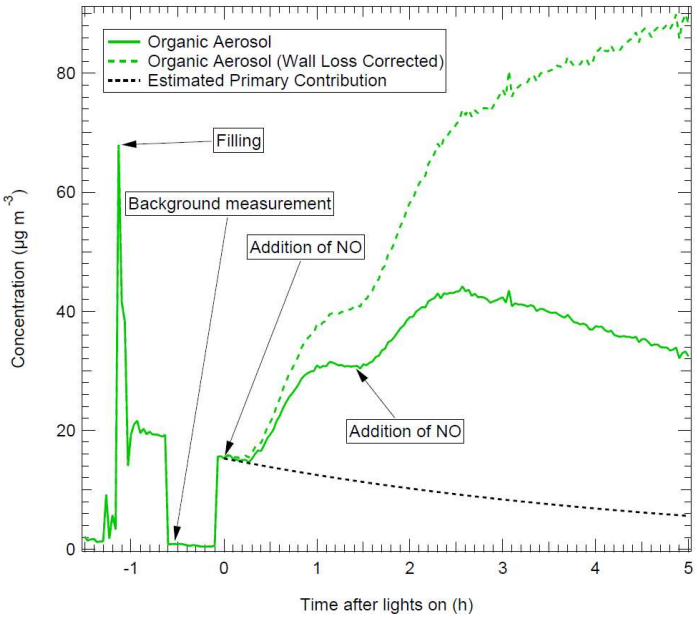

Figure 15: *Time series of a typical scooter smog chamber experiment (15.11.10). The green line indicates the concentration of organic aerosol in the smog chamber with respect to time after lights on as measured by the aerosol mass spectrometer. The dashed green line is the wall loss corrected aerosol mass concentration based on the loss rate of the primary organic aerosol (see text), shown in black.*

3.2.2 Smog chamber experiments on idling two stroke scooters

Figure 16 shows a schematic of the experimental online instrument used to measure the concentrations of reactive oxygen species (ROS). The same experimental design has previously been used in Taipei to study ROS in ambient aerosol.

Online particle bound ROS analysis utilised the fluorescence probe 2,7-dichlorofluorescein (DCFH) in solution. Particles were collected and continuously extracted on a wetted hydrophilic filter. The particle collector samples air at up to 5 litres per minute and collects particles larger than aerodynamic diameter 50 nm with greater than 95% efficiency. Particles are collected and extracted in an aqueous solution of horseradish peroxidase (HRP) (0.5 units per ml) allowing immediate reaction of ROS on collection. The concentration of ROS is characterised following subsequent reaction of the oxidised HRP with DCFH (5 µM) for 10 minutes at 40 ^{o}C, yielding the fluorescent product DCF in the continuous flow set-up. The concentration of DCF is measured using fluorescence spectroscopy in a flow-through cell and calibrated to ROS concentration with hydrogen peroxide. ROS data are normalised to the total carbon per m^3 (that is, moles hydrogen peroxide equivalent per mole aerosol carbon), determined from high resolution fitting of aerosol mass spectrometer data, and presented as a percentage.

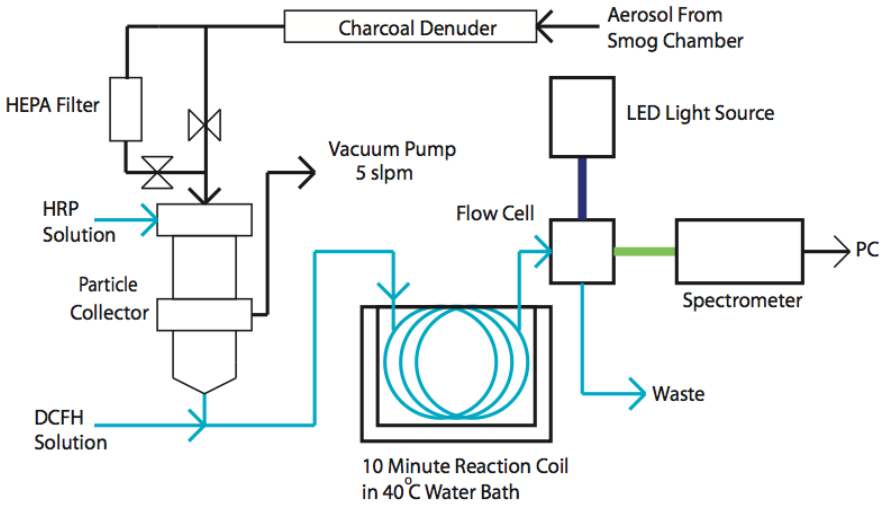

Figure 16: *A schematic of the online instrument used to measure particle bound reactive oxygen species (ROS) in aerosol from 2-stroke moped exhaust at the smog chamber.*

3.3 Results

3.3.1 Emission factors

Emissions factors (EF, g kg^{-1} fuel), shown in Fig. 17 and Table 7, were calculated using a carbon mass balance:

$$EF = \left(\frac{OC}{C_{CO2} + C_{CO} + C_{HC}} \right) \cdot W_C \,, \qquad (13)$$

where C denotes carbon mass, and the subscripts CO_2, CO, HC, carbon dioxide, carbon monoxide and hydrocarbon, respectively. W_c is the fuel carbon content (0.847 for gasoline).

For the idling scooter experiments C_{CO} and C_{CO2} were taken at the tailpipe using the FTIR. OC and C_{HC} were measured from the smog chamber and scaled up to the tailpipe concentration using the dilution ratio $CO_{tailpipe}/CO_{smog\ chamber}$. Meanwhile, for the driving cycles all concentrations were determined at the smog chamber.

Emission factors are given at known OH exposures, i.e. OH = $15 \cdot 10^6$ cm^{-3} h (equivalent to 15 hours in the atmosphere) for the idling and simulated low power 2S scooters. OH exposure (cm^{-3} h) was determined using the “OH clock” methodology of Barmet et al., (2012). Briefly, after allowing several minutes for equilibration and characterisation of the primary emissions, 1 µl (~20 ppbv) nine times deuterated butanol (butanol-D9, 98% Aldrich) was injected into the chamber. Since the reaction rate of butanol-D9 with OH, *k,* is known, the slope of its decay rate, measured with a quadrupole PTR-MS (idling 2S scooters) or PTR-ToF-MS (Ionicon Analytik, driving cycle 2S scooters) can be used to determine the OH concentration as a function of time *t*, [OH](*t*) , via:

$$[OH](t) = -\frac{slope(t)}{k} \,, \qquad (14)$$

For some of the idling scooter experiments butanol-D9 was not injected. In these cases the slope of the decay of toluene (present from the scooter emissions) together with its

reaction rate constant with OH were substituted in Eq. 14. Comparison between [OH] measured with toluene and with butanol-D9 (for the experiments where it was used) showed extremely good agreement over the first 5 hours, indicating that interference from other compounds at the same m/z was minimal [13].

The oxidation of VOCs in 2S scooter emissions produces significant SOA (g carbon (C) kg^{-1} fuel), exceeding, by up to a factor of 26, the POA emissions (Fig. 17, and Table 7). In addition, substantial toxic aromatic emissions (up to ~40% of emitted VOC volume) of benzene, toluene, and C2-C4-benzenes, which are recognised SOA precursors [14, 32], are present in the exhaust. Among the aromatics, benzene is of particular concern due to its carcinogenicity. Levels in the raw 2S scooter exhaust were as high as 300'000 µg m^{-3} or 146 ppm(v) from idling. The EU annual mean limit for benzene is 5 µg m^{-3} [35], while the US National Institute for Occupational Safety and Health (NIOSH) recommends that workers wear special breathing equipment when exposed to benzene at levels exceeding 1 ppm for 15 minutes. Waiting in traffic behind a 2S scooter, e.g. at junctions and while the scooter is idling, may therefore be highly deleterious to health. Figure 17 also shows POA, SOA, aromatic, and benzene emissions from a diesel-fuelled heavy duty and light duty vehicle [36], a four-stroke (4S) scooter and a gasoline light duty vehicle [34]. POA EFs are between 13.5 and 3500 times higher for 2S scooters than for other vehicles. Aged OA is in the range 3.4 to 186 times higher. It should be noted that absolute aerosol concentrations can influence these emission factors: higher measurement concentrations would lead to higher emission factors [3]. The lowest 2S scooter EF (3.4 times higher compared to gasoline car GLDV1) was measured at low concentration (~3 µg m^{-3}), therefore this EF may be underestimated by a factor of around 2.5 compared to the other EFs in Figure 17, measured at smog chamber suspended OA concentration of 50 µg m^{-3} or higher, according to the yield curve in Figure 18. SOA formation is most significant from idling scooter emissions, while smaller at higher engine loads. However, POA emissions are higher under the latter conditions, and the aggregate POA+SOA emission at high load is comparable to that from idling.

There are likely several reasons for these relatively large OA and aromatic emissions. Firstly, 2S engines, unlike 4S, require addition of lubricant oils to the fuel, some of which is emitted in the exhaust [37]. Secondly, during the 2S engine cycle some of the fresh fuel/air mixture passes directly through the engine, increasing VOC emissions, which may explain the high SOA formation. Thirdly, scooters generally utilise *rich combustion* (low air/ fuel ratio), improving drivability while producing higher CO, VOC and PM emissions (but lower NO_x). Accordingly, VOC emissions, in particular aromatics as found in raw gasoline, are also 16 to 390 times higher compared to those from other vehicles. Finally, scooter after-treatment systems are inherently inefficient due to their relatively small size and longer light-off times.

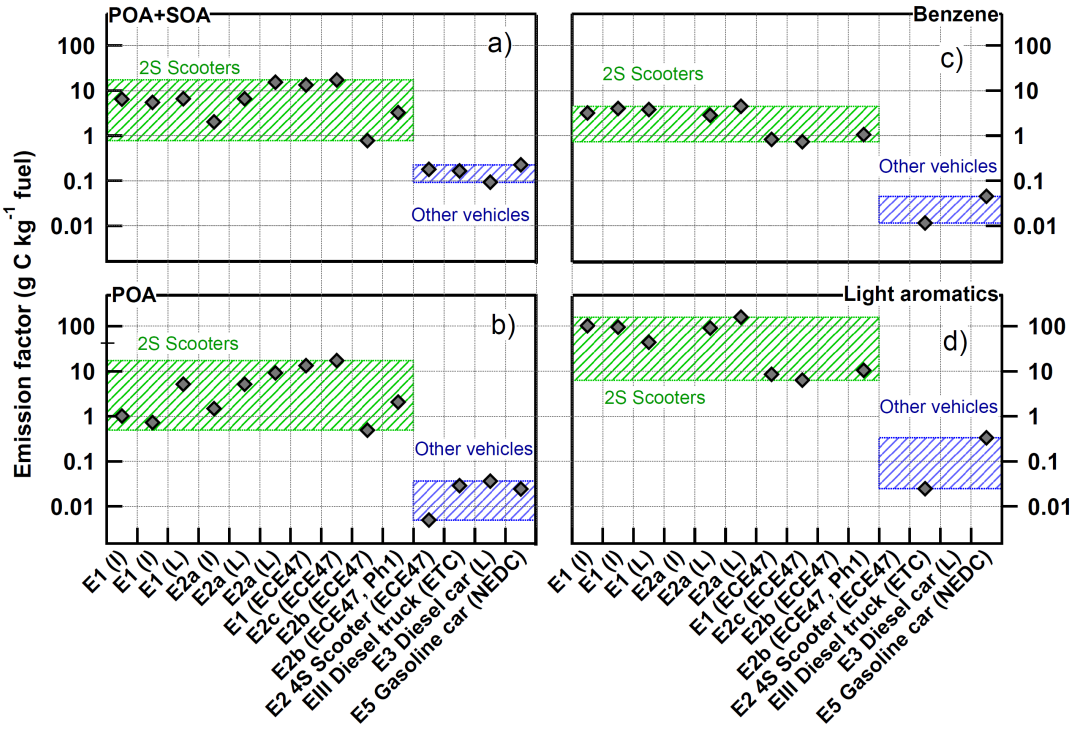

Figure 17: *Emission factors from two-stroke scooters and other vehicles Emission factors (EF) of a) aged OA (POA+SOA), b) POA, c) benzene, and d) light aromatics, for the Euro 1 (E1), and three Euro 2 (E2a, E2b, E2c Chirico et al., (in Prep)) 2S scooters. EFs from other vehicles are shown: a Euro III truck (EIII HDDV (Chirico et al., in Prep)), a Euro 2 4S-scooter, a Euro 3 diesel car (Chirico et al., 2010) and a Euro 5 gasoline car (Platt et al., 2012). Operating conditions given in parentheses: I= idle, L=simulated low power, ECE47, NEDC, and ETC are regulatory driving cycles for scooters, passenger cars, and trucks, respectively. Scooter idling and low power EFs are at OH=15·10^6 cm^{-3} h. EFs for scooter E2b are given at OH=1.5-3·10^6 cm^{-3} h, while for the Euro 5 gasoline car the SOA potential EF is at OH=12·10^6 cm^{-3} h). For the diesel car SOA was quantified during a study at unknown OH exposure (Chirico et al., 2010). Shaded regions show the range of EFs from all tests on 2S scooters (green) and other vehicles (blue).*

3.3.2 Secondary organic aerosol yields

A secondary organic aerosol (SOA) yield *y* is defined as:

$$y = \frac{\Delta C_{OA}}{\Delta VOC}, \qquad (15)$$

Where ΔC_{OA} is the organic aerosol production for a given change in volatile organic compound concentration ΔVOC. The SOA yields for an individual aromatic *compound i* as a function of aerosol loading may be estimated using *two-product fits* which assume that SOA partitioning behaviour of reacted products may be approximated by two products, *1* and *2* :

$$y_i = \Delta C_{OA} \cdot \left[\frac{\alpha_1 k_{om,1}}{1 + k_{om,1} \cdot C_{OA}} + \frac{\alpha_2 k_{om,2}}{1 + k_{om,2} \cdot C_{OA}} \right], \qquad (16)$$

Where C_{OA} is the organic aerosol loading (POA+SOA), measured using a high resolution time of flight mass spectrometer, and α_i and $k_{om,i}$ are the mass fraction and partitioning coefficients of gas phase species *i*, respectively. Using literature values of α_i and *kom,i* for aromatic hydrocarbons [32] a concentration-weighted predicted yield $y_{predicted}$ is calculated for the oxidation of aromatics in 2S scooter exhaust using:

$$y_{predicted} = \frac{\sum_i (y_i \cdot \Delta i)}{\sum_i \Delta i} \quad (17)$$

SOA yields from the literature for high NO_X conditions were used to calculate a predicted yield $y_{predicted}$ from the decay of aromatic hydrocarbons (benzene, toluene, xylenes, ethyl benzene, and C9 aromatics), measured with a proton transfer reaction mass spectrometer (PTRMS) from the smog chamber. $y_{predicted}$ is then compared with the apparent yield $y_{apparent}$:

$$y_{apparent} = C_{SOA} / \sum_i \Delta_i \quad (18)$$

Apparent yields closely match average concentration-weighted literature aromatic SOA yields [32] for idling, complete ECE47 driving cycles, and ECE47 phase one (Ph1), indicating that almost all SOA is from aromatic precursors (Figure 18a). SOA from ECE47 phase two (Ph2) alone is underestimated by Eq. 18, suggesting SOA production from unidentified compounds, emitted by the hot engine. Note that the total emission during a full cycle is dominated by Ph1, i.e. by cold engine emissions. Furthermore, a *Van Krevelen diagram* illustrates the aging of 2S scooter emissions, from oxygen O:C~0 to O:C~0.6. This elemental composition is consistent with that of previously observed SOA from aromatic precursors [38] (Figure 18b). We therefore conclude that SOA formation from 2S scooter emissions is likely from the oxidation of aromatics, in contrast to diesel SOA, which is predominantly from other precursors [3].

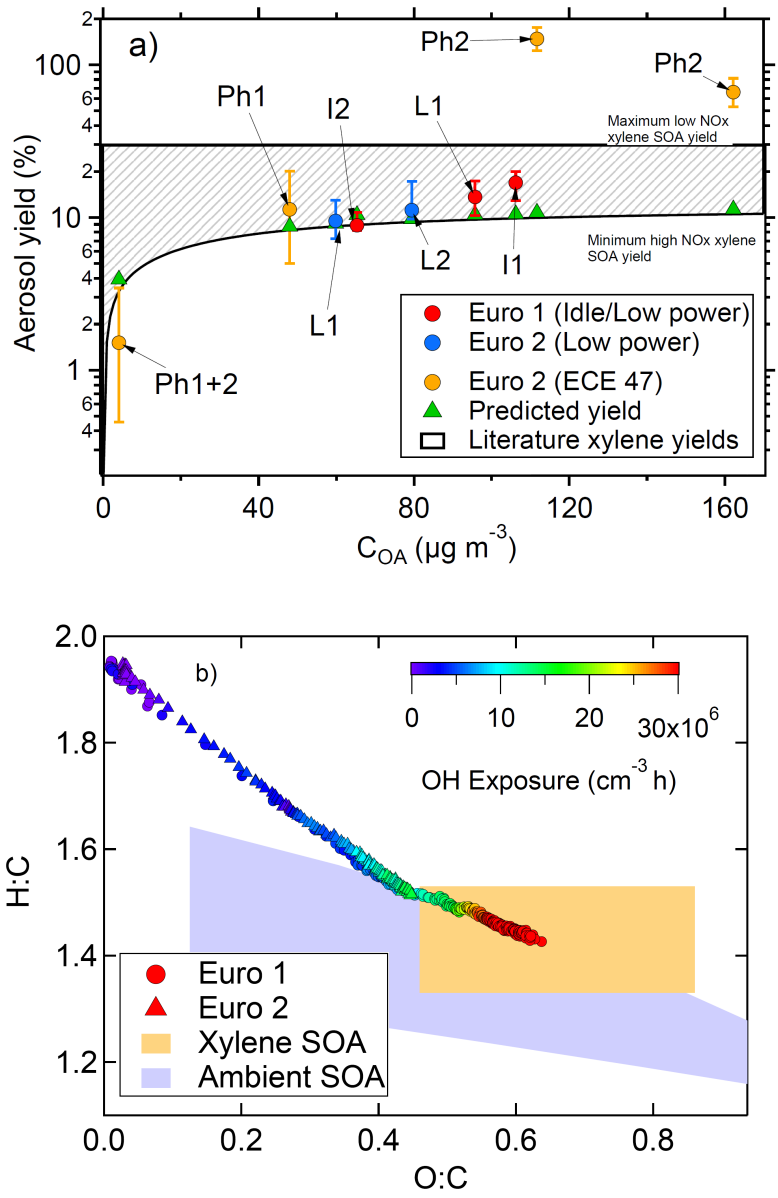

Figure 18: *a) Apparent SOA mass yields, calculated assuming that only light aromatic hydrocarbon oxidation contributes to the SOA (Eq. 1), as a function of suspended OA mass (C_{OA}). Error bars show the sensitivity of the apparent yield to the chamber wall loss factor, with higher and lower bars representing ± one standard deviation, respectively. Apparent yields for Euro 1 and 2 2S scooters E1a and E2a are shown in red and blue, respectively. Orange data points show the same calculation from aged emissions of a second E2 2S scooter (E2b) generated during driving cycles (ECE47) on a chassis dynamometer. Ph 1 and Ph 2 refer to the first and second phase of the ECE47, respectively. A predicted yield, for the mixture of all aromatics, for each experiment using two-product yield curves from Ng. et al., 2007 is shown (green triangles). The range of SOA yields for xylene, which are close to the aggregate predicted yield for all aromatics, combined are indicated by the shaded region. b) Elemental ratios of OA emissions from a Euro 1 (E1L1) scooter and a Euro 2 (E2aI1) as a function of photochemical age. Elemental ratios observed for xylene SOA [38] and for ambient SOA are shown, orange and purple, respectively.*

3.3.3 Contribution of two-stroke scooters to ambient air pollution

The results in Fig. 17 suggest that 2S scooters are 'asymmetric' polluters of OA and aromatics compared to other vehicles. Up to ~10% of all fuel for road transport in Asian urban areas e.g. Bangkok, Thailand, is consumed by 2S scooters (Fig. 19). Precise estimation of a relative contribution from 2S scooters is difficult since vehicle emissions controls vary on a country to country basis. However, taking the lower range limit from Fig 17, POA emissions would suggest relative contributions to roadside POA mass from 2S scooters of 60 to up to over 97% in the most extreme case. Aged OA would vary from 27 to 86% of tailpipe vehicular emissions.

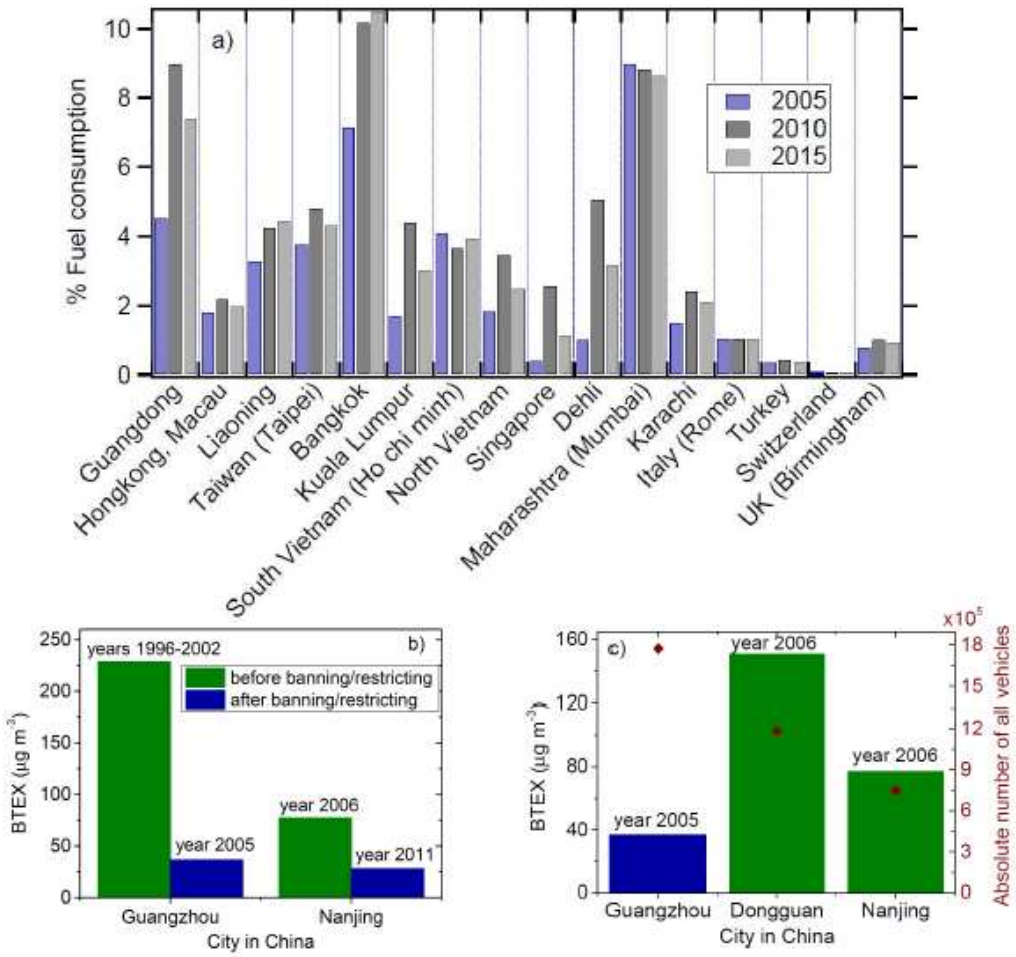

Figure 19: *Ambient and model data on two-stroke scooters a) Share of total fuel consumption by 2S in 2005, 2010 and 2015 from the Greenhouse gas Air pollution Interactions and Synergies, GAINS, model[39]. b) Roadside benzene, toluene, ethyl-benzene, and xylene (BTEX) before and after banning/ restricting 2S scooters in two Chinese cities, and c) roadside BTEX and number of vehicles in three Chinese cities. It must be noted that concentrations were measured at different time periods, and this effect is not accounted for.*

Furthermore, significantly elevated roadside concentrations of benzene, toluene, and C2-benzenes: ethylbenzene and xylene (BTEX) have been reported in Asian cities with large 2S scooter fleets, while concentrations in cities with large gasoline fleets but small

scooter fleets are much lower (Table 8). These field observations demonstrate our findings that 2S scooters are dominant polluters of aromatics. For China, vehicular aromatic emission correlates markedly stronger with 2S scooter fuel consumption (<13 % of total) than with fuel use by all vehicles combined, Fig. 20.

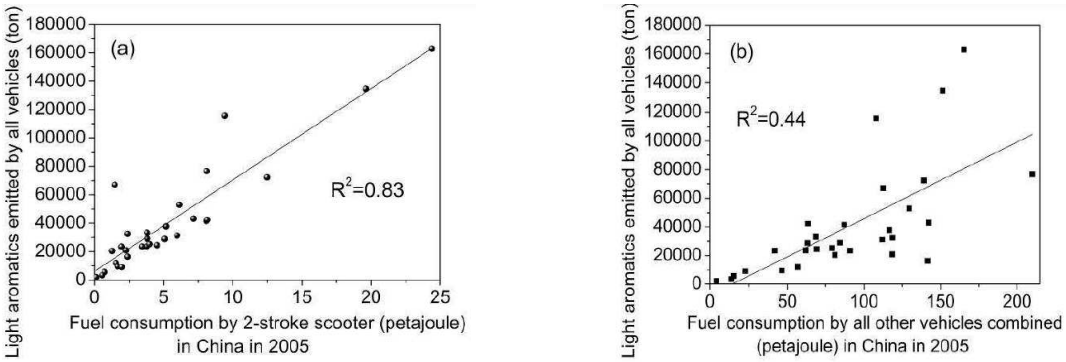

Figure 20: *On-road vehicle emissions of light aromatic compounds as a function of fuel consumption. Each data point in (a) and (b) represents the case of a province/municipality of China in 2005. The emission inventories of aromatics are provided by [40], and fuel consumption by different vehicle categories is calculated using the GAINS model [39] using International Energy Agency World Energy Outlook data on fuel sales. Note that the fuel consumed by 2-stroke scooters is only a small proportion (1-13%) of all fuel consumption. However, the total vehicle emissions of light aromatics correlate positively with fuel consumption by 2-stroke scooters (a) instead of with all other vehicles combined (b), indicating that 2-stroke scooters are the major contributors to traffic-related aromatic compounds emissions.*

Across the EU, 2S scooters consume an average of only 0.3 % of total fuel. This is close to the average in Switzerland, around 0.5%. However, our numbers suggest that reducing the numbers of these vehicles in operation would offer a cost effective way of mitigating vehicle OA and aromatic emissions, especially given the alternatives available (electric and 4S). In this regard China has taken the lead, banning or restricting motorbikes in many cities since the late 1990s [41]. This has led to a striking decrease in the traffic-related aromatic emissions in many Chinese cities. For example, the roadside BTEX concentrations decreased from 229 µg m-3 to 37 µg m-3 in Guangzhou and from 77 µg m-3 to 28 µg m-3 in Nanjing, respectively, after banning/restricting scooters (Fig. 19). Another complication in estimating relative contributions arises from the possibility of large contributions to OA from a small number of super-polluting vehicles (of all types). However, many scooters will likely fall into this super-polluting category, especially as a considerable number of scooters are in operation in some regions without any form of emissions control (scooters presented in this study are equipped with oxidation catalysts) and because emissions may be further exacerbated by poor maintenance and tampering, which is rife for scooters [42].

Table 8: *Roadside benzene, toluene, ethylbenzene and xylene (BTEX) concentrations in different cities (µg m^{-3})*

City	Time	Benzene	Toluene	Ethylbenzene	Xylene	Ref.
Guangzhou, China	Oct and Nov 1996	51.5	77.3	17.8	82.1	(Wang et al., 2002)
Guangzhou, China	Sep 2000	47.9	75.3	15.2	106.3	(Chan et al., 2002)
Guangzhou, China	Feb and Aug 2000	61.6	103.9	15.4	109.8	(Tang et al., 2008)
Guangzhou, China	Feb 2002	34.6	56.2	11.4	48.2	(Zhao et al., 2004)
Guangzhou, China	Sep 2005	6.6	15.1	4.0	11.1	(Tang et al., 2007)
Dongguan, China	Jan 2006	12.3	76.0	14.6	48.0	(Tang et al., 2007)
Macau	Nov 1995	34.9	85.9	24.1	95.6	(Wang et al., 2002)
Hong Kong	Jan and Feb 1998	24.9	68.9	2.5	14.5	(Chan et al., 2002)
Nanjing, China	April 2006 – Jan 2007	15.8	38.2	7.0	16.3	(Wang and Zhao, 2008)
Nanjing, China	Aug 2011	5.6	10.6	4.0	7.8	(Lan and Binh, 2012)
Changchun, China	Sep 1997 – Jul 1998	38.5	80.2	18.8	23.4	(Liu et al., 2000)
Taipei, Taiwan	Spring 1992	371.0	849.0	189.0	606.0	(Chan et al., 1994)
Taichung, Taiwan	1998	145.0	442.0	74.0	198.0	(Kuo et al., 2000)
Kyoto, Japan	May 2011	2.3	12.2	2.8	3.7	(Lan and Binh, 2012)
Osaka, Japan	May 2011	2.1	11.8	2.1	5.9	(Lan and Binh, 2012)
Bangkok, Thailand	Sep 2003	/	246.7	/	106.3	(Kim Oanh et al., 2008)
Kuala Lumpur, Malaysia	Aug 2011	48.0	105.6	15.8	82.6	(Lan and Binh, 2012)
HoChiMinh, Vietnam	Oct – Dec 2009	93.5	208.5	33.8	200.4	(Lan and Minh, 2013)
HoChiMinh, Vietnam	Oct 2011	87.0	200.1	39.2	150.9	(Lan and Binh, 2012)
Hanoi, Vietnam	Dec 2011	52.0	88.4	23.4	84.0	(Lan and Binh, 2012)
Singapore	May 2011	6.9	42.8	5.2	14.0	(Lan and Binh, 2012)
Delhi, India	Oct 2001 – Sep 2002	103.5	185.5	22.5	127.0	(Hoque et al., 2008)
Delhi, India	Jan – Dec 2001	358.5	74.8	31.3	37.6	(Srivastava, 2005)
Mumbai, India	May 2001 – April 2002	237.8	216.0	1.7	0.7	(Srivastava et al., 2006)
Karachi, Pakistan	Dec 1998 – Jan 1999	93.9	246.9	/	249.0	(Barletta et al., 2002)
Rome, Italy	Jan, May, July, Oct 2000	6.2	44.1	8.2	41.4	(Fuselli et al., 2001)
Izmir, Turkey	Aug – Sep 1998	46.3	102.8	29.3	177.1	(Muezzinoglu et al., 2001)
Zurich, Switzerland	Oct 1993	6.0	/	/	7.4	(Monn and Hangartner, 1996)
London, UK	July 1991 – June 1992	15.6	25.8	4.2	18.7	(Derwent, 1995)
London, UK	Jan – Dec 1996	6.0	13.6	3.2	12.8	(Derwent et al., 2000)
Birmingham, UK	2005 – 2006 (13 months)	2.0	9.5	1.7	5.4	(Vardoulakis et al., 2011)

3.3.4 Reactive oxygen species in scooter exhaust

We also examined the health implications of the 2S scooter SOA (other than those from the mass increase) using online measurements of particle-bound, water soluble reactive oxygen species (ROS, see Sect. 3.2.2), which are linked to negative health effects [43]. ROS is undetectable in POA, but accounts for 0.5-1% carbon in the aged OA, suggesting

that PM emissions initially become increasingly toxic with aging (Figure 21). Increasing ROS is consistent with the higher O:C ratio of the aerosol and in line with a previous study showing increased oxidative potential with aging for 2S scooter emissions, albeit at aerosol and oxidant loadings much higher than under ambient conditions [43]. After 1-2 hours of irradiation ROS stabilises or decreases, as reported previously for organic peroxides, likely due to decomposition processes [44, 45].

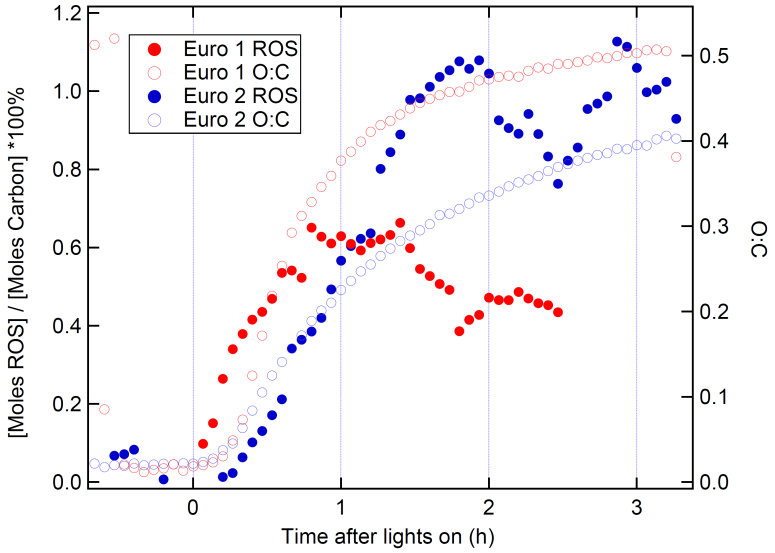

Figure 21: *Percentage of water soluble reactive oxygen species (ROS) and elemental O:C ratios of organic aerosol as a function of time after lights on in the smog chamber from Euro 1 (red) and Euro 2 (blue) two-stroke scooter exhaust emissions. ROS concentration measured in moles hydrogen peroxide equivalents is normalised to the molar organic carbon concentration per m^3 inside the smog chamber to give a percentage.*

4 Effect of alkylated fuels on emissions from two- and four-stroke scooters

4.1 Introduction

Due to their agility in traffic, low price, low maintenance costs, and ease of parking Powered Two Wheelers (PTWs: mopeds and scooters with engine displacement ≤ 50 cc, and motorcycles) are a practical and convenient means of transport, especially in urban environments at temperate latitudes. In Europe (EU27) for instance the number of circulating PTWs has increased from about 31.3 millions up to 37.4 millions from 2003 to 2011 [46]. PTWs are popular in urban areas where the majority of the population lives, which amplifies their negative impact on human health [47]. They are known to be strong emitters of pollutants because of their simple engine and after treatment technology resulting in a partially unburned exhaust, and in the case of 2-strokers also because of the use of lube oil mixed with the fuel [37, 48, 49]. Their typical use is for short distances and therefore at cold engine conditions, with consequently large emissions. In addition, information in the scientific literature about PTWs is scarce compared to passenger cars and no research about secondary organic aerosol

particles (SOA) from PTWs has been reported so far. SOA, formed in the atmosphere through the photochemical oxidation of volatile organic compounds and consequent gas to particle conversion, represents a significant fraction of the ambient tropospheric aerosol [50]. A number of recent studies elucidated their physico-chemical properties necessary to evaluate the impact on air pollution, climate and human health. Nevertheless, significant gaps persist in our understanding of SOA formation and sources [8]. Specifically for the air quality field, the question arises as to whether limitations on primary particle emissions from internal combustion engines are sufficient to control the ambient particle mass and number concentrations. Evidently this is not the case if vehicles are important SOA sources. For these reasons we measured regulated and unregulated primary emissions and for the first time quantified SOA formation from a 2-stroke and a 4-stroke scooter during legislated driving cycles in a chassis dynamometer test cell using the mobile smog chamber (See Sect. 2 for details). Moreover since aromatic compounds in fuels are known to be important SOA precursors [14], we also compared emissions from scooters fuelled with standard petrol and oil against the use of a reformulated alkylate fuel (almost free of aromatic compounds) and synthetic lube oil with low ash forming potential (ultra-clean oil, hereafter). These fuels are designed to produce cleaner emissions, hence reducing health risks and increase engine lifetime.

4.2 Methodology

The generalised procedure for smog chamber experiments is described in Sect. 2. Specific vehicle emissions laboratory procedures as pertaining to the scooter alkylate study are outlined in this section. Experiments were conducted in a certified chassis dynamometer test cell (Vehicle Emissions Laboratories, Joint Research Centre of the European Commission, JRC-Ispra, Italy) combined with the mobile smog chamber (see Sect 2). The scooter-specific set up is illustrated in Fig. 22. Instruments and methods deployed to characterize primary emissions are listed in Table 9. For these experiments we used two marketable and quite recent scooters (registration in 2010), one 2-stroker and one 4-stroker (2S and 4S, respectively, when abbreviated in Figures and Tables), both equipped with a 2-way-catalyst (for hydrocarbon and carbon monoxide reduction) as an example of the circulating European fleet. The scooters' characteristics are summarized in Table 10.

The legislated ECE-47 driving cycle (Dir.97/24/EC, 1997) was run on a chassis dynamometer (Roller bench 48; AVL Zoellner GmbH, Germany) combined with a constant volume sampler (CVS) critical flow venturi dilution tunnel system (typical average dilution ≈ 27; typical dilution tunnel flow ≈ 5 m^3 /min). It consists of 8 modules of

sharp accelerations up to a brief constant speed of 50 km/h and decelerations down to 0 km/h, see Fig. 23, dashed black curve. Depending on the country of vehicle registration, maximum speed can be limited to values lower than 50 km/h. In this study, a maximum speed of 45 km/h was reached as prescribed by the Italian legislation (actual speed, shaded grey area in Fig. 23). For legislative purposes, only the last 4 modules of the driving cycle, commonly referred to as the second phase, or hot phase (Ph2, hereafter when abbreviated) are considered. In our analysis also the first 4 modules (the first phase, Ph1, or cold phase, hereafter) were included, since this is more representative of real-world driving, where engines are often started cold. Scooters were fuelled either with certified reference fuel (European Emission Certification Fuel - CEC RF-02-99) and synthetic oil (API TC, Jaso FC, ISO-LEGD, 2% vol in the 2-stroker only) or with alkylate fuel (Lantmannen Aspen Petroleum AB) and ultra-clean oil (Stihl HP Ultra, 2% vol in the 2-stroker only). A comparison of basic fuels properties is given in Table 11; the fuel and oil analysis were performed on purpose for our study and independently by a specialised lab, following UNI-EN/ASTM methodologies. The alkylate fuel is rich in short chain single-bond hydrocarbons and has a low content of alkenes, oxygenates and aromatic compounds. Alkylate fuels are commonly used by professionals in hand held machinery (gardening, for instance) and are normally not available at petrol stations for on-road vehicles. Due to their cleaner formulation, in particular their low aromatic content, they are good candidates for experimental studies on secondary organic aerosol and in general on organic compounds from internal combustion engines. We ran a total of 15 experiments (see Table 2) at stable, controlled conditions of temperature, 19.1-21.3℃, and relative humidity, 55-65% RH inside the test cell. For sake of reproducibility, all tests started at well defined cold engine conditions after a soak time of several hours (≈ 24h) at constant T ≈ 21◦C in the test cell, thus allowing the initial engine oil temperature (measured with thermocouples inside the engine) to differ less than 1℃ from the test cell temperature.

Table 9: *Vehicle emission laboratory (VELA) Instruments and methods. Tailpipe (TP) measurements are online at 1Hz; Constant volume sampler (CVS) measurements are sampled in Tedlar bags and analysed offline, integrated over the entire driving cycle and separately over the cold and hot phases.* [1]*Non–dispersive Infrared;* [2]*Chemiluminescence Detector;* [3]*Flame Ionisation Detector;* [4]*Gas Chromatography;* [5] *Fourier Transform Infrared Spectroscopy.*

Compound/ Property	Sampling location	Technique	Model
CO, CO_2	TP, CVS	NDIR[1]	Advance Optima, ABB (TP); AMA i60, AVL (CVS)
NOx	TP, CVS	CLD[2]	As above
THC	TP, CVS	FID[3]	As above
VOCs	CVS	GC-FID[4]	Agilent 6890
Small HC, N-species	TP	FTIR[5]	MKS 2030HS

Table 10: *Technical details of the scooters used to investigate the effect of alkylated fuels*

Vehicle type	Technology	Engine displacement	Power	Mileage	Year
2-stroke (2S)	Carburetor 2-way oxy cat	49.4 cc	3.2 kW at 7500 rpm	1700	2010
4-stroke (4S)	Carburetor 2-way oxy cat	49.9 cc	3.4 kW at 7250 rpm	2500	2010

Table 11: *Fuel properties from independent and certified ISO/ISO-EN/ASTM analysis performed by an external, specialized lab.*

Property/ Compound	Standard fuel	Alkylate fuel	Unit
Aromatics	29.6	<0.4	%vol
Alkenes	4.2	0.1	%vol
Alkanes	61.3	>99.6	%vol
Oxygenates	4.9	<0.1	%vol
Benzene	0.2	<0.01	%vol
H-content	13.16	15.5	%wt
C-content	85.95	84.5	%wt
O-content	0.9	<0.1	%wt
Density (15 C°)	759.2	692.4	kg/m^3

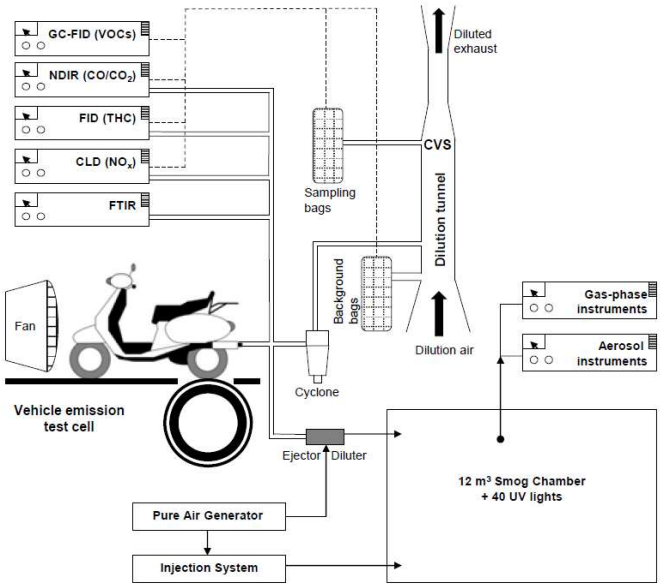

Figure 22: *Schematic of the test facility and instrumentation. The scooter exhaust is collected at the tailpipe and transferred via heated lines (190◦ C) to online instrumentation (FID, NDIR, CLD, FTIR - see Table 1). The exhaust is also directed to a dilution tunnel as required by the legislation for subsequent offline analysis (dashed lines). Part of the exhaust is injected in the 12 m^3 smog chamber for secondary aerosol formation.*

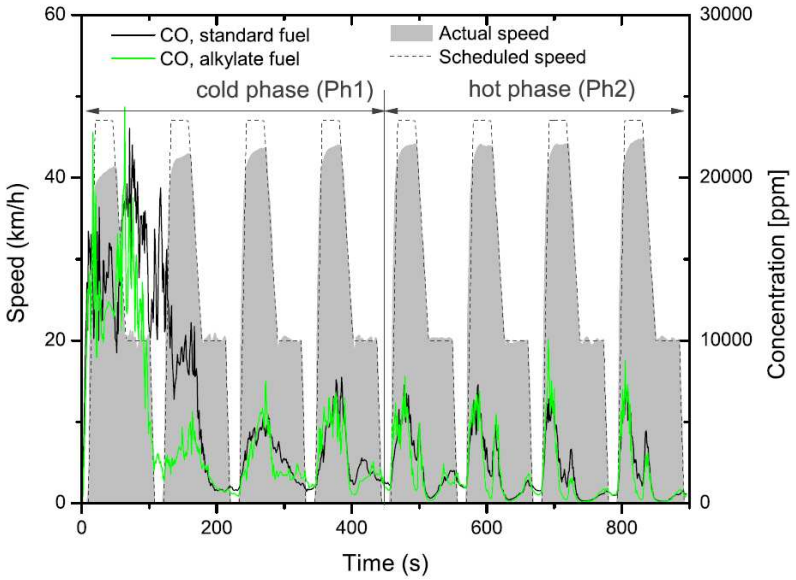

Figure 23: *Averaged tailpipe CO concentration measured at the tailpipe with FTIR for the 2-stroke scooter with standard fuel (black curve) and alkylate fuel (green curve) during an ECE-47 driving cycle. Theoretical speed (dashed black curve) reaches higher peaks than actual speed (gray shaded area) because of speed limitations enforced by legislation of the country of vehicle registration (Italy). CO emissions are largest in the first two modules of the cycle with standard fuel, followed by a repetitive pattern for the rest of the cycle. Alkylate fuel tests exhibit lower emissions especially in the cold phase. Note that only the hot phase is considered for type approval tests.*

4.2.1 Tailpipe and CVS measurements

In most countries worldwide, vehicles have to comply with emission standards that traditionally include total hydrocarbons (THC), carbon monoxide (CO), nitrogen oxides (NOx), particulate mass (PM) and carbon dioxide (CO_2). We refer to them as regulated compounds hereafter, even though CO_2 is not regulated by EU legislation for type approval emission tests. Instead, manufacturers are obliged to ensure that their entire light duty vehicle fleet does not emit more than an average of 130 g/km of CO_2 by 2015 and 95 g/km by 2020. No CO_2 limits are envisaged for PTWs. In particular, Euro 2 scooters have limits only on THC+NOx (1.2 g/km) and CO (1 g/km) considered only over the second half of the driving cycle (hot phase, see also Table 5). Gaseous emissions were analysed in accordance with Directive Dir.70/220/EEC (1970): Tedlar bags (3 bags per test, one for the first phase, one for the second phase and one for the entire cycle) were filled with diluted exhaust from the CVS

(Automatic Bag Sampler, CGM electronics) and CO, THC, NOx, and CO_2 concentrations were measured with the techniques summarized in Table 9 by an integrated measurement system (AMA i60 Exhaust Measurement System, AVL). The same compounds were also measured online (at 1Hz) at the scooter tailpipe (via a heated transfer line at T = 191 ℃ to ABB Advance Optima Modular Analyzers). CO_2 signals comparison allows the estimation of the tailpipe exhaust volumetric flow rate by the CO_2 tracer method (see for instance Clairotte et al., 2012 [12]). In addition, a heated line (191 ℃) conveyed tailpipe emissions to a Fourier Transform Infrared Spectrometer (FTIR, MKS Multigas analyzer 2030–HS) for online measurements (at 1 Hz) of short chain hydrocarbons, nitrogen containing species (NO, NO_2, N_2, O_2, NH_3 and HCN) and other

oxygenated organics (e.g., formaldehyde, acetaldehyde). CVS diluted emissions were also collected in Tedlar bags for offline analysis with dual flame gas chromatography (GC-FID, Agilent 6890 with Markes Unity 2 desorber). We applied to vehicle emissions the procedure for ambient air GC-FID analysis described in detail in Latella et al. (2005) for the quantification of the 29 volatile organic compounds (VOCs) listed as the main ozone precursors in the European Directive on tropospheric ozone (Dir.2002/3/EC, 2002).

4.3 Results and discussion

4.3.1 Regulated compounds

Figure 23 shows the time resolved tailpipe CO concentration for the 2-stroker measured with FTIR and averaged over all tests, during the ECE-47 legislated driving cycle, which is split at t = 448 s into a first, cold phase and a second, hot phase. The CO concentration is higher in the first two modules of the cycle when the engine is colder and combustion is incomplete. Tests with alkylate fuel and ultra-clean oil combination (green curve) exhibit lower concentrations than standard fuel tests for t =0−200 s. Differences become smaller and signals tend to overlap for t ≥ 200 s. A sudden drop is visible at t ≈ 100 s when using the alkylate fuel, indicating cleaner combustion and/or better efficiency of the 2-way catalyst. Note that by only sampling the hot phase, as prescribed by the legislation, the CO reduction in the cold phase would not be considered. Results for regulated compounds measured with prescribed methods are displayed as emission factors (mass/distance) in Fig. 24 and included in the summary Table 13. The 2-stroker emits much more CO, THC and PM than the 4-stroker, especially during the cold phase where combustion is less efficient. It emits about twice as much CO as the Euro 2 scooter studied in Clairotte et al., (2011) [12] and up to 5 times more than the Euro 5 car in Platt et al. (2012) [34].

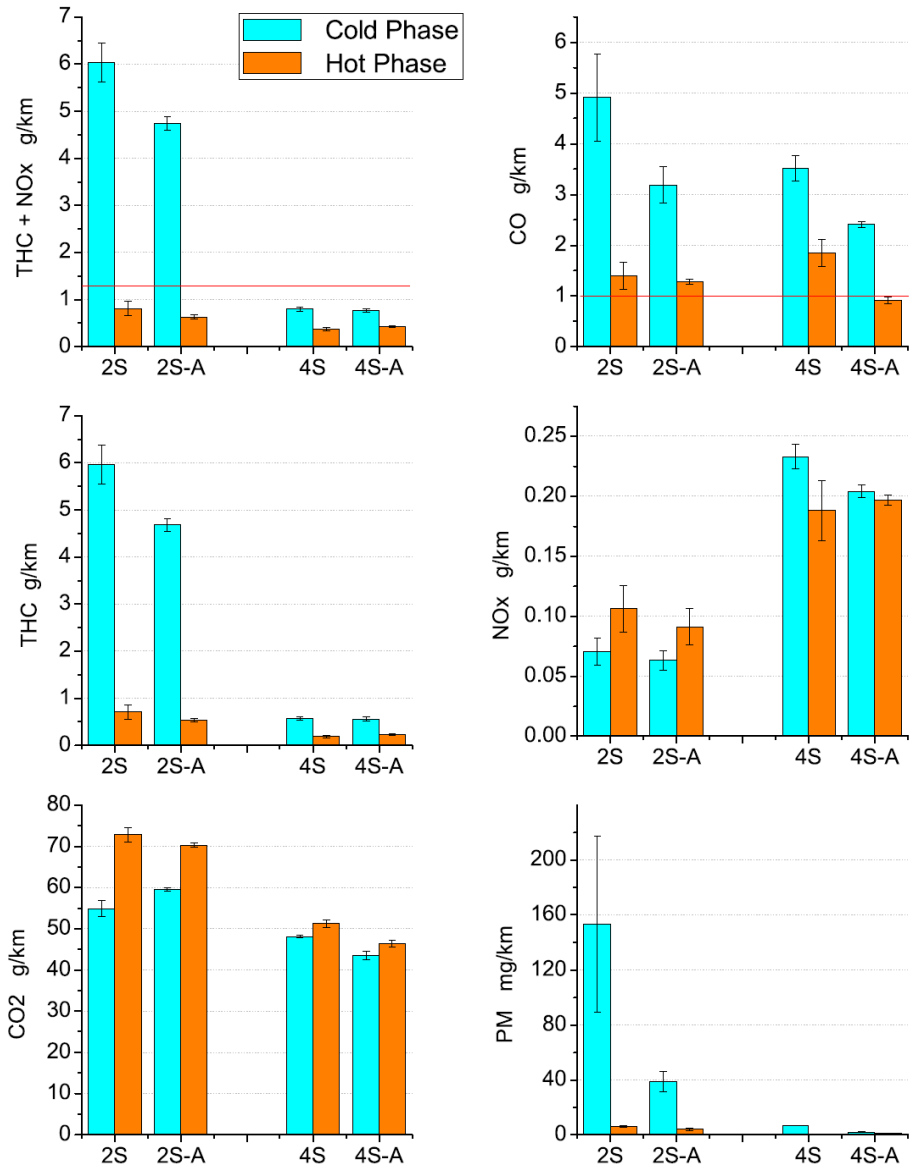

Figure 24: *Average emission factors (mass/distance) of regulated compounds grouped by scooter and fuel types, and split into cycle phases. The 2-stroker (2S) emits more THC, CO, and PM (dominated by cold phase emissions) than the 4-stroker (4S). The use of the alkylate fuel reduces THC, CO, PM and NOx of the 2S (2S-A, where A stands for alkylate) and CO, PM, NOx of the 4S (see text for details). THC+NOx and CO are limited by EU legislation at 1.2 g/km and 1 g/km, respectively (red horizontal line in the uppermost panels, see text for details). All values are summarized in Table 13 Error bars are explained in Table 12.*

Table 12: *Number of tests (N) grouped by vehicle, fuel and test type. Results for regulated and unregulated compounds are based on N and N(FTIR) tests, respectively, while SOA results are based on N(SOA) tests. The error analysis hereafter reports 1σ when test number is N>2; half of the minimum-to-maximum range when N=2. Notation: 2S-A and 4S-A refer to the 2- and 4-stroker fuelled with alkylate fuel.*

Test type	Analysis		
	N	N(FTIR)	N(SOA)
2S Ph1+Ph2	7	7	2
2S-A Ph1+Ph2	3	3	2
4S Ph1+Ph2	3	3	2
4S-A Ph1+Ph2	2	1	2
2S Ph2	(7)	(7)	2
2S-A Ph2	(3)	(3)	2

The 4-stroker emits ≈ 30% less CO than the 2-stroker, mainly because of more complete combustion. In particular, the scooters in our study slightly exceeded Euro 2 CO standards (uppermost right panel in Fig. 24), most likely because of normal emission degradation due to vehicle use. In fact, emission standards are set for the registration of a prototype vehicle, and in-use vehicles do not have necessarily to comply with them. Instead, the scooters must pass a less severe periodical inspection of the tailpipe exhaust, (due by law in 2014, in our case), with a warm engine CO limit of 3.5% vol.

For example, in our study [CO] ≤ 1% vol, see Figure 23. NO_X emissions, which are mainly thermally produced at high temperature from the nitrogen and oxygen in the combustion air, have a more levelled temporal profile (not shown here), or even opposite behaviour compared to CO, with larger amounts in the hot phase. The 2-stroker, due to its simpler engine technology and generally colder engine temperature, features less NO_X than the 4-stroker. Note that a 2-way catalyst does not act to reduce NO_X emissions, but only those of CO and THC. This contributed to the two orders of magnitude difference between the 2-stroker NO_X emission factor and that of the modern car in Platt et al. (2012) [34] in hot engine conditions (≈ 0.1 g/km vs. ≈ 0.002 g/km), when the car could benefit from the light-off of a 3-way catalyst (which acts also on NO_X). The use of the alkylate fuel and ultra-clean oil combination is clearly beneficial for compounds emitted mainly in the cold phase: THC, CO and PM. The effect is important for CO and PM (e.g., up to 35% and 75% reduction of CO and PM, see Table 6) and less pronounced for THC and in general in the hot phase. PM reduction is one of the main reasons for using ultra-clean lubricant oil in professional 2-stroke machinery where the presence of unburned lube oil droplets in the exhaust and generally colder exhaust temperature facilitate condensation of gaseous compounds on primary particles. A certified analysis of the 2-stroke lube oils used in this study commissioned to an in dependent, external lab reports ash-forming material = 0.005% mass/mass for the ultra-clean oil against 0.1 % mass/mass for the standard

***Table 13**: Summary of emission factors. Errors in parenthesis are 1σ or half of the minimum-to-maximum range based on the number of tests in Table 12. NA: not available; nd: not determinable because below detection limit.*

Compound	Method	2S-Ph1	2S-Ph2	2S-A-Ph1	2S-A-Ph2	4S-Ph1	4S-Ph2	4S-A-Ph1	4S-A-Ph2
Regulated (g/km)									
CO	NDIR	4.92(0.86)	1.40(0.27)	3.19(0.36)	1.29(0.06)	3.52(0.25)	1.84(0.27)	2.41(0.06)	0.91(0.06)
CO Euro2 limit	NDIR	–	1	–	1	–	1	–	1
NOx	CLD	0.07(0.01)	0.11(0.02)	0.60(0.01)	0.09(0.01)	0.23(0.01)	0.19(0.02)	0.20(0.01)	0.20(0.01)
THC	FID	5.96(0.40)	0.71(0.15)	4.68(0.13)	0.54(0.04)	0.56(0.04)	0.19(0.02)	0.56(0.04)	0.22(0.02)
THC+NOx Euro2 limit		–	1.2	–	1.2	–	1.2	–	1.2
CO_2	NDIR	54.9(1.9)	72.8(1.7)	59.5(0.4)	70.3(0.5)	48.0(0.3)	51.2(0.9)	43.5(0.9)	46.3(0.8)
PM (mg/km)	Filter	153(64)	6.10(0.62)	39(8)	4.16(0.97)	6.94	0.33	1.98(0.34)	0.99(0.47)
Non regulated (mg/km)									
N_2O	FTIR	nd	nd	nd	nd	2.16(0.14)	1.61(0.56)	2.14	0.69
NH_3	FTIR	nd	nd	nd	nd	0.66(0.12)	2.27(0.13)	0.10	0.2
Methane (CH_4)	FTIR	97.0(4.8)	56(16)	157(8)	72(11)	24.11(0.01)	13.8(1.2)	35.3	17.72
Acetylene (C_2H_2)	FTIR	75(14)	15.4(5.4)	50.5(2.9)	5.9(1.6)	26.47(0.65)	4.73(0.81)	35.2	5.34
Ethylene (C_2H_4)	FTIR	247(12)	138(26)	250.3(3.8)	138.1(9.6)	34.97(0.78)	10.34(0.91)	33.96	11.62
Ethane (C_2H_6)	FTIR	25.7(3.3)	17.9(5.1)	39.9(2.9)	26.6(5.2)	6.61(0.06)	3.47(0.08)	10.91	7.65
Propylene (C_3H_6)	FTIR	155.5(7.4)	55(11)	247.6(9.7)	66.0(8.9)	20.8(2.5)	8.2(2.1)	31.61	10.84
1-3-Butadiene (C_4H_6)	FTIR	45.9(4.8)	16.2(4.3)	25.3(3.4)	10.2(3.8)	8.0(1.4)	3.79(0.60)	4.36	2.4
2-Methylpropene (C_4H_8)	FTIR	118.7(7.7)	28.2(5.5)	236.5(7.2)	48.3(8.3)	11.6(1.2)	5.57(0.94)	28.28	10.84
2-methyl-2-butene (C_5H_{10})	FTIR	258(36)	84(28)	245(31)	72(18)	NA	NA	NA	NA
Octane (C_8H_{18})	FTIR	NA	NA	NA	nd	42.89(1.32)	16.67(3.74)	nd	nd
o-xylene (C_8H_{10})	FTIR	NA	NA	nd	nd	42.2(11.81)	10.55(8.45)	nd	nd
Isocyanic acid (HNCO)	FTIR	NA	NA	107(34)	33.4(7.9)	NA	NA	NA	NA
Formaldehyde (CH_2O)	FTIR	79.8(7.8)	58.7(7.9)	110.4(4.7)	58.4(1.8)	9.99(0.20)	4.71(0.24)	13.23	7.88
Acetaldehyde (C_2H_4O)	FTIR	NA	NA	73.05(4.64)	19.85(2.06)	10.01(1.22)	5.20(0.95)	11.18	5.66
Methanol (CH_4O)	FTIR	8.22(0.84)	2.8(0.4)	6.43(0.15)	2.29(0.52)	2.47(0.06)	1.20(0.19)	2.99	1.41
Ethanol (C_2H_6O)	FTIR	299(24)	27.5(7.3)	42(19)	24(14)	NA	NA	NA	NA

oil (method:UNI EN ISO 6245:2005). Lubricating oil formulation is suggested to contribute up to 95% to the total exhaust particle mass (e.g., Aalander et al., 2005, and references therein [51]).

No significant benefit was observed for CO_2 emissions which were about 75 g/km and g/km, for the 2-stroker and the 4-stroker, respectively. On the other hand, a comparison with the carbon containing species CO and THC yields a remarkable 36% of total carbon not related to CO_2 emissions in the cold phase, decreasing to 7% in the hot phase. This suggests low engine efficiency and high potential for unregulated emissions compared to a Euro 5 car, where the relative contribution is on the order of 1%. In general, the PTW contribution to CO_2 from global transport is marginal. Moreover, considering that PTWs emit lower amounts of CO_2 compared to passenger cars, and that only one tenth of the energy is necessary to manufacture and recycle them, the increase in trips done by PTWs would actually have a positive effect in the overall reduction of CO_2 emissions from road transport [46].

4.3.2 Unregulated compounds

Table 13 reports emission factors for selected species amongst which, alkanes, alkenes, alkynes, oxygenated and nitrogen containing species (beyond the regulated compounds emission factors plotted in Fig. 24). Nitrous oxide (N_2O) and ammonia (NH_3) are only present in the 4-stroker exhaust, while previous studies reported both compounds for other Euro 2 2-strokers (e.g., Clairotte et al., 2012 [12]), confirming a large degree of unpredictability for the simple technology of 2-stroke engines. N_2O is catalytically produced, and therefore the older 4-stroker catalyst (larger mileage) together with higher engine temperatures related to NOx production could partially explain the presence of N_2O. It remains unclear why, like in Clairotte et al. (2012) [12], emissions are larger during the cold phase. Similarly to N_2O, NH_3 is produced on the catalyst surface, via H_2 formed in the water-gas-shift reaction of CO. Higher catalyst temperatures are usually associated to larger NH_3 emissions, which could explain why we found more NH_3 in the hot phase. In particular, NH_3 emissions have peaks exceeding 20 ppm (not shown here) during accelerations in the hot phase. These emissions are even higher than the only existing EU limit on NH_3 established for heavy duty engines in the upcoming EURO VI legislation (EC-No595, 2009). N_2O and NH_3 are of concern for climate science and air quality, the former being a greenhouse gas and the latter an aerosol and toxic SOA precursor. In terms of CO_2 equivalent mass the greenhouse gases N_2O (100–year Global Warming Potential GWP = 298) and methane (GWP = 25) are negligible compared to direct CO_2 emissions from the scooters.

As for the light hydrocarbon and oxygenated species monitored by the FTIR at the tailpipe (amongst which the toxic formaldehyde and 1-3-butadiene), the cold phase emissions were predominant for both scooters, in good agreement with the regulated THC without any exception. The effect of alkylate fuel and ultra-clean oil combination is species dependent, with prevailing larger emissions for the 4-stroker, and no overall net effect for the 2-stroker.

The barplot in Fig. 25 displays the effect of the use of alkylate fuel on the tailpipe diluted emission (CVS sampling) of VOCs measured with GC-FID following the legislated methodology described in Paragraph 2.3. VOC results are broken down by aromatic (benzene, toluene, ethylbenzene, m/p-xylene, o-xylene, 1-2-3-trimethylbenzene, 1-3-5 trimethylbenzene, 1-2-4-trimethylbenzene) and non-aromatic compounds mainly C2-C8 alkanes and alkenes. The aromatic content of the exhaust drops dramatically for both scooters, while the other VOCs remain the same within experimental variability, as expected by the alkylate fuel formulation (see Table 11). In terms of total amounts, the 2-

stroker emits twice as much as the 4-stroker, mainly in the first phase (only 0.6% produced in the second phase of the 2-stroker). VOCs emission factors were used to calculate the Ozone Formation Potential (OFP) with the incremental reactivity method proposed by Carter et al. (1994) [52], see Table 13. As expected by the emission pattern in Fig. 25, the 2-stroker OFP is much larger than that of the 4-stroke (up to an order of magnitude), deriving mainly from the cold phase emissions. The use of the alkylate fuel has no significant effect for the 2-stroker up to a moderate effect for the 4-stroker.

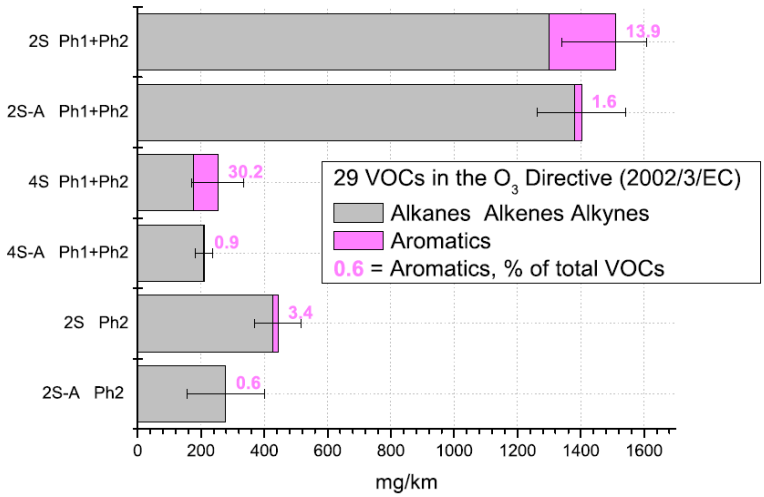

Figure 25: *Average emission factors of VOCs measured by GC-FID (see methodology in Par. 2.2) broken down by aromatic and non-aromatic compounds (8 and 21 species, respectively, see text for details). Tests are grouped by scooter type, fuel, and phase of the driving cycle (Ph1+Ph2 = entire cycle). Sampling design is consistent with smog chamber tests in Table 4. Bar labels represent the percentage of aromatics on total VOCs. Error bars are minimum and maximum values of total VOCs based on the number of tests in Table 12.*

4.3.3 Secondary organic aerosol

Figure 26 shows concentrations of carbonaceous gas and condensed phase species measured from the mobile smog chamber after injection of the 2-stroker exhaust as a function of time after lights on (left axes). Secondary species are produced after lights on, for example peroxy acetyl nitrate (PAN, grey curve), benzoic acid (cyan curve) and SOA. The observed increase in aerosol concentration after wall loss correction is taken as the SOA production for a given emission sample. The organic aerosol concentration is corrected for wall losses using black carbon (BC) measurements as a tracer in Eq. 12. Primary emissions, including primary organic aerosol (POA) are taken from average concentrations measured before irradiation. Figure 26 illustrates the difference between hot phase emissions from the 2-stroker when using standard and alkylate fuels and ultra-clean oil combination. For the standard fuel a large mass increase is observed (800 mg/kg.fuel) due to SOA formation, with aged OA/POA ratio = 16, while for the alkylate emissions, aged OA/POA = 2. In absolute mass a much smaller increase is observed (40 mg/kg.fuel), suggesting that fuel composition affects SOA production. To the best of our knowledge these results show for the first time that scooter emissions generated during ECE47 driving cycles produce significant SOA, in addition to previously observed high primary aerosol emissions (e.g., Adam et al., 2010 [48]). Notably for some tests, e.g. the hot phase of the 2-and 4-stroker, SOA largely exceeds the primary emissions of POA and BC. As a consequence, our current understanding of the contribution of scooter emissions to ambient PM does not capture a significant, and possibly the largest fraction, of the total emissions. Absolute masses of both primary and secondary components are converted into emission factors (formation factors, for secondary species) per mass of fuel (EF_{MASS} , right axes) using Eq. 13. Emission factors of BC, POA, and formation potential of SOA are summarised in Tables 14 and 15, and shown in Fig. 27, in

mass/distance calculated based on Eq. 13 (see Fig. 28 for emission factors and potential of SOA production in mass/mass of fuel). Figure 29 shows high resolution mass spectra obtained for primary and secondary aerosols during experiments on scooters. These spectra demonstrate that aged OA contains considerably more oxidised fragments than the primary emission.

The 2-stroker hot phase and the 4-stroker entire cycle aged exhaust produces amounts of secondary material which is larger than (i) primary particulate emission in Fig. 25, (ii) PM emission factors measured with the legislated method shown in Fig. 23, and (iii) even larger than the emission limit for modern passenger cars (Euro 5 PM limit = 5 mg/km, primary only), confirming that SOA contribution to ambient PM from scooters may be important. Furthermore, the 4-stroker shows significantly lower primary emissions, but a relatively large SOA production (a similar phenomenon is reported for a Euro 5 gasoline car in Platt et al., 2013 [34]). However, it still offers significant reduced emissions compared to the 2-stroker even when the relatively large SOA formation is taken into account.

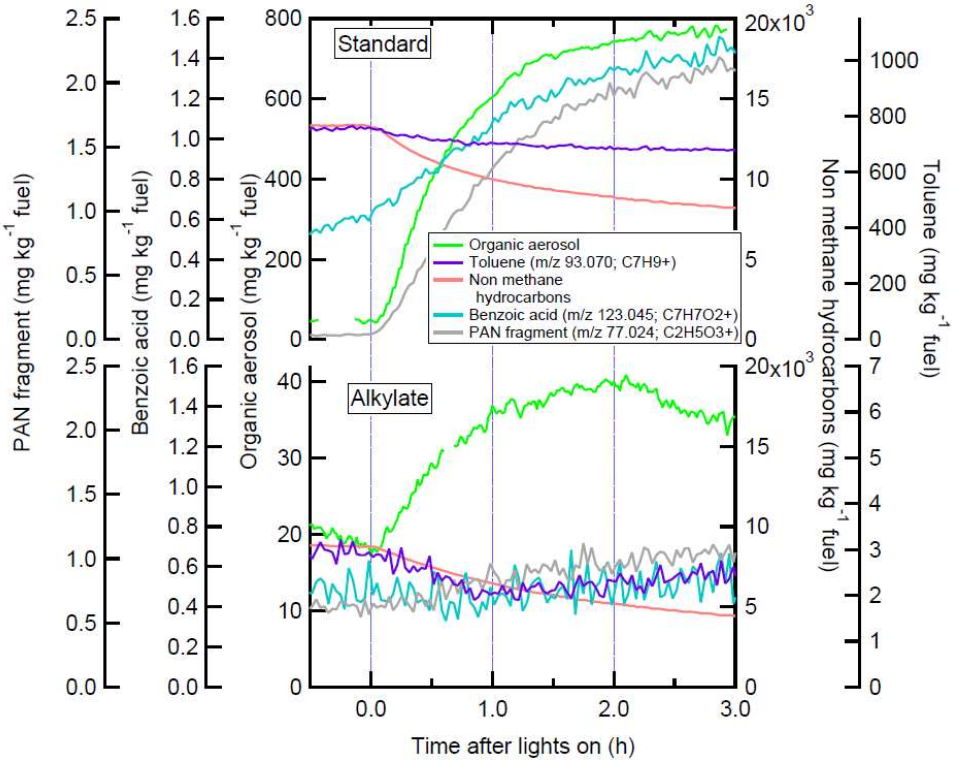

Figure 26: *Emission factors (mg/kg.fuel, wall loss corrected) of various species calculated from concentrations measured inside the smog chamber as a function of time after lights on for the 2-stroker (hot phase only) using standard (top panel) and alkylate fuel (bottom panel).*

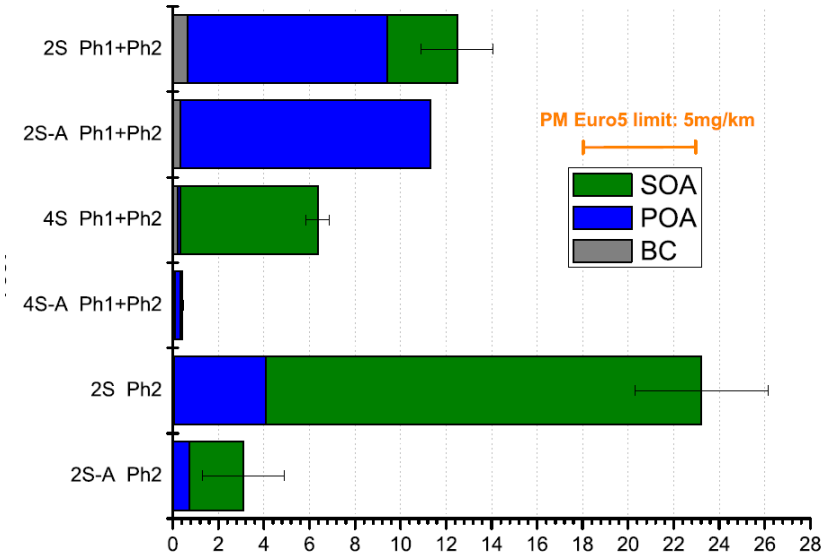

Figure 27: *Average emission factors (mg/km) of BC and POA, and SOA production from scooter emissions measured after aging in the mobile smog chamber, grouped by vehicle type, fuel, and sampled phase (Ph1+Ph2 = entire driving cycle). Error bars show the maximum and minimum observed values for SOA formation. For sake of comparison, the orange bar (upper right corner) displays the Euro 5 limit for light duty passenger cars: when using standard fuel and oil SOA production from the scooters is close to or exceeds that limit.*

Figure 27 shows that alkylate fuels significantly reduce SOA formation from emissions of both 2- and 4- stroke scooters, generated during a full driving cycle. We conclude that this reduced SOA formation stems from the almost complete removal of aromatic compounds from the exhaust (Fig. 25), identified by Platt et al. (2013) [34] as predominant SOA precursors in the case of 2-stroke engines. This mitigation in total primary and secondary particulate mass is only seen for the SOA (similar POA emissions are observed for both types of fuels), further highlighting the importance of secondary pollutants to a comprehensive understanding of vehicle emissions. Figure 27 also shows that there is less potential for mitigation when considering the hot phase of the driving cycle only. Note that the results shown for individual phases refer to separate tests where only part of the cycle was injected into the chamber, meaning that the combined emission factors over a full cycle do not necessarily correspond to the sum of the tests on individual phases. That is, although much reduced, considerable SOA is formed from hot phase emissions of the 2-stroker run on alkylate fuel. This suggests the presence of additional, as yet unidentified, SOA precursors produced when the engine is hot. The benefit of alkylate fuels is thus seen over the course of a full driving cycle, rather than the regulatory hot phase. Therefore alkylate fuels and ultra-clean oils are of benefit not only due to the removal of toxic aromatics and olefins, but also because they have potential to

reduce PM pollution.

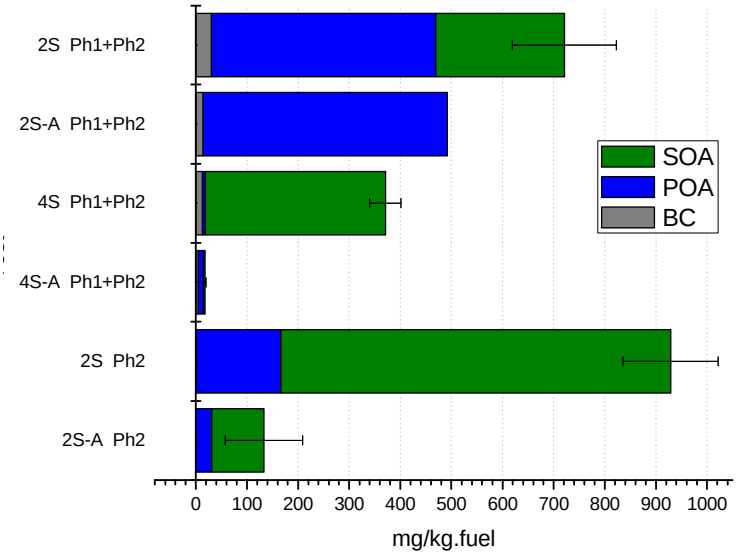

Figure 28: *Average emission factors (mg/kg fuel) of BC, POA, and SOA from scooter emissions measured after aging in the mobile smog chamber, grouped by vehicle type, fuel, and sampled phase. Scooter emissions using standard fuel clearly produce SOA, which may be in excess of the primary emissions. Alkylate fuel reduces, and in some cases (2S-A Ph1+Ph2 and 4S-A Ph1+Ph2) completely prevents, SOA formation.*

Generally, OH exposure times were in the range (1.5 − 3) 10^6 cm^3h, corresponding to an aging time of 1.5 – 3 hours in the ambient atmosphere assuming a global annual mean OH concentration of 10^6 molecules cm^{-3}, suggesting that the already significant SOA formation quantified here may be a lower limit of the ambient SOA formation potential. This is further exemplified by the large fraction of unreacted toluene shown in Fig. 26 (purple curve). Note that OH exposure was generally higher for the alkylate emission aging experiments (for those experiments where it could be determined) and that for one smog chamber experiment with alkylate fuel an additional OH source (nitrous acid, HONO) was added to the chamber, boosting the total OH exposure to around $30 \cdot 10^6$ cm^3 h. Even with these higher OH exposures less SOA was produced from the alkylate fuel emissions. An estimation of SOA formation from aromatic emissions (for 2-stroke scooters using standard fuel) at longer OH exposure times will be presented in a forthcoming paper and further experiments are planned on these issues.

Table 14. *Black carbon (BC), primary organic aerosol (POA) and secondary organic aerosol (SOA) grouped by scooter and fuel types. For the 2-stroker also the results over the hot phase alone (Ph2) are available.*

	BC	POA	SOA
Test	**mg/kg_fuel**		
2S Ph1+Ph2	30.62	438.82	251.48
2S-A Ph1+Ph2	14.18	477.71	0.00
4S Ph1+Ph2	13.03	5.97	351.67
4S-A Ph1+Ph2	4.94	10.26	2.42
2S Ph2	1.48	164.81	762.49
2S-A Ph2	0.00	31.39	101.71

Table 15*. Same as Table 14 with units in mg/km*

	BC	POA	SOA
Test	**mg/km**		
2S Ph1+Ph2	0.64	8.78	3.07
2S-A Ph1+Ph2	0.33	11.00	0.00
4S Ph1+Ph2	0.22	0.10	6.03
4S-A Ph1+Ph2	0.11	0.24	0.06
2S Ph2	0.04	4.04	19.15
2S-A Ph2	0.00	0.72	2.38

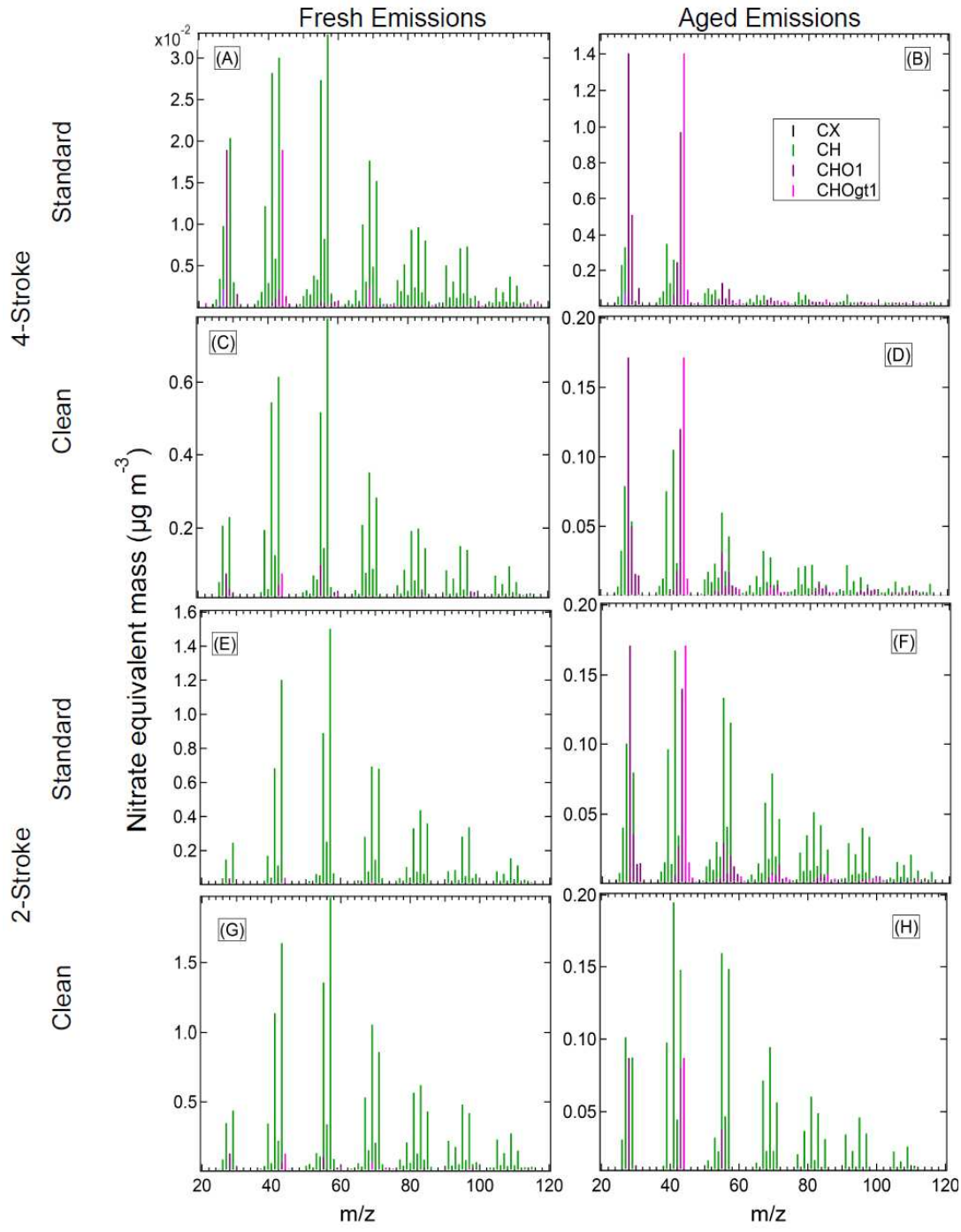

Figure 29. *High resolution aerosol mass spectra measured from the mobile smog chamber of fresh primary and aged emissions from a 4-stroke scooter on standard fuel (A and B) and alkylate fuel (C and D) and a 2-stroke scooter on standard fuel (E and F) and clean fuel and lubricant oil (G and H). Nitrate equivalent mass is*

The benefit summary in Table 16 is related to the two scooters considered in this study, and should not be read to draw general conclusions on global atmospheric impact of PTWs. Nevertheless, strong indications for emission improvements can be deduced if one reasonably assumes that standard versus alkylate fuels would have the same qualitative behaviour when tested on similar simple engines. Considering that particulate pollution is one of the main concerns both in the urban environment and for the climate

change, the use of alkylate fuels and low ash forming potential lube oils seem to be a promising alternative. The best option is likely the electrification of the scooters as is done in many cities in China.

Table 16: *Benefits from the use of alkylate fuel versus standard fuel as percentage of emission factor improvement. Results are given for driving cycle phases and entire cycle. Note that only the hot phase (Ph2) of the cycle is considered for legislation.*

Compound	2S-Ph1	2S-Ph2	2S-Ph1+Ph2	4S-Ph1	4S-Ph2	4S-P
THC	22	23	22	1	-18	-4
NOx	11	14	13	13	-5	5
THC+NOx	21	22	22	4	-12	-1
CO	35	8	29	31	50	38
CO_2	-8	3	-2	9	10	10
PM	75	32	73	72	-200	59
Aromatics (VOCs)	NA	89	89	NA	NA	97
Total VOCs	NA	37	7	NA	NA	17
SOA	NA	87	100	NA	NA	99
N_2O	NA	NA	NA	1	57	25
NH_3	NA	NA	NA	84	91	90
Formaldehyde	-38	0	-22	-33	-67	-44
1-3-butadiene	45	37	43	46	37	43
MTBE	51	3	49	-111	-198	-134
CH_4	-62	-28	-49	-46	-28	-40
OFP	NA	30	0	NA	NA	31

5 Smog chamber study on emissions from heavy duty vehicles

5.1 Introduction

Heavy duty diesel vehicles (HDDVs) are a small but significant fraction (13%, Fig. 30) of the total European vehicle fleet. However, while the average annual distance driven by passenger cars is ca. 14000km, HDDVs typically drive 10 times further in the EU, or 3 times further in Switzerland per year with an average fuel consumption ten times higher than that of passenger cars. An assessment of PM pollution from vehicular sources thus requires knowledge of emissions from HDDVs.

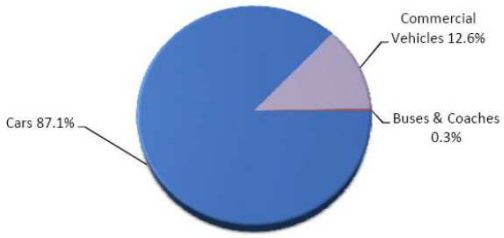

Figure 30: *Contribution of heavy duty vehicles to the European vehicle fleet.*

Furthermore, despite the recent economic downturn and corresponding decrease in registration of new HDDVs (Fig. 31) the number in circulation has actually increased (Fig. 32).

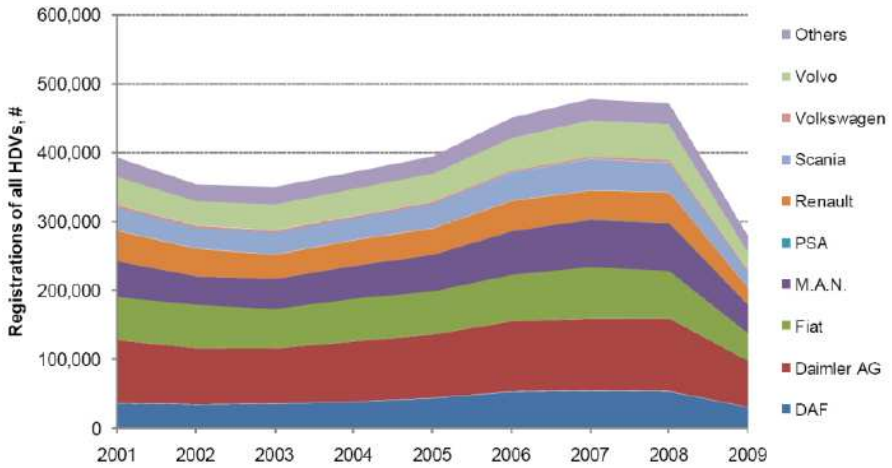

Figure 31: *Yearly registration of new heavy duty diesel vehicles by brand.*

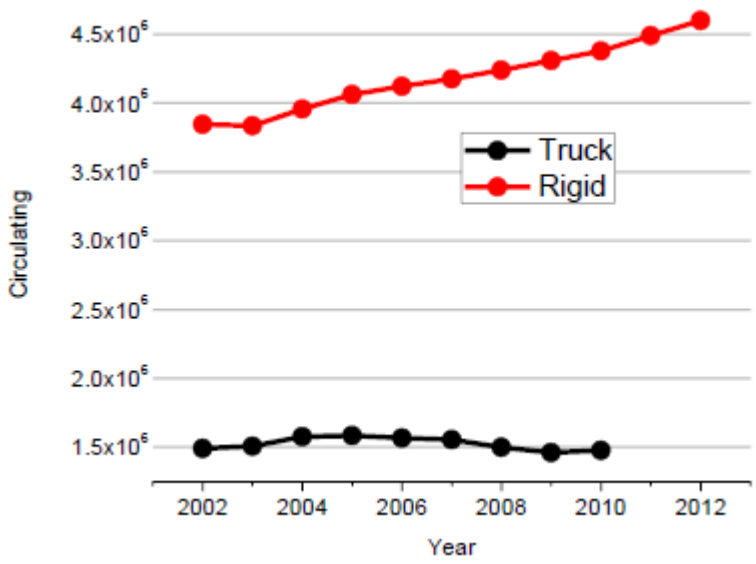

Figure 32: *Number of heavy duty diesel vehicles in circulation in the EU by year. Data are shown for articulated vehicles and un articulated vehicles (labelled rigid).*

Current European emission standards for HDDVs (Table 17) apply only to engine test bench tests (not driving cycles) and work is needed to determine emissions under realistic driving conditions. Estimations of SOA from HDDVs is also completely lacking in the literature, even though it may contribute significantly to particulate pollution. For this reason we investigated secondary aerosol formation and tailpipe emissions from HDDVs. Furthermore we investigated the effect of substituting part of the diesel fuel for liquid petroleum gas (LPG) during driving for one vehicle equipped with 'Flexi fuel' technology. LPG should theoretically limit CO_2 emissions as it produces less CO_2 per unit of energy released, though it's overall effect on vehicle engine efficiency during driving (and hence true CO_2 emission) is unknown.

Table 17: *European emission standards for heavy duty diesel vehicles. The current stage, Euro V, is highlighted.*

Stage	Date	Test	CO	NMHC	CH_4[a]	NOx	PM[b]
			g/kWh				
Euro III	*1999.10 EEV only*	ETC	*3.0*	*0.40*	*0.65*	*2.0*	*0.02*
	2000.10		5.45	0.78	1.6	5.0	0.16[c]
Euro IV	2005.10		4.0	0.55	1.1	3.5	0.03
Euro V	2008.10		4.0	0.55	1.1	2.0	0.03
Euro VI	2013.01	WHTC	4.0	0.16[d]	0.5	0.46	0.01

a - for gas engines only (Euro III-V: NG only; Euro VI: NG + LPG)
b - not applicable for gas fueled engines at the Euro III-IV stages
c - PM = 0.21 g/kWh for engines < 0.75 dm^3 swept volume per cylinder and a rated power speed > 3000 min^{-1}
d - THC for diesel engines
e - for diesel engines; PN limit for positive ignition engines TBD

5.2 Methodology

We investigated emissions from two in use HDDVs. Table 18 provides technical details of these vehicles (Table 2 also provides details of the smog chamber conditions). The vehicles were operated during the European Transient Cycle (ETC, Fig. 33) which consists of three phases designed to simulate urban, rural, and motorway driving. The tests were performed on chassis dynamometers inside a vehicle testing cell after a mandatory soaking time at ambient temperature, -7 or 22℃, of at least 6 hours. The trucks were driven with a simulated load of 12.5t. The set up of the experiments is illustrated in Fig. 34. The procedure for tailpipe measurements is detailed in Chapter 4.2.1. Smog chamber experiments were conducted according to procedures outlined in Chapter 2.

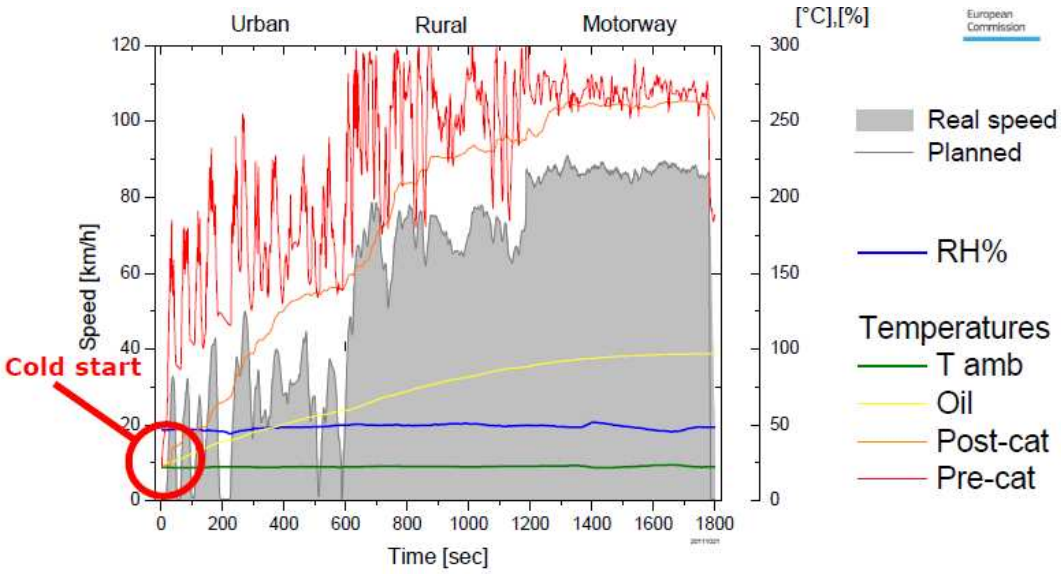

Figure 33: *European Transient Cycle (grey), which consists of urban, rural, and motorway modules during which the heavy duty vehicles of this project were operated. The cold start (highlighted) was included. Also indicated, the pre- and post-catalyst and oil temperature of the second HDDV during the cycle. Test cell temperature and humidity were stable during the test.*

Table 18: *Technical details for the two heavy duty diesel vehicles investigated as part of this project. DOC refers to a diesel oxidation catalyst.*

	Model	Year	Power	After-treatment	Category	Fuel	Mileage
Truck 1	DAF XF105 12.9L 19.5 ton	2007	340kW	SCR (Urea) DOC (THC,CO) Without DPF	Euro V	Diesel B5 Diesel/LPG, 50%	350000 km Ca.
Truck 2	MAN TGX 12.4L 19 ton	2009	324kW	DPF SCR DOC	Euro V	Diesel B5	250000 km Ca.

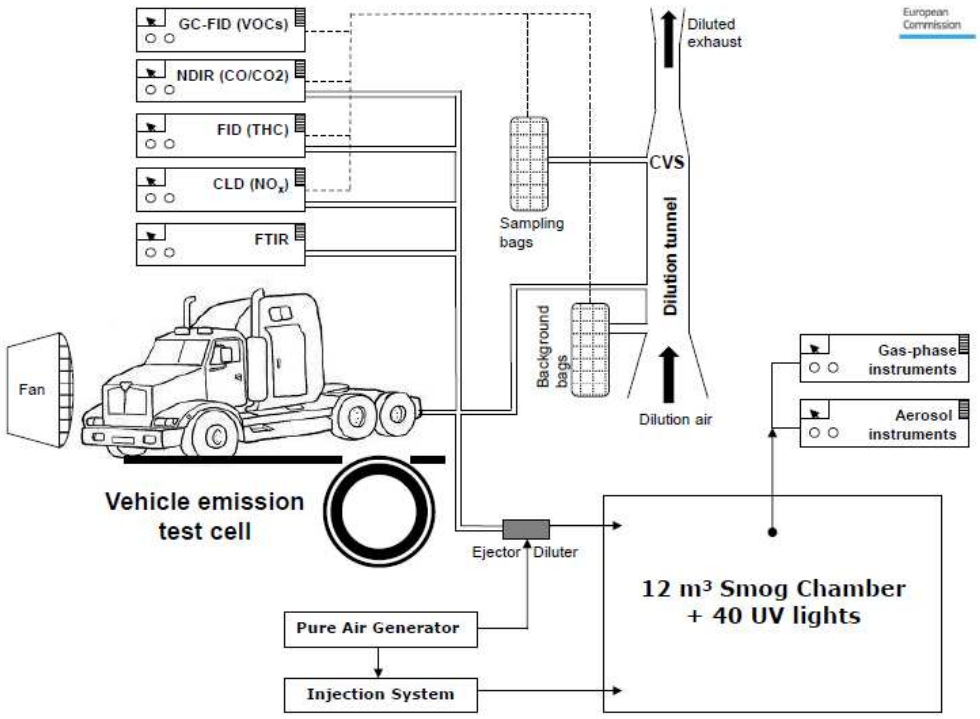

Figure 34: *Schematic of the test facility and instrumentation. The HDDV exhaust is collected at the tailpipe and transferred via heated lines (190◦ C) to online instrumentation (FID, NDIR, CLD, FTIR - see Table 1). The exhaust is also directed to a dilution tunnel as required by the legislation for subsequent offline analysis (dashed lines). Part of the exhaust is injected in the 12 m^3 smog chamber for secondary aerosol formation.*

5.3 Results and discussion

5.3.1 Regulated compounds

Figs. 35, 36 shows that for the regulated compounds (g/km) both HDDVs perform better than mandated even by the upcoming Euro VI legislation (Table 17). In all tests LPG faired worse. Generally most emission was during the cold start, as expected. Indeed, the LPG performed worse during driving cycles than Euro III engines typically perform on test benches. Tests at -7℃ produced elevated emissions, likely due to an increased length of the cold start period. Fig. 37 shows that the after treatment system typically did not engage until the motorway driving segment of the cycle. This, together with the relatively high cold start emissions, highlights that such vehicles are more suited to the motorway driving for which they are designed, but less suited to more confined driving such as in urban areas.

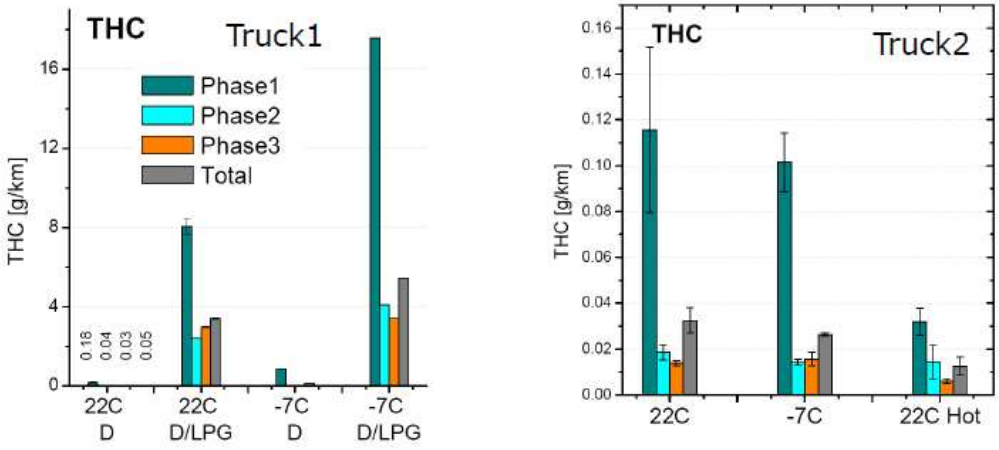

Figure 35: *Emissions of total hydrocarbon (THC) during the three phases of the ETC driving cycle for the two HDDVs of this study. LPG indicates the results of tests where truck one utilised its flexi fuel capacity and burned partly LPG during the cycle*

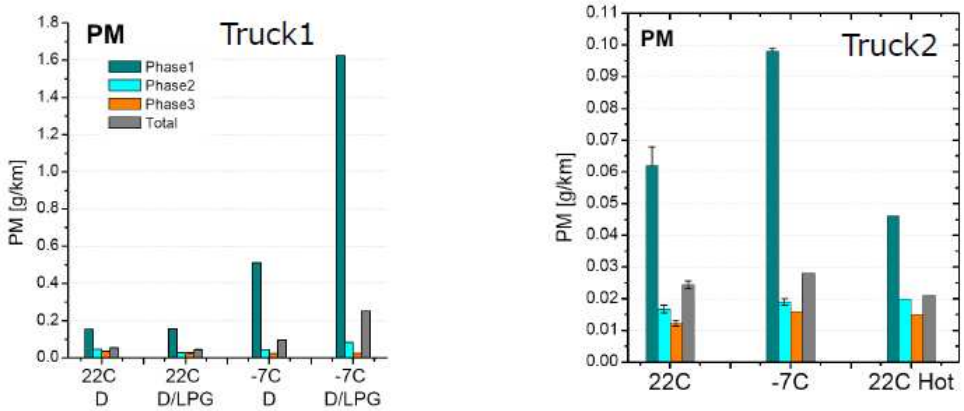

Figure 36: *Emissions of particulate matter (PM) during the three phases of the ETC driving cycle for the two HDDVs of this study. LPG indicates the results of tests where truck one utilised its flexi fuel capacity and burned partly LPG during the cycle.*

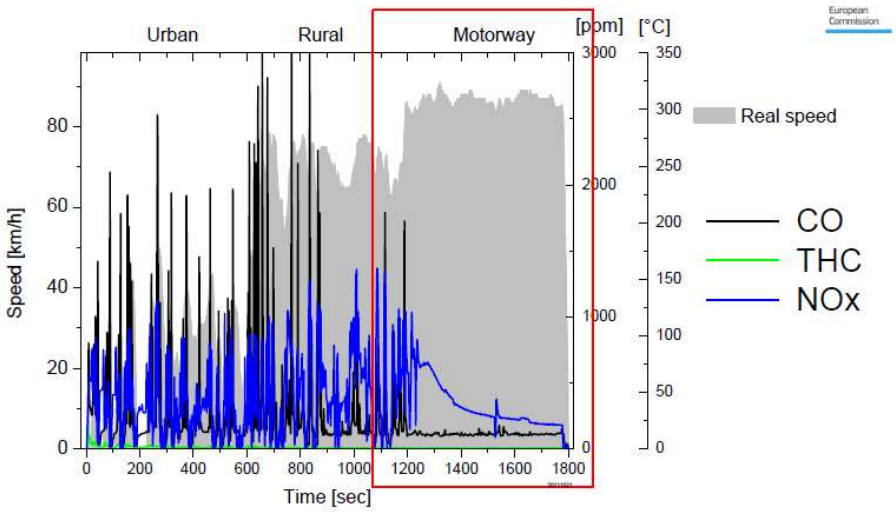

Figure 37: *Emissions of THC, CO and NOx from a heavy duty vehicle during the ETC driving cycle. Only during motorway driving (highlighted) does the NO_x after treatment system engage.*

5.3.2 Unregulated compounds

Fig. 38 shows that HDDV2, equipped with a diesel particle filter (DPF) produced significantly higher NO_2 emissions (accounting for almost all NO_X) during the low temperature (-7℃) tests. Some slip of NH_3 (produced during NO_2 reduction) is observed especially in the LPG case.

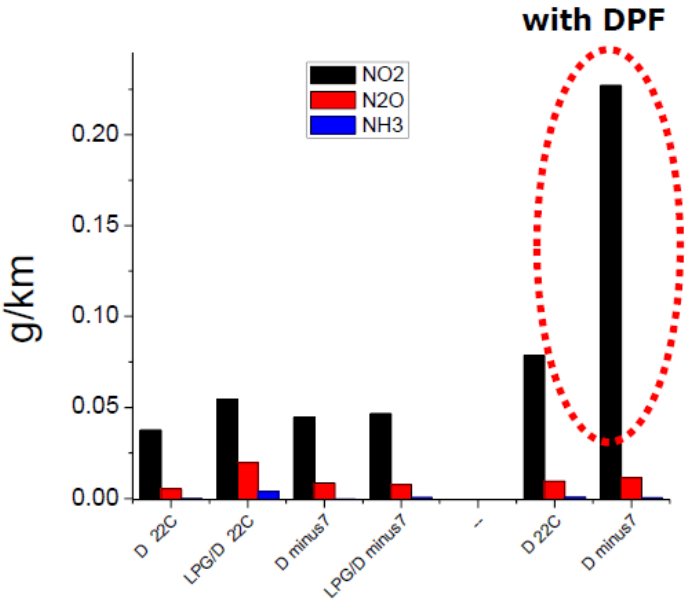

Figure 38: *Emission of nitrogen containing species during full ETC driving cycles from the two trucks of this study*

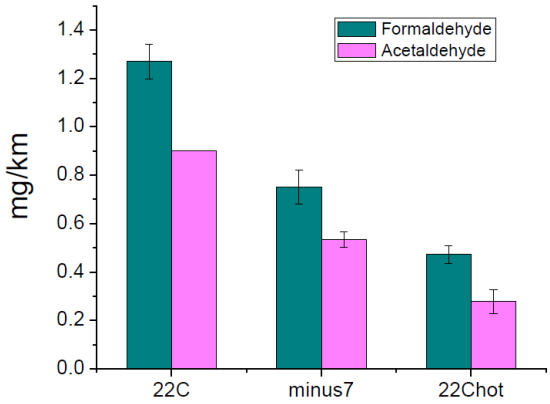

Figure 39: *Tailpipe concentrations of formaldehyde and acetaldehyde from HDDV2 during a full ETC driving cycle*

Figure 39 highlights that not all emissions are exacerbated by low temperature conditions. Carbonyl compounds, as measured by offline high pressure liquid chromatography, are highest at 22℃ compared to -7° C, though still lower during tests where only hot (motorway segment) driving was sampled. Oxidised hydrocarbons could in theory act as SOA precursors, requiring fewer oxidation steps to become highly oxidised and condensable.

5.3.3 Secondary organic aerosol

Figures 40 and 41 show that in the case of the two trucks of this study, the production of secondary aerosol is of minor concern. Assuming that the two HDDVs here are representative of newer HDDVs (EuroV onwards), only a small contribution to SOA might be expected as compared to scooters (chapter 3) and passenger cars (chapter 6). Note that the emission factors presented here are in per mass fuel and that fuel consumption is higher for HDDVs than passenger cars. The low SOA formation may be a result of the lean, efficient combustion in a large diesel engine, which typically would produce lower hydrocarbons (but higher NOx). For both trucks a considerable increase in SOA formation is observed at the low temperature condition: 50 and 25 times higher SOA formation is observed for HDDV1 and HDDV2, respectively. This may be a consequence of 1) increased VOC emission and/or 2) an increased aromatic fraction up to 60% of emitted VOC volume at -7℃ compared to 4-6% at 22℃ . Aromatics are known SOA precursors. Even in the cold case, SOA is still much smaller than the primary emission.

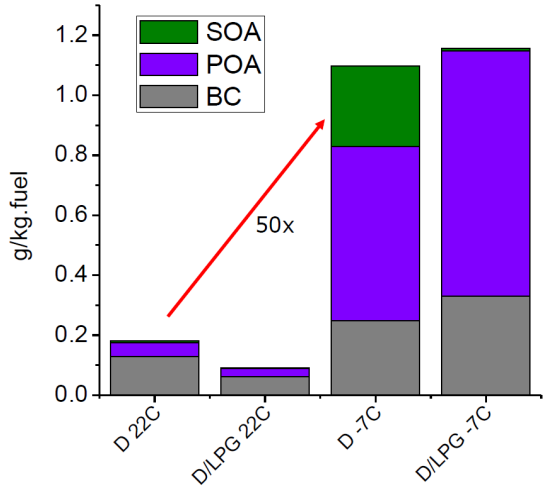

Figure 40: *Emission factors (g kg^{-1} fuel) for black carbon, primary organic aerosol (POA) and formation of secondary organic aerosol (SOA), determined from the smog chamber during experiments on HDDV1*

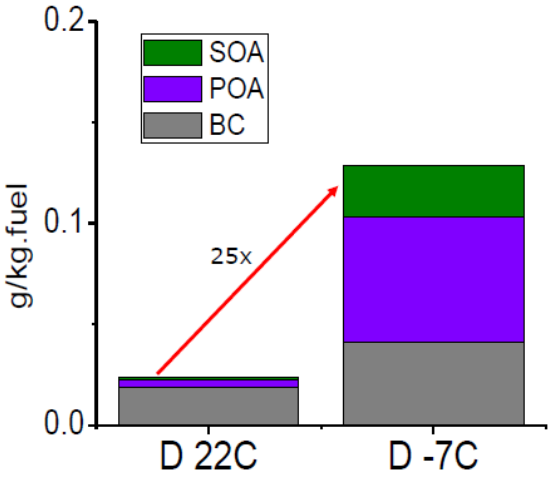

Figure 41: *Emission factors (g kg^{-1} fuel) for black carbon, primary organic aerosol (POA) and formation of secondary organic aerosol (SOA), determined from the smog chamber during experiments on HDDV2*

The deployment of the flexi fuel, LPG, capability for HDDV1 appears to reduce SOA formation. This is probably as LPG is a much lighter fuel than diesel and so produces less material capable of condensing upon oxidation. However, since formed SOA is not a large fraction of the total PM, this would not be enough to suggest that LPG is beneficial. Furthermore, results for the primary emission are mixed, being lower at 22℃ and higher at -7℃, while NOx was higher from HDDV1 when it wa s operated with LPG.

6 Smog chamber studies on emissions from light duty vehicles

6.1 Introduction

Unfortunately, little or no information on SOA formation from vehicle emissions exists in the literature. Furthermore, how SOA production varies by vehicle type (e.g. diesel or gasoline, vehicle legislative standard etc.) and thus the relative contribution of different vehicle classes to ambient PM, remains poorly constrained. For example, top-down estimations of SOA production from vehicle exhaust have yielded contradictory results. Recent ambient aerosol mass spectrometer measurements in the L.A. Basin concluded that secondary organic aerosol (SOA) from gasoline vehicle emissions can dominate background urban organic aerosol [6]. Conversely, another recent study has suggested, using raw diesel fuel combined with tunnel measurements, that diesel vehicles produce more SOA than gasoline vehicles [7]. Bottom-up estimations of SOA production from real tailpipe vehicular emissions are therefore needed. It is particularly important to investigate light duty vehicles such as passenger cars as these represent the largest fraction of the fleet and are operated in urban environments where their impact is higher since population density is also higher.

6.2 Methodology

Chapter 2 details extensively the methodology used to investigate emissions from passenger vehicles. Light duty vehicles were investigated under warm (22 ℃) and cold (-7 ℃) ambient operating conditions (see also Table 2), as well as at high (90%) and low (40-60%) relative humidity. Three GLDVs were studied: GLDV 1 (see chapter 2, multiport injection, no PM regulation), and two direct injection vehicles, from hereon in GLDV2 and GLDV3. Two diesel passenger cars, DLDV1 and DLDV2 from here on in, both equipped with diesel particle filters (DPF) were also studied.

Table 19 : European emission standards for light duty vehicles (g km^{-1})

Tier	**Date**	**CO**	**THC**	**NMHC**	**NOx**	**HC+NOx**	**PM***
Diesel							
Euro 1	July 1992	2.72	-	-	-	0.97	0.13
Euro 2	January 1996	1.0	-	-	-	0.7	0.08
Euro 3	January 2000	0.64	-	-	0.50	0.56	0.05
Euro 4	January 2005	0.50	-	-	0.25	0.30	0.025
Euro 5	September 2009	0.50	-	-	0.180	0.230	0.005
Euro 6	September 2014	0.50	-	-	0.080	0.170	0.005

Gasoline							
Euro 1	July 1992	2.72	-	-	-	0.97	-
Euro 2	January 1996	2.2	-	-	-	0.5	-
Euro 3	January 2000	2.3	0.20	-	0.15	-	-
Euro 4	January 2005	1.0	0.10	-	0.08	-	-
Euro 5	September 2009	1.0	0.10	0.068	0.060	-	0.005
Euro 6	September 2014	1.0	0.10	0.068	0.060	-	0.005

*For gasoline vehicles, applies only to direct injection vehicles

6.3 Results

Emission factors (EFs) of primary and secondary pollutants for diesel and light duty vehicles determined from smog chamber data using Eq. 13. Figure 42 shows an example of PM measurements from a smog chamber experiment on GLDV2 at 22℃, 40% RH.

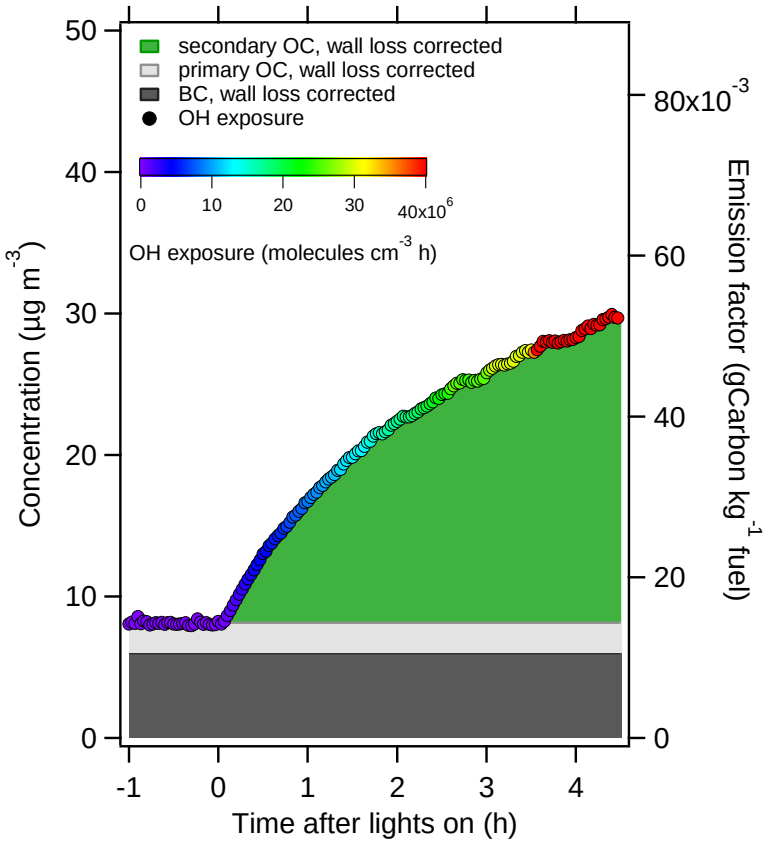

Figure 42: *Wall loss corrected smog chamber concentrations (left axis) of secondary organic carbon (OC); primary OC; and black carbon (BC) vs. time after lights on in the smog chamber during aging of emissions from a gasoline light duty vehicle. The right axis shows the same data expressed as an emission factor, in g Carbon kg^{-1} fuel based on Eq. 13. The colour scale indicates the OH exposure (see Sect. 2.3.2). For this experiment SOA (expressed in terms of secondary OC, dominates).*

Primary EFs, shown in Table 20 for GLDV1 were determined from smog chamber data using Eq. 13 (g kg^{-1} fuel, EF_{MASS}) and Eq. 19 (g km^{-1}, EF_{KM}):

$$EF_{KM} = EF_{MASS} \cdot e \cdot \rho \quad , \qquad (19)$$

Where e is fuel efficiency and ρ the fuel density. HC and NMHC are reported in units of carbon mass, i.e. grams C kg^{-1} fuel.

Table 20: *Emission factors for regulated compounds calculated for a Euro 5 gasoline light duty vehicle (GLDV1) from smog chamber data and VELA (CVS) data, averaged over two experiments, and Euro 5 limit values for gasoline light duty vehicles. For smog chamber data, the range of observed values, lowest-highest is given.*

	CO	THC	NMHC	NO_X
From Smog Chamber Data				
EF_{MASS} (g kg^{-1} fuel)	12.69-13.87	0.91-1.06	0.77-0.86	0.72-1.06
EF_{KM} (g km^{-1})	0.50-0.55	0.036-0.042	0.030-0.034	0.028-0.041
From CVS Data				
EF_{MASS} (g kg^{-1} fuel)	18.84±0.68	1.75±0.21	1.75±0.21	0.89±0.14
EF_{KM} (g km^{-1})	0.741±0.03	0.069±0.009	0.069±0.009	0.035±0.005

Fig. 43 shows exhaust VOCs measured at the CVS using GC-FID in addition to normalised methane and formaldehyde measured at the tailpipe and condensed phase material measured in the smog chamber for GLDV1. Data are presented as a carbon mass balance for fresh and aged emissions. An estimate of the aged gas phase (Fig. 43, aged emissions, grey) is made by subtracting the aged secondary organic carbon from the initial VOC. The aged gas therefore incorporates gas phase reaction products including CO and CO_2. Note that a considerable fraction of lighter hydrocarbons are produced, and that the aromatic hydrocarbon fraction (~10 %) is somewhat reduced compared to the raw fuel used (29 %) indicating that raw fuel is not a good proxy for vehicular emitted hydrocarbon, at least not in this case. The large unidentified fraction of the hydrocarbon emission may include smaller oxygenated compounds, e.g. ethanol, longer chain and branched alkanes and measurement uncertainty. Most of this THC emission (>90 %) occurs at the start of the driving cycle (see Fig. 5), when the catalyst is cold, as is to be expected based from previous studies showing the importance of the cold start, e.g. (Weilenmann et al., 2009).

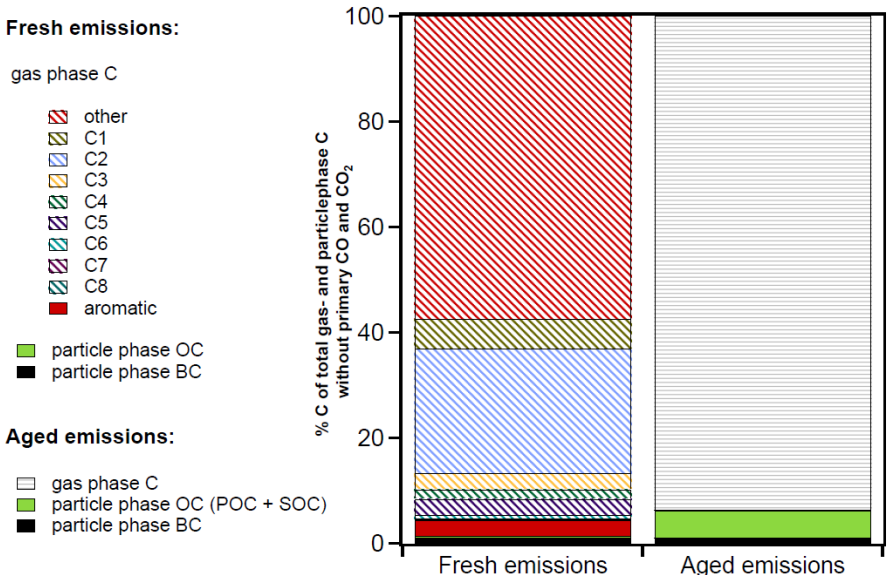

Figure 43: *Composition of fresh and smog chamber aged exhaust emissions from a euro 5 gasoline light duty vehicle (GLDV 1, Exp. 2), and raw gasoline fuel. Data are presented as a carbon mass balance. The following species were included: C1: methane and formaldehyde, C2: ethane, acetylene and ethane, C3: propane and propene, C4 isobutane, n-butane, trans-2-butene, 1-butene, cis-2-butene, and 1,3-butadiene, C5: 2-methylbutane, n-pentane, trans-2-pentene, 1-pentene, and isoprene, C6: 2-methylpentane and hexane, C7: n-heptane, C8: 2,2,4-trimethylpentane and n-octane.*

As shown from the CVS data in Table 20, GLDV1 complies with Euro 5 regulations. Furthermore, emission of regulated compounds is close to those previously observed from a Euro 5 GLDV during the NEDC cycle ([53], and Internal Communication, Joint Research Centre) as well as from a Euro 4 GLDV tested during different driving cycles (Chirico et al., in prep.).

Table 21 shows EF_{KM} for carbonaceous aerosol from all passenger cars tested in this study, which are also presented in Fig. 47. Primary PM is determined using gravimetric analysis of filters taken at the CVS. The primary emission is speciated as black carbon and primary organic aerosol using the ratio OC/BC measured at the smog chamber. Values for SOC are taken at OH exposures of $10 \cdot 10^6$ $cm^{-3}h$ (SOC_{10h}), as well as for the maximum exposure, $(30\text{-}150) \cdot 10^6$ $cm^{-3}h$.

$$y_{bulk} = SOC_{10h} / THC \qquad (20)$$

Secondary organic aerosol is calculated by applying bulk yields (see Eq. 20) to emissions of total hydrocarbon measured at the tailpipe using FTIR and corrected for partitioning to a background concentration of 10 μgm^{-3} (Eq. 16).

$$SOC_{10h} = THC * y_{bulk} \qquad (21)$$

Where THC is the total hydrocarbon emission per km.

Table 21: *Emission factors (mg/km) for particulate matter (PM), black carbon (BC), primary organic carbon (POC) and secondary organic carbon (SOC) from the passenger cars of this study*

Vehicle	Temperature °C	PM	BC	POC	SOC $10\times10^6 cm^{-3}$ h	Maximum
GLDV1	22	1.40	0.58	0.82	1.19	1.63
GLDV2	22	1.59	0.77	0.12	1.03	1.41
GLDV3	22	3.85	2.75	1.10	0.57	0.78
DLDV1	22	0.27	-	-	0.24	4.38
DLDV2	22	0.69	0.23	0.46	0.09	1.71
GLDV1	-7	5.81	2.75	0.18	4.24	5.81
GLDV2	-7	13.38	7.87	0.60	6.27	8.60
GLDV3	-7	8.72	8.72	0.00	2.86	3.93
DLDV1	-7	1.39	0.46	0.92	0.19	3.42
DLDV2	-7	0.73	0.62	0.11	0.14	2.56

Black carbon (BC) emission factors were calculated using aethalometer data, presented in Fig. 11. The Ángström exponent (α), a standardised parameter describing the decrease in light absorbance with respect to wavelength for BC, and a useful tool for source apportionment [54] is also shown in Fig. 11 for Exp. 2 with GLDV1. The initial value of 1.2 was obtained for aerosols from the gasoline car, which is higher than values reported for diesel cars (Sandradewi 2008 [54] and references therein). A slow reduction of α during the experiment was observed, except immediately after the UV-light switch-on, where a transient increase of α is observed. These changes could be caused by an increase of coating thickness due to condensation or evaporation, and oxidation of the adsorbed species.

As Fig. 44 shows, POA emissions from GLDV1 are lower than those previously reported for a Euro 3 diesel vehicle equipped with an oxidation catalyst, but no DPF [15]. An alternative, gravimetric measurement of primary PM measured from the CVS is also reported in Table 21, as PM. PM emission factors are close to the combined OA+BC taken from the chamber (see Fig. 8), suggesting that there are only small errors in the reported primary emission factors. Small variation in the methodologies likely results from a number of factors including, but not limited to, i) adsorption artefacts on the filters ii) effects due to lower-than-smog chamber dilution in the CVS iii) error in the Aethalometer estimation of BC iv) error in the SMPS measurement due to differences in effective and mobility diameters. A High resolution AMS mass spectrum of the POA from GLDV1 is presented in Fig. 45. POA emissions are highly hydrocarbon like, containing very few oxidised fragments.

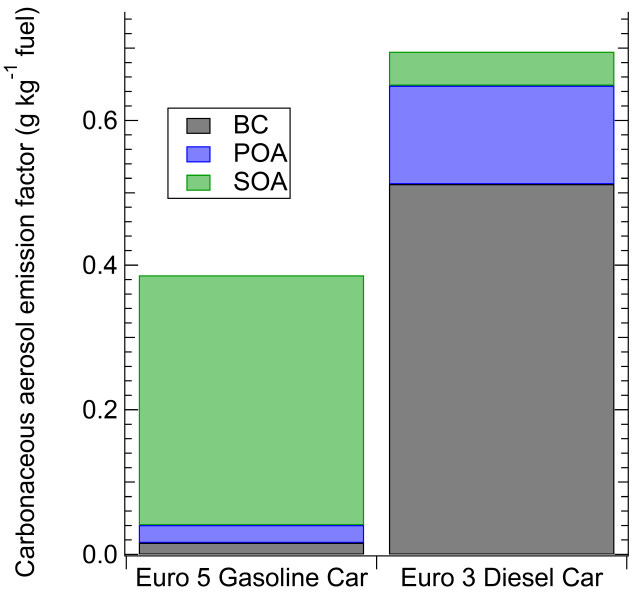

Figure 44: *Primary aerosol emission factors and secondary organic aerosol formation factors calculated for the Euro 5 gasoline light duty vehicle (GLDV) (average over Exp. 1 and 2) of this study and the results of a previous smog chamber study on a Euro 3 diesel passenger car (with oxidation catalyst, but without diesel particle filter, DPF) [15]. The diesel emissions are dominated by black carbon (BC, black) and primary organic aerosol (POA, blue) with only a small secondary organic aerosol (SOA, green) fraction. Conversely, a large fraction of the GLDV emission comprises SOA after aging. The large SOA fraction for the GLDV suggests a larger contribution from gasoline vehicles to ambient particulate pollution than has so far been recognised based on primary emissions. Further, future use of DPFs would remove almost all of the primary BC and POA emissions from diesel vehicle emissions, in which case the total particulate emissions (i.e. POA + SOA) for the GLDV may exceed those of a diesel vehicle. It should be noted that smog chamber OA concentrations in [15] were lower (<30 µg m^{-3}) than those in this study, leading to lower emission factors due to lower partitioning to the aerosol phase*

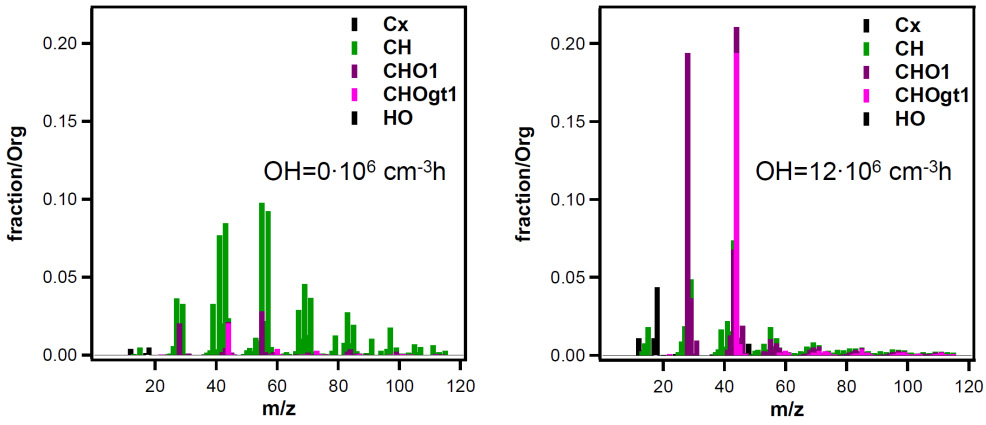

Figure 45: *High resolution aerosol mass spectra measured at the mobile smog chamber of fresh primary and aged OA emission at an OH exposure of 12·10^{6} cm^{-3} h from a gasoline light duty vehicle*

A comparison between all vehicles and tests is shown in Fig. 45.

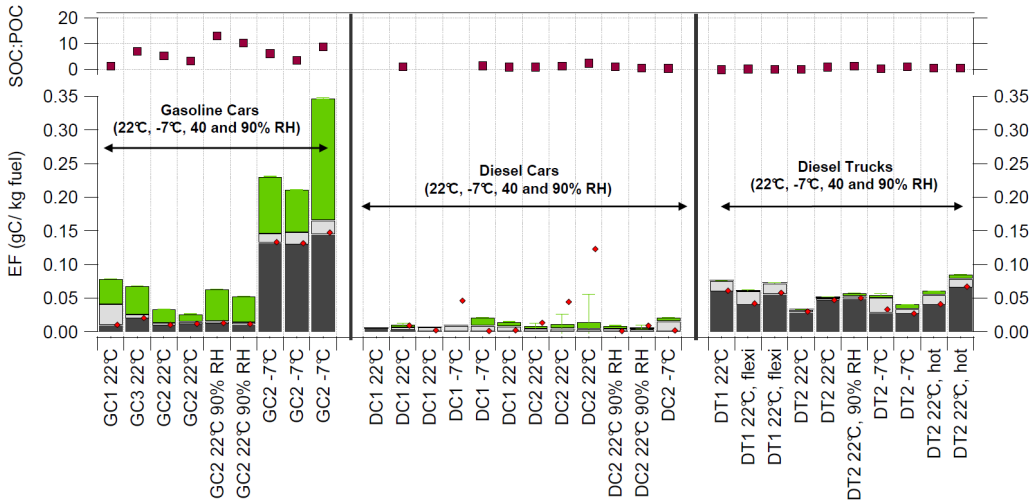

Figure 46: *Emission factors (g C kg^{-1} fuel) from gasoline cars and diesel passenger cars and trucks, of primary (light grey) and secondary organic carbon (green) and black carbon (dark grey). Also, shown the relative increase SOC/POC and detection limits for each experiment. Note that for many tests with the diesel car the PM was below detection and thus only a maximum emission factor could be determined.*

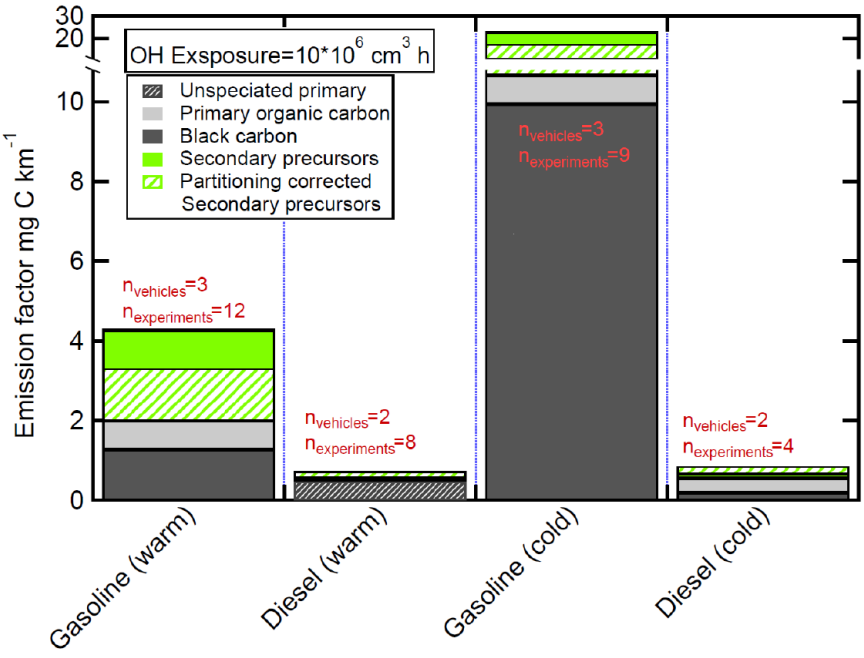

Figure 47: *Average emission factors of PM speciated as black carbon or primary organic carbon where possible, as well as secondary organic carbon (shown as emitted precursors to SOC) in mg carbon (C) km^{-1} at an OH exposure of $10*10^6 cm^{-3} h$ from three Euro 5 gasoline and two Euro 5 diesel light duty vehicles. Also shown, an estimation of SOC at a background concentration of 10 ug m^{-3} to account for the effects of portioning (shaded green, Eq. 16) compared to the absolute, measured value. The number of tests is also given for each vehicle/ condition as well as number of vehicles tested.*

Primary emission factors at 22 ℃ (warm, Fig. 47) a re around 3 times higher for the Euro 5 gasoline cars tested than for the Euro 5 diesel passenger cars. Secondary organic carbon is also much higher, meaning that total carbonaceous PM is higher in the case of

modern gasoline car. This is likely a direct consequence of the use of a diesel particle filter (DPF) for the diesel cars and generally lower VOC emissions (i.e. less SOA precursors). The average THC emission for gasoline vehicles in this study (smog chamber data, cold start included) was 40 mg km^{-1}, while a value of 96.5 mg km^{-1} has also been reported for a Euro 5 GLDV from an NEDC cycle [53]. Diesel engines operate under lean conditions with a higher air/fuel ratio in comparison to the spark ignition engines typically used by GLDVs. Our results suggest that the impact of diesel vehicles on ambient PM concentrations may further decrease in Europe where more vehicles on the road are likely to be equipped with DPFs in order to meet regulations, furthermore all heavy duty diesel vehicles are expected to require DPFs in order to meet Euro VI legislation [55]. A DPF has close to 100 % efficiency in terms of particle mass when used correctly. However, the potential use of a gasoline particle filter (GPF) in gasoline vehicles would be ineffective at reducing hydrocarbon emissions which may lead to SOA formation**.**

A second important point shown in Figs. 46 and 47 is that the cold temperature emission is higher for the gasoline car, while diesel is unaffected. We suggest that the main effect of the cold ambient conditions was not on chemistry inside the smog chamber, rather an effect on the test vehicle. This is because the cold start lasts longer at colder temperatures and gasoline vehicles are known have significantly higher emissions during cold start compared to hot driving, while for diesel vehicles this effect is much less pronounced [56]. Furthermore both THC emissions and SOC formation were 7 times higher at cold conditions for the gasoline car suggesting a similar bulk yield (Eq. 19). For the GLDV2 vehicle we found an increase of the SOC formation when increasing the relative humidity from 50 to 90% by roughly a factor 3. In contrast, no significant effect was found for a diesel vehicle.

Indicated in Fig. 10 is the O:C ratio of the POA and of the aged OA from GLDV1, which increase with time and OH exposure in the chamber. Normalised high resolution mass spectra of the fresh (primary) and aged aerosol for GLDV1 are also shown in Fig 44. An increasing O:C, reflecting increasing oxygen content following oxidisation, is predicted by theory [50] and has been observed in ambient datasets [57]. Highly aged ambient aerosols typically have O:C ratios approaching unity, whereas urban combustion related aerosol have been observed in the range 0.06-0.1 [58]. The O:C ratio of 0.7 observed here is the same as that of the ambient observed low volatility oxygenated organic aerosol (LV-OOA) [57]. This increase is observed during all experiments at similar OH exposures as ambient under conditions [58]. Previous smog chamber studies, performed at similar PM concentrations to those here, on a wide range of emissions from wood burning [59] to biogenic SOA precursors [57], could not often reproduce such an O:C increase (values below 0.5 are typically reported). Recent aging experiments by Nordin et al., (2013) [60] on the aging of emissions from older Euro 2-4 idling gasoline cars also produce SOA with lower O:C (~0.4) than observed in this study. This suggests that the emissions of this Euro 5 car operated under the conditions of this study have a unique VOC profile, that yield upon oxidation high amounts of highly oxidized SOA. Generally, long-chain hydrocarbons with many oxygen atoms are thermodynamically unstable, while highly oxidised aerosol is more likely to be produced in fewer generations from smaller precursor hydrocarbons [61]. Therefore this suggests that the remarkably high O:C ratio here results from the oxidation and condensation of smaller, unknown SOA precursor hydrocarbons or processes.

6.4 Secondary organic aerosol yields from gasoline emissions

Eq. 15 defines a SOA yield (yield=aerosol produced/ hydrocarbon reacted). Unfortunately, information on how much of initial hydrocarbon emission has reacted inside the smog chamber to produce SOA during this study is not available; the THC analyser does not discriminate between the initial VOC and gas phase reaction products. However Fig. 43 indicates that despite significant SOA production, only around 5 % of emitted VOC and particle phase carbon condenses to the particle phase in the case of gasoline cars at an OH exposure of 12×10^{6} molecules cm^{-3} h. I.e. a large SOA yield is not required in order to account for the SOA production from vehicle emissions.

An estimated maximum SOA production ($\Delta OA_{predicted}$) from light aromatic hydrocarbons in the emissions (benzene, toluene, C2-benzenes, C3-benzenes or naphthalene) can be determined using

$$\Delta OA_{predicted} = \sum_i (\Delta_i \times Y_i) \quad , \qquad (22)$$

where Δ_i is the change in concentration of an aromatic hydrocarbon *i*, measured from the smog chamber using PTR-ToF-MS and Y_i is the low NO_X SOA yield of aromatic *i*. SOA yields for benzene, toluene, and *m*-xylene (~0.3) are taken from Ng et al., (2007) [32]. The low NO_X SOA yield for *m*-xylene is used for all C2 and C3 benzenes, while the SOA yield for naphthalene (0.73) is taken from Chan et al., (2009) [62]. Low NO_X yields are used since these are higher than high NO_X yields, thereby allowing a maximum estimation, (even though high NO_X yields would likely be more applicable for an accurate estimation). Fig. 48 shows that, using this methodology $\Delta OA_{predicted}$ accounts for <20 % of the observed SOA production. Candidate non aromatic (unknown) precursors may include smaller, highly oxygenated hydrocarbons, as suggested by the high O:C ratio of the aged OA. Odum et al., (1997) [14] assume that the composition of gasoline vehicle exhaust matches that of raw gasoline and suggest that SOA formation from gasoline vehicle emissions may be accounted for by aromatic oxidation. However, Fig. 43 shows that although there would be enough aromatic hydrocarbons in the raw fuel to produce the SOA observed here while only requiring modest SOA yields, the VOC composition of the exhaust over a full driving cycle is significantly different to that of raw gasoline. Strikingly, the total carbon content of the aged OA is actually higher than the total carbon emitted as light aromatic hydrocarbons. This demonstrates that, at least in the case of this vehicle, aromatics in raw gasoline cannot be used to account for SOA production. This result is consistent with previous vehicle emission aging studies [3, 63]. However, these results contradict Nordin et al., (2013) [60] who suggest that around 60 % of gasoline SOA may be explained by aromatic oxidation. This may be a consequence of the different methodology employed, Nordin et al., (2013) [60] used older test vehicles which were operated under engine idling and relatively low temperature (ambient, outdoor). This suggests an influence of driving conditions on SOA formation. To understand and quantify SOA formation from vehicles, emissions generated under controlled, repeatable, and as realistic as possible conditions may be required.

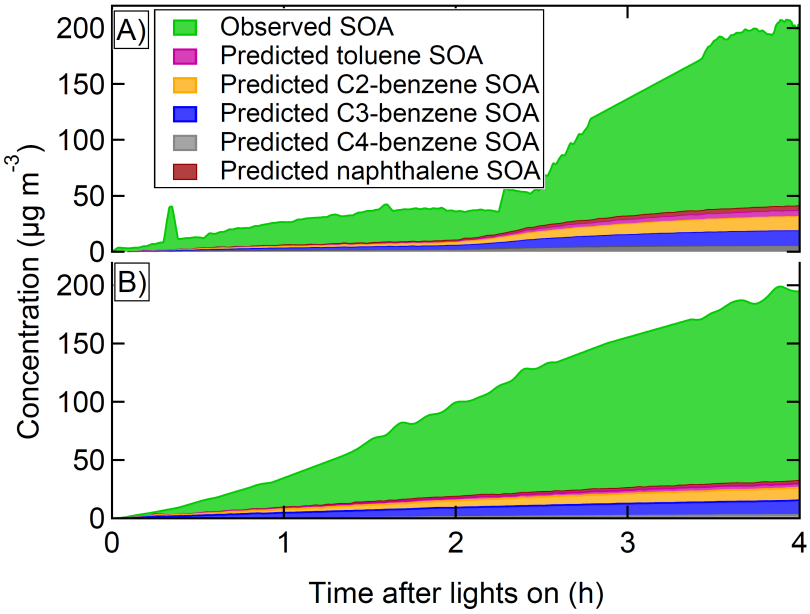

Figure 48: *Observed secondary organic aerosol (SOA) formation, wall loss corrected, green, in the mobile smog chamber during aging of emissions from a Euro 5 gasoline light duty vehicle and predicted SOA formation based on measurement of aromatic*

hydrocarbon decay for Exp 1 (A) and Exp 2 (B). Low NO_X yields are used to predict SOA from the aromatics in order to provide an upper limit. Only a small fraction of observed SOA is explained by the oxidation of aromatic hydrocarbons.

7 Development of a flow tube reactor for the study of combustion emissions

In addition to the mobile smog chamber measurements discussed previously, the Ispra 2013 measurement campaign served as the first deployment of a continuous flow reactor developed at PSI. The flow reactor was intended to complement chamber measurements in two ways: (1) improve measurement statistics by providing a near real-time measurement of secondary organic aerosol (SOA) formation potential (compared to the one-experiment-per-day protocol required by the smog chamber), and (2) investigate the SOA formation potential as a function of location in the regulatory driving cycle. Results obtained during the Ispra campaign are promising with respect to the first objective, while the second requires modifications to the reactor system.

In the PSI flow reactor (Fig. 49), emissions are continuously sampled (3.5 L min^{-1}), mixed with humidified air (1 L min^{-1}) and a flow (0.5 L min^{-1}) containing either O_3 or HONO, which serve as OH precursors. The humidified air is produced by flowing air through a Nafion humidifier (Perma Pure LLC, Toms River, NJ, USA), O_3 is produced by irradiating air with a mercury lamp at 185 nm, and HONO is generated by the reaction of $NaNO_2$ with H_2SO_4. The mixed flow then enters the reaction zone, which consists of a fused silica glass tube (28 cm diameter, 100 cm length).

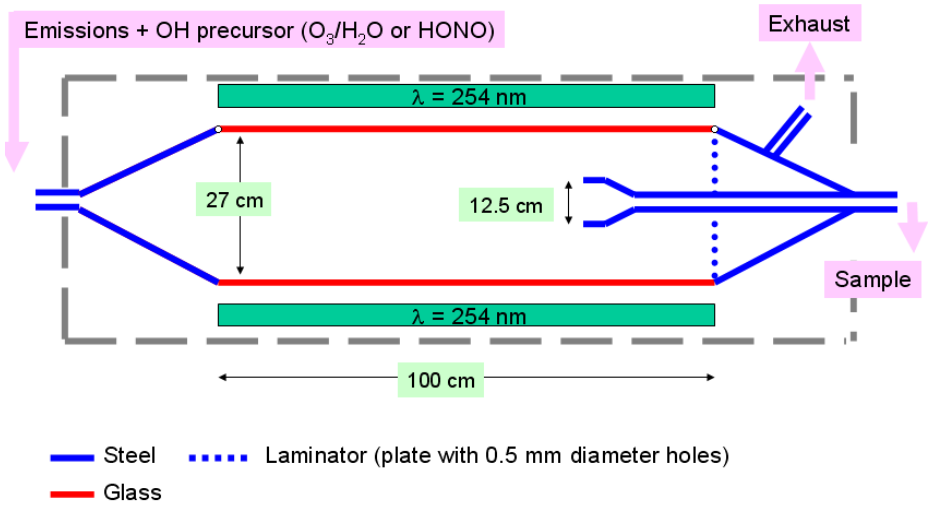

Fig. 49: *Schematic of the PSI flow reactor.*

Here the mixture is irradiated by a bank of 4 mercury grid lamps (BHK Inc., Ontario, CA, USA) at 254 nm, producing OH radicals. The flow enters through a conical stainless steel flange to reduce jets and turbulent mixing. A fraction of the flow (1 L min^{-1}) is sampled isokinetically from the center of the tube using a moveable stainless steel sampling probe (12 cm diameter). The remainder of the flow is exhausted through an aluminium flange drilled with 60 0.5 mm holes to encourage laminar flow through the reactor. Exposure time is governed by probe position, while OH radical concentrations are controlled by the injected O_3 concentration. During the Ispra campaign, the reactor sampled from either (1) a constant volume sampler (CVS) attached to the vehicle tailpipe during regulatory driving cycles, or (2) directly from the smog chamber. Results obtained from position (1) are discussed below.

Prior to the measurement campaign, reactor residence time was investigated using pulses of test particles (NH_4NO_3 with diameter = 300 nm). A mode residence time of 5 minutes was observed (consistent with laminar flow conditions), with the signal decaying to ~10% of maximum after 11 min. However, test measurements following the Ispra campaign demonstrated that this decay to 10% of maximum signal required 45 to 60

min,, and these post-tests were more consistent with behavior during the campaign. We speculate that leaks around the edges of the laminator and/or clogging in the laminator hole degraded the reactor performance. As a result, the reactor behaved more similarly to a stirred flow reactor rather than a laminar flow reactor. Thus it was not possible to resolve SOA production potential as a function of test cycle phase, and OH exposure (OH concentration x time) was not well defined, because a range of exposures were present in the system.

Nonetheless, even in this sub-optimal state the reactor was able to qualitatively demonstrate differences between vehicle SOA production potentials consistent with chamber measurements. Figure 50 shows the time-integrated organic mass concentration (mass concentration x time) for representative tests of gasoline, flexi-fuel, and diesel vehicles at -7 and 22 C. The asymptotic limit approached by these functions is related to the total OA emission factor, and is dominated by SOA in all cases. The figure suggests that, after aging, gasoline vehicle emissions produce approximately an order of magnitude more OA at -7 C than 22 C, consistent with chamber measurements (see Fig. 2). Time-integrated OA from flexi-fuel cars was on the order of the 22 C gasoline experiments, with diesel cars an additional order of magnitude lower (again roughly consistent with chamber measurements). Test-to-test variations were on the order of +/- 20%. While these measurements require additional corrections for e.g. dilution and fuel consumption before OA emission factors can be calculated, the qualitative agreement with chamber measurements suggests this may be a productive method for rapid estimation of SOA production potentia

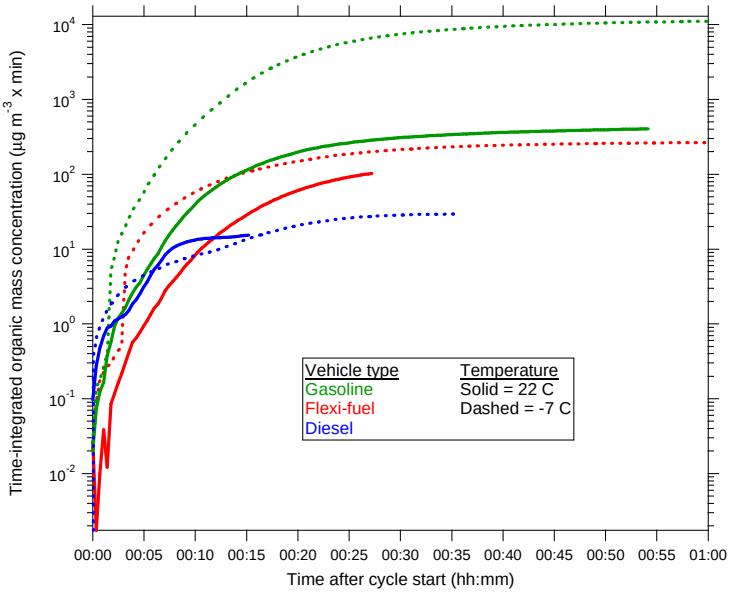

Fig. 50*. Time-integrated OA mass concentrations for gasoline, flexi-fuel, and diesel cars at -7 and 22 C.*

Glossar

Begriff	Bedeutung
2S	Two-stroke
4S	Four-stroke
AMS	Aerosol mass spectrometer
BC	Black carbon
BTEX	Benzene, toluene, ethyl benzene, and xylenes
C3H6	Propene
CE	Collection efficiency
CH4	Methane
CO	Carbon monoxide
CO2	Carbon dioxide
CPC	Condensation particle counter
CVS	Constant volume sampler
DAQ	Data acquisition unit
DI	Direct injection
DLDV	Diesel light duty vehicle
DPF	Diesel particle filter
EF	Emission factor
ETC	European transient cycle
EU	European Union
FID	Flame ionisation detector
GC-FID	Gas chromatography flame ionisation detector
GLDV	Gasoline light duty vehicle
H2O	Water
HC	Hydrocarbon
HDDV	Heavy duty diesel vehicle
HR-FTIR	High resolution Fourier transformed infra red
HRP	Horse radish peroxidase
HR-ToF-AMS	High resolution time-of-flight aerosol mass spectrometer
HONO	Nitrous acid
JRC	Joint Research Center
LPG	Liquid petroleum gas
MPI	Multipoint injection
N2	Nitrogen
NEDC	New European Driving Cycle
NH3	Ammonia
NO3	Nitrate
NO2	Nitrogen dioxide
NO	Nitrogen monoxide
NOx	Oxides of nitrogen, NO+NO2
NMHC	Non methane hydrocarbon
O3	Ozone
OA	Organic aerosol
OC	Organic carbon
OFP	Ozone forming potential
OH	Hydroxyl radical

PM	Particulate matter
POA	Primary organic aerosol
POC	Primary organic carbon
ppb	Parts per billion
ppb(v)	Parts per billion by volume
ppm	Parts per million
ppmC	Parts per million of carbon
ppm(v)	Parts per million by volume
ppt	Parts per trillion
ppt(v)	Parts per trillion by volume
PSI	Paul Scherrer Institute
PTR-ToF-MS	Proton transfer reaction time-of-flight mass spectrometer
PTW	Powered two-wheeler
RH	Relative humidity
ROS	Reactive oxygen species
SCR	Selective catalytic reduction
SMPS	Scanning mobility particle sizer
SOA	Secondary organic aerosol
SOC	Secondary organic carbon
THC	Total hydrocarbon
TWC	Three way catalyst
UV	Ultraviolet radiation
VELA	Vehicle emissions laboratory
VOC	Volatile organic compound

Literaturverzeichnis

[1]	Seinfeld, J.H. and S.N. Pandis, ***Atmospheric Chemistry and Physics***, ed. J.H. Seinfeld and S.N. Pandis. 2006: Wiley.
[2]	IPCC, ***Contribution of Working Group I to the Fourth Assessment Report of the Intergovernmental Panel on Climate Change***. 2007: Cambridge University Press.
[3]	Robinson, A.L., et al., **Rethinking organic aerosols: Semivolatile emissions and photochemical aging**. Science, 2007. **315**(5816): p. 1259.
[4]	Zhang, Q., et al., **Ubiquity and dominance of oxygenated species in organic aerosols in anthropogenically-influenced Northern Hemisphere midlatitudes.** Geophysical Research Letters, 2007. **34**(13): p. L13801.
[5]	EEA, **EMEP/ CORINAIR Emission Inventory Guidebook**. 2006, European Environment Agency: http://reports.ee.europa.eu/EMEPCORINAIR4, last accessed May 2nd 2012.
[6]	Bahreini, R., et al., **Gasoline emissions dominate over diesel in formation of secondary organic aerosol mass.** Geophysical Research Letters, 2012. **39**(6): p. L06805.
[7]	Gentner, D.R., et al., **Elucidating secondary organic aerosol from diesel and gasoline vehicles through detailed characterization of organic carbon emissions.** Proceedings of the National Academy of Sciences, 2012. **109**(45): p. 18318-18323.
[8]	Hallquist, M., et al., **The formation, properties and impact of secondary organic aerosol: current and emerging issues.** Atmospheric Chemistry and Physics, 2009. **9**(14): p. 5155.
[9]	Presto, A.A., et al., **Fine particle and organic vapor emissions from staged tests of an in-use aircraft engine**. Atmospheric Environment, 2011. **45**: p. 3603-3612.
[10]	Barlow, T.J., et al., **A reference book of driving cycles for use in the measurement of road vehicle emissions.** Vol. 1. 2009.
[11]	Taira, M. and Y. Kanda, **Continuous generation system for low-concentration gaseous nitrous acid**. Analytical Chemistry, 1990. **62**(6): p. 630-633.
[12]	Clairotte, M., et al., **Online Characterization of Regulated and Unregulated Gaseous and Particulate Exhaust Emission from Two-Stroke Mopeds: A Chemometric Approach**. Analytica Chimica Acta, 2011.
[13]	Barmet, P., et al., *OH clock determination by proton transfer reaction mass spectrometry at an environmental chamber.* Atmospheric Measurement Techniques, 2012. **5**: p. 647-656.
[14]	Odum, J.R., et al., **Aromatics, reformulated gasoline, and atmospheric organic aerosol formation**. Environmental science and technology, 1997. **31**(7): p. 1890-1897.
[15]	Chirico, R., et al., **Impact of aftertreatment devices on primary emissions and secondary organic aerosol formation potential from in-use diesel vehicles: results from smog chamber experiments.** Atmospheric Chemistry and Physics, 2010. **10**(23): p. 11545-11563.
[16]	Song, C., et al., **Impact of propene on secondary organic aerosol formation from m-xylene**. Environmental science and technology, 2007. **41**(20): p. 6990-6995.
[17]	DeCarlo, P.F., et al., **Field-deployable, high-resolution, time-of-flight aerosol mass spectrometer**. Analytical Chemistry, 2006. **78**(24): p. 8281-8289.
[18]	Middlebrook, A.M., et al., **Evaluation of composition-dependent collection efficiencies for the Aerodyne aerosol mass spectrometer using field data**. Aerosol Science and Technology, 2012. **46**(3): p. 258-271.
[19]	Matthew, B.M., A.M. Middlebrook, and T.B. Onasch, **Collection efficiencies in an Aerodyne Aerosol Mass Spectrometer as a function of particle phase for laboratory generated aerosols.** Aerosol Science and Technology, 2008. **42**(11): p. 884-898.
[20]	Williams, L.R., et al., **Characterization of an aerodynamic lens for transmitting particles> 1 micrometer in diameter into the Aerodyne aerosol mass spectrometer**. Aerosol Measurement Techniques Discussions, 2013. **6**: p. 5033–5063.
[21]	Saathoff, H., et al., **Coating of soot and (NH4) 2SO4 particles by ozonolysis products of [alpha]-pinene**. Journal of aerosol science, 2003. **34**(10): p. 1297-1321.
[22]	Paulsen, D., et al., **Secondary Organic Aerosol Formation by Irradiation of 1, 3, 5-Trimethylbenzene-NO x-H2O in a New Reaction Chamber for Atmospheric Chemistry and Physics.** Environmental science and technology, 2005. **39**(8): p. 2668-2678.
[23]	Carter, W.P.L., **National Renewable Energy Laboratory (US), Environmental chamber studies of atmospheric reactivities of volatile organic compounds: Effects of varying chamber and light source.** 1995: Statewide Air Pollution Research Center.
[24]	Atkinson, R., et al., **Evaluated kinetic and photochemical data for atmospheric chemistry: Volume I-gas phase reactions of Ox, HOx, NOx and SOx species.** Atmospheric Chemistry and Physics, 2004. **4**(4): p. 1461-1738.
[25]	Atkinson, R., et al., **Evaluated kinetic and photochemical data for atmospheric chemistry:**

Volume II: gas phase reactions of organic species. Atmospheric Chemistry and Physics, 2006. **6**(11): p. 3625-4055.

[26] DeMore, W.B., et al., **Chemical kinetics and photochemical data for use in stratospheric modeling.** 1997, Jet Propulsion Lab., California Inst. of Tech., Pasadena, CA.

[27] Johnston, H.S., H.F. Davis, and Y.T. Lee, **NO3 Photolysis product channels: Quantum yields from observed energy thresholds.** The Journal of Physical Chemistry, 1996. **100**(12): p. 4713-4723.

[28] Malicet, J., et al., **Ozone UV spectroscopy. II. Absorption cross-sections and temperature dependence**. Journal of atmospheric chemistry, 1995. **21**(3): p. 263-273.

[29] Prinn, R.G., et al., **Evidence for substantial variations of atmospheric hydroxyl radicals in the past two decades**. Science, 2001. **292**(5523): p. 1882-1888.

[30] Donahue, N.M., et al., **Aging of Secondary Organic Aerosol via Gas-Phase OH Radical Reactions.** Proceedings of the National Academy of Sciences of the United States of America, 2012. **109**: p. 13503-13508.

[31] Geivanidis, S., et al., **Study on possible new measures concerning motorcycle emissions**. Arisotle University Thessaloniki, Thessaloniki, 2008.

[32] Ng, N.L., et al., **Secondary organic aerosol formation from m-xylene, toluene, and benzene**. Atmospheric Chemistry and Physics, 2007. **7**: p. 3909-3922.

[33] Lan, T.T.N. and N.T.T. Binh, **Daily roadside BTEX concentrations in East Asia measured by the Lanwatsu, Radiello and Ultra I SKS passive samplers.** Science of the Total Environment, 2012. **441**: p. 248-257.

[34] Platt, S.M., et al., **Secondary organic aerosol formation from gasoline vehicle emissions in a new mobile environmental reaction chamber**. Atmospheric Chemistry and Physics, 2013. **13**(18): p. 9141-9158.

[35] EC, **European Commission Regulation No 692/2008 of 18 July 2008 implementing and amending Regulation (EC) No 715/2007 of the European Parliament and of the Council on type-approval of motor vehicles with respect to emissions from light passenger and commercial vehicles (Euro 5 and Euro 6) and on access to vehicle repair and maintenance information**. Official Journal of the European Communities, 2008. **L199**.

[36] Chirico, R., et al., **Chassis dynamometer measurements of organic mass, particle number, and regulated and unregulated gas emissions from mopeds and heavy duty vehicles**. in Prep.

[37] Spezzano, P., P. Picini, and D. Cataldi, **Contribution of unburned lubricating oil and gasoline-derived n-alkanes to particulate emission from non-catalyst and catalyst-equipped two-stroke mopeds operated with synthetic lubricating oil.** Journal of Environmental Monitoring, 2008. **10**(10): p. 1202-1210.

[38] Chhabra, P.S., R.C. Flagan, and J.H. Seinfeld, **Elemental analysis of chamber organic aerosol using an aerodyne high-resolution aerosol mass spectrometer.** Atmospheric Chemistry and Physics, 2010. **10**(9): p. 4111-4131.

[39] Klaassen, G., C. Berglund, and F. Wagner, **The GAINS Model for Greenhouse Gases-Version 1.0: Carbon Dioxide (CO2). IIASA Interim Report IR-05-53.** International Institute for Applied Systems Analysis (IIASA), Laxenburg, Austria, 2005.

[40] Cai, H. and S.D. Xie, **Tempo-spatial variation of emission inventories of speciated volatile organic compounds from on-road vehicles in China.** Atmospheric Chemistry and Physics, 2009. **9**(18): p. 6983-7002.

[41] Yang, C.J., **Launching strategy for electric vehicles: Lessons from China and Taiwan.** Technological Forecasting and Social Change. **77**(5): p. 831-834.

[42] Santino, D., P. Picini, and L. Martino, **Particulate matter emissions from two-stroke mopeds**. ENEA Italy, SAE Naples, 2001: p. 01-068.

[43] McWhinney, R.D., et al., **Evaluation of the Effects of Ozone Oxidation on Redox-Cycling Activity of Two-Stroke Engine Exhaust Particles.** Environmental science & technology, 2005.

[44] Mertes, P., et al., **Development of a sensitive long path absorption photometer to quantify peroxides in aerosol particles (Peroxide-LOPAP).** Atmospheric Measurement Techniques, 2012. **5**: p. 2339-2348.

[45] Surratt, J.D., et al., **Chemical composition of secondary organic aerosol formed from the photooxidation of isoprene.** The Journal of Physical Chemistry A, 2006. **110**(31): p. 9665-9690.

[46] ACEM, **Association des Constructeurs Europeans de Motocycles: ACEM year boon 2011-Facts and figures on PTWs in Europe**. *Available at htto:??www.acem.eu; accessed July 2011.* 2011.

[47] WUP, **World Urbanization Prospects: The 2011 Revision. Edited by: United Nations Department of Economic and Social Affairts. Available at: http://esa.un.org/wup/index.thm** *Accessed on: April 1sr, 2013.* 2011.

[48] Adam, T., et al., **Chemical Characterization of Emissions from Modern Two-Stroke Mopeds Complying with Legislative Regulation in Europe (EURO-2).** Environmental science and technology, 2010. **44**(1): p. 505-512.

[49]	Prati, M.V. and M.A. Costagliola**, Emissions of fine particles and organic compounds from mopeds.** Environmental Engineering Science, 2009. **26**(1): p. 111-122.
[50]	Jimenez, J.L., et al., *Evolution of organic aerosols in the atmosphere.* Science, 2009. **326**(5959): p. 1525.
[51]	Aalander, T., et al., **Particle emissions from a small two-stroke engine: effects of fuel, lubricating oil, and exhaust aftertreatment on particle characteristics**. Aerosol science and technology, 2005. **39**(2): p. 151-161.
[52]	Carter, W.P.L., **Development of ozone reactivity scales for volatile organic compounds.** Air \& waste, 1994. **44**(7): p. 881-899.
[53]	EC, **Regulated emissions of a Euro 5 passenger car measured over different driving cycles.** 2010, European Commission Joint Research Centre (JRC) Institute for Environment and Sustainability: http://www.unece.org/fileadmin/DAM/trans/doc/2010/wp29grpe/WLTP-DHC-04-03e.pdf last accessed July 9th 2012
[54]	Sandradewi, J., et al., **A study of wood burning and traffic aerosols in an Alpine valley using a multi-wavelength Aethalometer**. Atmospheric Environment, 2008. **42**(1): p. 101-112.
[55]	Johnson, T.V., **Diesel emission control in review**. SAE International Journal of Fuels and Lubricants, 2008. **1**(1): p. 68-81.
[56]	Weilenmann, M., J.-Y. Favez, and R. Alvarez, **Cold-start emissions of modern passenger cars at different low ambient temperatures and their evolution over vehicle legislation categories.** Atmospheric environment, 2009. **43**(15): p. 2419-2429.
[57]	Ng, N.L., et al., **Organic aerosol components observed in Northern Hemispheric datasets from Aerosol Mass Spectrometry.** Atmospheric Chemistry and Physics, 2010. **10**: p. 4625-4641.
[58]	Aiken, A.C., et al., **O/C and OM/OC ratios of primary, secondary, and ambient organic aerosols with high-resolution time-of-flight aerosol mass spectrometry.** Environmental Science and Technology, 2008. **42**(12): p. 4478-4485.
[59]	Heringa, M.F., et al., **Investigations of primary and secondary particulate matter of different wood combustion appliances with a high-resolution time-of-flight aerosol mass spectrometer.** Atmospheric Chemistry and Physics, 2011. **11**: p. 5945-5957.
[60]	Nordin, E.Z., et al., **Secondary organic aerosol formation from idling gasoline passenger vehicle emissions investigated in a smog chamber.** Atmospheric Chemistry and Physics, 2013. **13**: p. 6101-6116.
[61]	Kroll, J.H., et al., **Carbon oxidation state as a metric for describing the chemistry of atmospheric organic aerosol.** Nature Chemistry, 2011. **3**(2): p. 133-139.
[62]	Chan, A.W.H., et al., **Secondary organic aerosol formation from photooxidation of naphthalene and alkylnaphthalenes: implications for oxidation of intermediate volatility organic compounds (IVOCs).** Atmos. Chem. Phys, 2009. **9**(9): p. 3049-3060.
[63]	Grieshop, A.P., et al., **Laboratory investigation of photochemical oxidation of organic aerosol from wood fires 1: measurement and simulation of organic aerosol evolution**. Atmospheric Chemistry and Physics, 2009. **9**(4): p. 1263-1277.

Projektabschluss

Schweizerische Eidgenossenschaft
Confédération suisse
Confederazione Svizzera
Confederaziun svizra

Eidgenössisches Departement für
Umwelt, Verkehr, Energie und Kommunikation UVEK
Bundesamt für Strassen ASTRA

FORSCHUNG IM STRASSENWESEN DES UVEK Version vom 09.10.2013

Formular Nr. 3: Projektabschluss

erstellt / geändert am: 12.12. 2013

Grunddaten

Projekt-Nr.:	ASTRA 2010/021
Projekttitel:	Sekundärer Feinstaub vom Verkehr (S-Feinstaub)
Enddatum:	31.12.2013

Texte

Zusammenfassung der Projektresultate:

Der Verkehr ist bekannt als Quelle von Feinstaub, darunter kohlenstoffhaltigem krebserregendem Russ. In der vorliegenden Studie konnte gezeigt werden, dass der Feinstaub, welcher durch flüchtige Kohlenwasserstoffemissionen und nachfolgender Oxidation in der Atmosphäre entsteht (Sekundärer organischer Feinstaub - SOA), für alle Fahrzeugkategorien wichtig, oft deutlich bedeutsamer ist als der direkt emittierte Feinstaub. Diese Resultate wurden durch mobile Smogkammerexperimente an den Motorenprüfständen des europäischen Forschungszentrums in Ispra, Italien erarbeitet. Die wichtigsten Resultate sind im Folgenden zusammengefasst. Dabei muss festgehalten werden, dass sie auf relativ kleinen Stichproben (2-3 Fahrzeuge pro Fahrzeugkategorie) beruhen und deshalb entsprechende Unsicherheiten aufweisen.

- Moderne (Euro 5) Personenwagen mit Benzin produzieren im Durchschnitt mehr sekundären organischen Feinstaub und emittieren auch mehr primäres organisches Aerosol (im Durchschnitt sechsmal mehr) als Euro-5-Personenwagen mit Diesel, welche wie üblich mit Partikelfilter ausgerüstet sind. Der überwiegende Anteil der SOA-Vorläuferstoffe wird bei den Benzinfahrzeugen während des Kaltstarts emittiert, also solange der Katalysator seine Funktion noch nicht erfüllen kann.

- Kalte Umgebungstemperaturen (-7°C versus 22°C) haben bei Benzinfahrzeugen dramatische Effekte auf die Kaltstartemissionen und die SOA-Bildung. Die Abgasemissionen von VOC und von kohlenstoffhaltigem Feinstaub (inklusive SOA) steigen um ein Mehrfaches an, während bei Personenwagen mit Diesel kein Temperatureffekt feststellbar ist. Der Beitrag von Benzinfahrzeugen an die Belastung mit kohlenstoffhaltigem Aerosol ist somit im Winter wegen den hohen Emissionen während des verlängerten Kaltstarts deutlich erhöht.

- Zweitakt-Mopeds sind extreme Emittenten. Bezogen auf den verbrauchten Treibstoff emittieren sie höchste Mengen an primärem Feinstaub und toxischen gasförmigen Aromaten. Zudem bilden sie beträchtliche Mengen von SOA. Die gesamte kohlenstoffhaltige Feinstaubmasse (POA+BC+SOA) ist etwa 100-mal (Median) höher als bei einem Benzinfahrzeug. Selbst wenn nur ein kleiner Teil der Fahrzeugflotte aus Mopeds besteht und diese nur einen geringen Anteil des gesamten Treibstoffs verbrauchen, können sie zum dominanten verkehrsbedingten Feinstaub-Produzenten werden. Dies trifft insbesondere in Teilen von Süd-Ost-Asien, Afrika und Südeuropa zu. Auch in Europa und der Schweiz ist ihr Beitrag an den verkehrsbedingten Feinstaub relevant - trotz ihres sehr kleinen Anteils am Treibstoffverbrauch.

- Bei den untersuchten Lastwagen ist im Gegensatz zu den Personenwagen der Anteil des sekundär produzierten Feinstaubes im Vergleich zu den Emissionen vergleichsweise gering.

Schweizerische Eidgenossenschaft
Confédération suisse
Confederazione Svizzera
Confederaziun svizra

Eidgenössisches Departement für
Umwelt, Verkehr, Energie und Kommunikation UVEK
Bundesamt für Strassen ASTRA

Zielerreichung:

Die gesetzten Ziele wurden erreicht. Die Bedeutung des sekundären Feinstaubs vom Verkehr konnte bei verschiedenen Bedingungen (Temperatur, Feuchte) dokumentiert werden.

Baumaschinen-Experimente wurden wurden in Absprache mit der Begleitkommission keine durchgeführt und durch eine grössere Anzahl Wiederholungen bei den Personenwagen-Experimente ersetzt.

Folgerungen und Empfehlungen:

- 2-Takt-Mopeds ist keine adäquate Technologie in der heutigen Zeit. Die toxischen Emisssionen und das Feinstaubbildungspotential sind massiv.

- Die Entwicklung von technischen Verbesserungen zur Reduktion von partikel- und gasförmigen Emissionen bei Benzinfahrzeugen, insbesondere beim Kaltstart, sollten höhere Priorität bekommen

Publikationen:

Platt, S. M., I. El Haddad, A. A. Zardini, M. Clairotte, C. Astorga, R. Wolf, J. G. Slowik, B. Temime-Roussel, N. Marchand, I. Jezek, L. Drinovec, G. Mocnik, O. Mohler, R. Richter, P. Barmet, F. Bianchi, U. Baltensperger, and A. S. H. Prevot (2013) Secondary organic aerosol formation from gasoline vehicle emissions in a new mobile environmental reaction chamber, Atmospheric Chemistry and Physics, 13(18), 9141-9158.

Weitere Publikationen wurden eingereicht und sind in Vorbereitung

Der Projektleiter/die Projektleiterin:

Name: Prevot Vorname: Andre

Amt, Firma, Institut: Labor für Atmosphärenchemie, Paul Scherrer Institut

Unterschrift des Projektleiters/der Projektleiterin:

Schweizerische Eidgenossenschaft
Confédération suisse
Confederazione Svizzera
Confederaziun svizra

Eidgenössisches Departement für
Umwelt, Verkehr, Energie und Kommunikation UVEK
Bundesamt für Strassen ASTRA

FORSCHUNG IM STRASSENWESEN DES UVEK

Formular Nr. 3: Projektabschluss

Beurteilung der Begleitkommission:

Beurteilung:

Das Projekt wurde sachkundig und sorgfältig durchgeführt. Die Resultate und der Schlussbericht weisen hohe fachliche Qualität auf und sind national und international von Interesse. Es resultieren wertvolle Erkenntnisse über die Bildung von sekundärem organischem Aerosol (einem Bestandteil des lungengängigen Feinstaubs PM10) aus Vorläuferemissionen verschiedener Fahrzeugkategorien des Strassenverkehrs. Die Resultate geben Hinweise, in welche Richtung sich Technik und Abgasgesetzgebung künftig entwickeln sollten. Die Projektziele wurden weitgehend erreicht.

Umsetzung:

Die Verminderung der strassenverkehrsbedingten Luftbelastung durch lungengängigen Feinstaub PM10 zum Schutz der Umwelt und der Gesundheit ist eine wichtige Aufgabe (Vollzug der Umweltschutzgesetzgebung).
Die Identifikation und Quantifizierung der relevanten Feinstaub-Bildungsprozesse aus Vorläuferemissionen des Strassenverkehrs durch das Projekt "Sekundärer Feinstaub vom Verkehr" trägt zu einer gezielten Minderungsstrategie bei. Die wichtigsten Ursachen für die Bildung beträchtlicher Mengen an sekundärem organischem Feinstaub konnten identifiziert werden.

weitergehender Forschungsbedarf:

- Untersuchungen von Euro 6 Personenwagen und Euro VI Lastwagen (Auswirkung neuester Technologie);
- Untersuchungen von zusätzlichen Fahrzeugen für eine bessere statistische Abstützung, allenfalls gekoppelt mit Tunnelmessungen und Parkhausemissionen, um die aktuelle Flotte im Durchschnitt zu erfassen.
- Detaillierte Untersuchungen zu kombinierten Effekten von Ammoniak und Verkehrsemissionen.

Einfluss auf Normenwerk:

kein unmittelbarer Einfluss

Der Präsident/die Präsidentin der Begleitkommission:

Name: Schiess Vorname: Martin

Amt, Firma, Institut: Bundesamt für Umwelt, Abteilung Luftreinhaltung und Chemikalien

Unterschrift des Präsidenten/der Präsidentin der Begleitkommission:

Verzeichnis der Berichte der Forschung im Strassenwesen

Stand: 31.10.2013

Bericht-Nr.	Projekt Nr.	Titel	Jahr
1422	ASTRA 2011/006_OBF	Fracture processes and in-situ fracture observations in Gipskeuper	2013
1421	VSS 2009/901	Experimenteller Nachweis des vorgeschlagenen Raum- und Topologiemodells für die VM-Anwendungen in der Schweiz (MDATrafo)	2013
1420	SVI 2008/003	Projektierungsfreiräume bei Strassen und Plätzen	2013
1419	VSS 2001/452	Stabilität der Polymere beim Heisseinbau von PmB-haltigen Strassenbelägen	2013
1416	FGU 2010/001	Sulfatwiderstand von Beton: verbessertes Verfahren basierend auf der Prüfung nach SIA 262/1, Anhang D	2013
1415	VSS 2010/A01	Wissenslücken im Infrastrukturmanagementprozess "Strasse" im Siedlungsgebiet	2013
1414	VSS 2010/201	Passive Sicherheit von Tragkonstruktionen der Strassenausstattung	2013
1413	SVI 2009/003	Güterverkehrsintensive Branchen und Güterverkehrsströme in der Schweiz Forschungspaket UVEK/ASTRA Strategien zum wesensgerechten Einsatz der Verkehrsmittel im Güterverkehr der Schweiz Teilprojekt B1	2013
1412	ASTRA 2010/020	Werkzeug zur aktuellen Gangliniennorm	2013
1411	VSS 2009/902	Verkehrstelematik für die Unterstützung des Verkehrsmanagements in ausserordentlichen Lagen	2013
1410	VSS 2010/202_OBF	Reduktion von Unfallfolgen bei Bränden in Strassentunneln durch Abschnittsbildung	2013
1409	ASTRA 2010/017_OBF	Regelung der Luftströmung in Strassentunneln im Brandfall	2013
1408	VSS 2000/434	Vieillissement thermique des enrobés bitumineux en laboratoire	2012
1407	ASTRA 2006/014	Fusion des indicateurs de sécurité routière : FUSAIN	2012
1406	ASTRA 2004/015	Amélioration du modèle de comportement individuell du Conducteur pour évaluer la sécurité d'un flux de trafic par simulation	2012
1405	ASTRA 2010/009	Potential von Photovoltaik an Schallschutzmassnahmen entlang der Nationalstrassen	2012
1404	VSS 2009/707	Validierung der Kosten-Nutzen-Bewertung von Fahrbahn-Erhaltungsmassnahmen	2012
1403	SVI 2007/018	Vernetzung von HLS- und HVS-Steuerungen	2012
1402	VSS 2008/403	Witterungsbeständigkeit und Durchdrückverhalten von Geokunststoffen	2012

Bericht-Nr.	Projekt Nr.	Titel	Jahr
1401	SVI 2006/003	Akzeptanz von Verkehrsmanagementmassnahmen-Vorstudie	2012
1400	VSS 2009/601	Begrünte Stützgitterböschungssysteme	2012
1399	VSS 2011/901	Erhöhung der Verkehrssicherheit durch Incentivierung	2012
1398	ASTRA 2010/019	Environmental Footprint of Heavy Vehicles Phase III: Comparison of Footprint and Heavy Vehicle Fee (LSVA) Criteria	2012
1397	FGU 2008/003_OBF	Brandschutz im Tunnel: Schutzziele und Brandbemessung Phase 1: Stand der Technik	2012
1396	VSS 1999/128	Einfluss des Umhüllungsgrades der Mineralstoffe auf die mechanischen Eigenschaften von Mischgut	2012
1395	FGU 2009/003	KarstALEA: Wegleitung zur Prognose von karstspezifischen Gefahren im Untertagbau	2012
1394	VSS 2010/102	Grundlagen Betriebskonzepte	2012
1393	VSS 2010/702	Aktualisierung SN 640 907, Kostengrundlage im Erhaltungsmanagement	2012
1392	ASTRA 2008/008_009	FEHRL Institutes WIM Initiative (Fiwi)	2012
1391	ASTRA 2011/003	Leitbild ITS-CH Landverkehr 2025/30	2012
1390	FGU 2008/004_OBF	Einfluss der Grundwasserströmung auf das Quellverhalten des Gipskeupers im Belchentunnel	2012
1389	FGU 2003/002	Long Term Behaviour of the Swiss National Road Tunnels	2012
1388	SVI 2007/022	Möglichkeiten und Grenzen von elektronischen Busspuren	2012
1387	VSS 2010/205_OBF	Ablage der Prozessdaten bei Tunnel-Prozessleitsystemen	2012
1386	VSS 2006/204	Schallreflexionen an Kunstbauten im Strassenbereich	2012
1385	VSS 2004/703	Bases pour la révision des normes sur la mesure et l'évaluation de la planéité des chaussées	2012
1384	VSS 1999/249	Konzeptuelle Schnittstellen zwischen der Basisdatenbank und EMF-, EMK- und EMT-DB	2012
1383	FGU 2008/005	Einfluss der Grundwasserströmung auf das Quellverhalten des Gipskeupers im Chienbergtunnel	2012
1382	VSS 2001/504	Optimierung der statischen Eindringtiefe zur Beurteilung von harten Gussasphaltsorten	2012
1381	SVI 2004/055	Nutzen von Reisezeiteinsparungen im Personenverkehr	2012
1380	ASTRA 2007/009	Wirkungsweise und Potential von kombinierter Mobilität	2012

Bericht-Nr.	Projekt Nr.	Titel	Jahr
1379	VSS 2010/206_OBF	Harmonisierung der Abläufe und Benutzeroberflächen bei Tunnel-Prozessleitsystemen	2012
1378	SVI 2004/053	Mehr Sicherheit dank Kernfahrbahnen?	2012
1377	VSS 2009/302	Verkehrssicherheitsbeurteilung bestehender Verkehrsanlagen (Road Safety Inspection)	2012
1376	ASTRA 2011/008_004	Erfahrungen im Schweizer Betonbrückenbau	2012
1375	VSS 2008/304	Dynamische Signalisierungen auf Hauptverkehrsstrassen	2012
1374	FGU 2004/003	Entwicklung eines zerstörungsfreien Prüfverfahrens für Schweissnähte von KDB	2012
1373	VSS 2008/204	Vereinheitlichung der Tunnelbeleuchtung	2012
1372	SVI 2011/001	Verkehrssicherheitsgewinne aus Erkenntnissen aus Datapooling und strukturierten Datenanalysen	2012
1371	ASTRA 2008/017	Potenzial von Fahrgemeinschaften	2011
1370	VSS 2008/404	Dauerhaftigkeit von Betonfahrbahnen aus Betongranulat	2011
1369	VSS 2003/204	Rétention et traitement des eaux de chaussée	2012
1368	FGU 2008/002	Soll sich der Mensch dem Tunnel anpassen oder der Tunnel dem Menschen?	2011
1367	VSS 2005/801	Grundlagen betreffend Projektierung, Bau und Nachhaltigkeit von Anschlussgleisen	2011
1366	VSS 2005/702	Überprüfung des Bewertungshintergrundes zur Beurteilung der Strassengriffigkeit	2010
1365	SVI 2004/014	Neue Erkenntnisse zum Mobilitätsverhalten dank Data Mining?	2011
1364	SVI 2009/004	Regulierung des Güterverkehrs Auswirkungen auf die Transportwirtschaft Forschungspaket UVEK/ASTRA Strategien zum wesensgerechten Einsatz der Verkehrsmittel im Güterverkehr der Schweiz TP D	2012
1363	VSS 2007/905	Verkehrsprognosen mit Online -Daten	2011
1362	SVI 2004/012	Aktivitätenorientierte Analyse des Neuverkehrs	2012
1361	SVI 2004/043	Innovative Ansätze der Parkraumbewirtschaftung	2012
1360	VSS 2010/203	Akustische Führung im Strassentunnel	2012
1359	SVI 2004/003	Wissens- und Technologientransfer im Verkehrsbereich	2012
1358	SVI 2004/079	Verkehrsanbindung von Freizeitanlagen	2012
1357	SVI 2007/007	Unaufmerksamkeit und Ablenkung: Was macht der Mensch am Steuer?	2012
1356	SVI 2007/014	Kooperation an Bahnhöfen und Haltestellen	2011

Bericht-Nr.	Projekt Nr.	Titel	Jahr
1355	FGU 2007/002	Prüfung des Sulfatwiderstandes von Beton nach SIA 262/1, Anhang D: Anwendbarkeit und Relevanz für die Praxis	2011
1354	VSS 2003/203	Anordnung, Gestaltung und Ausführung von Treppen, Rampen und Treppenwegen	2011
1353	VSS 2000/368	Grundlagen für den Fussverkehr	2011
1352	VSS 2008/302	Fussgängerstreifen (Grundlagen)	2011
1351	ASTRA 2009/001	Development of a best practice methodology for risk assessment in road tunnels	2011
1350	VSS 2007/904	IT-Security im Bereich Verkehrstelematik	2011
1349	VSS 2003/205	In-Situ-Abflussversuche zur Untersuchung der Entwässerung von Autobahnen	2011
1348	VSS 2008/801	Sicherheit bei Parallelführung und Zusammentreffen von Strassen mit der Schiene	2011
1347	VSS 2000/455	Leistungsfähigkeit von Parkierungsanlagen	2010
1346	ASTRA 2007/004	Quantifizierung von Leckagen in Abluftkanälen bei Strassentunneln mit konzentrierter Rauchabsaugung	2010
1345	SVI 2004/039	Einsatzbereiche verschiedener Verkehrsmittel in Agglomerationen	2011
1344	VSS 2009/709	Initialprojekt für das Forschungspaket "Nutzensteigerung für die Anwender des SIS"	2011
1343	VSS 2009/903	Basistechnologien für die intermodale Nutzungserfassung im Personenverkehr	2011
1342	FGU 2005/003	Untersuchungen zur Frostkörperbildung und Frosthebung beim Gefrierverfahren	2010
1341	FGU 2007/005	Design aids for the planning of TBM drives in squeezing ground	2011
1340	SVI 2004/051	Aggressionen im Verkehr	2011
1339	SVI 2005/001	Widerstandsfunktionen für Innerorts-Strassenabschnitte ausserhalb des Einflussbereiches von Knoten	2010
1338	VSS 2006/902	Wirkungsmodelle für fahrzeugseitige Einrichtungen zur Steigerung der Verkehrssicherheit	2009
1337	ASTRA 2006/015	Development of urban network travel time estimation methodology	2011
1336	ASTRA 2007/006	SPIN-ALP: Scanning the Potential of Intermodal Transport on Alpine Corridors	2010
1335	VSS 2007/502	Stripping bei lärmmindernden Deckschichten unter Überrollbeanspruchung im Labormassstab	2011
1334	ASTRA 2009/009	Was treibt uns an? Antriebe und Treibstoffe für die Mobilität von Morgen	2011
1333	SVI 2007/001	Standards für die Mobilitätsversorgung im peripheren Raum	2011
1332	VSS 2006/905	Standardisierte Verkehrsdaten für das verkehrsträgerübergreifende Verkehrsmanagement	2011

Bericht-Nr.	Projekt Nr.	Titel	Jahr
1331	VSS 2005/501	Rückrechnung im Strassenbau	2011
1330	FGU 2008/006	Energiegewinnung aus städtischen Tunneln: Systemeevaluation	2010
1329	SVI 2004/073	Alternativen zu Fussgängerstreifen in Tempo-30-Zonen	2010
1328	VSS 2005/302	Grundlagen zur Quantifizierung der Auswirkungen von Sicherheitsdefiziten	2011
1327	VSS 2006/601	Vorhersage von Frost und Nebel für Strassen	2010
1326	VSS 2006/207	Erfolgskontrolle Fahrzeugrückhaltesysteme	2011
1325	SVI 2000/557	Indices caractéristiques d'une cité-vélo. Méthode d'évaluation des politiques cyclables en 8 indices pour les petites et moyennes communes.	2010
1324	VSS 2004/702	Eigenheiten und Konsequenzen für die Erhaltung der Strassenverkehrsanlagen im überbauten Gebiet	2009
1323	VSS 2008/205	Ereignisdetektion im Strassentunnel	2011
1322	SVI 2005/007	Zeitwerte im Personenverkehr: Wahrnehmungs- und Distanzabhängigkeit	2008
1321	VSS 2008/501	Validation de l'oedomètre CRS sur des échantillons intacts	2010
1320	VSS 2007/303	Funktionale Anforderungen an Verkehrserfassungssysteme im Zusammenhang mit Lichtsignalanlagen	2010
1319	VSS 2000/467	Auswirkungen von Verkehrsberuhigungsmassnahmen auf die Lärmimmissionen	2010
1318	FGU 2006/001	Langzeitquellversuche an anhydritführenden Gesteinen	2010
1317	VSS 2000/469	Geometrisches Normalprofil für alle Fahrzeugtypen	2010
1316	VSS 2001/701	Objektorientierte Modellierung von Strasseninformationen	2010
1315	VSS 2006/904	Abstimmung zwischen individueller Verkehrsinformation und Verkehrsmanagement	2010
1314	VSS 2005/203	Datenbank für Verkehrsaufkommensraten	2008
1313	VSS 2001/201	Kosten-/Nutzenbetrachtung von Strassenentwässerungssystemen, Ökobilanzierung	2010
1312	SVI 2004/006	Der Verkehr aus Sicht der Kinder: Schulwege von Primarschulkindern in der Schweiz	2010
1311	VSS 2000/543	VIABILITE DES PROJETS ET DES INSTALLATIONS ANNEXES	2010
1310	ASTRA 2007/002	Beeinflussung der Luftströmung in Strassentunneln im Brandfall	2010
1309	VSS 2008/303	Verkehrsregelungssysteme - Modernisierung von Lichtsignalanlagen	2010
1308	VSS 2008/201	Hindernisfreier Verkehrsraum - Anforderungen aus Sicht von Menschen mit Behinderung	2010

Bericht-Nr.	Projekt Nr.	Titel	Jahr
1307	ASTRA 2006/002	Entwicklung optimaler Mischgüter und Auswahl geeigneter Bindemittel; D-A-CH - Initialprojekt	2008
1306	ASTRA 2008/002	Strassenglätte-Prognosesystem (SGPS)	2010
1305	VSS 2000/457	Verkehrserzeugung durch Parkierungsanlagen	2009
1304	VSS 2004/716	Massnahmenplanung im Erhaltungsmanagement von Fahrbahnen	2008
1303	ASTRA 2009/010	Geschwindigkeiten in Steigungen und Gefällen; Überprüfung	2010
1302	VSS 1999/131	Zusammenhang zwischen Bindemitteleigenschaften und Schadensbildern des Belages?	2010
1301	SVI 2007/006	Optimierung der Strassenverkehrsunfallstatistik durch Berücksichtigung von Daten aus dem Gesundheitswesen	2009
1300	VSS 2003/903	SATELROU Perspectives et applications des méthodes de navigation pour la télématique des transports routiers et pour le système d'information de la route	2010
1299	VSS 2008/502	Projet initial - Enrobés bitumineux à faibles impacts énergétiques et écologiques	2009
1298	ASTRA 2007/012	Griffigkeit auf winterlichen Fahrbahnen	2010
1297	VSS 2007/702	Einsatz von Asphaltbewehrungen (Asphalteinlagen) im Erhaltungsmanagement	2009
1296	ASTRA 2007/008	Swiss contribution to the Heavy-Duty Particle Measurement Programme (HD-PMP)	2010
1295	VSS 2005/305	Entwurfsgrundlagen für Lichtsignalanlagen und Leitfaden	2010
1294	VSS 2007/405	Wiederhol- und Vergleichspräzision der Druckfestigkeit von Gesteinskörnungen am Haufwerk	2010
1293	VSS 2005/402	Détermination de la présence et de l'efficacité de dope dans les bétons bitumineux	2010
1292	ASTRA 2006/004	Entwicklung eines Pflanzenöl-Blockheizkraftwerkes mit eigener Ölmühle	2010
1291	ASTRA 2009/005	Fahrmuster auf überlasteten Autobahnen Simultanes Berechnungsmodell für das Fahrverhalten auf Autobahnen als Grundlage für die Berechnung von Schadstoffemissionen und Fahrzeitgewinnen	2010
1290	VSS 1999/209	Conception et aménagement de passages inférieurs et supérieurs pour piétons et deux-roues légers	2008
1289	VSS 2005/505	Affinität von Gesteinskörnungen und Bitumen, nationale Umsetzung der EN	2010
1288	ASTRA 2006/020	Footprint II - Long Term Pavement Performance and Environmental Monitoring on A1	2010
1287	VSS 2008/301	Verkehrsqualität und Leistungsfähigkeit von komplexen ungesteuerten Knoten: Analytisches Schätzverfahren	2009
1286	VSS 2000/338	Verkehrsqualität und Leistungsfähigkeit auf Strassen ohne Richtungstrennung	2010

Bericht-Nr.	Projekt Nr.	Titel	Jahr
1285	VSS 2002/202	In-situ Messung der akustischen Leistungsfähigkeit von Schallschirmen	2009
1284	VSS 2004/203	Evacuation des eaux de chaussée par les bas-cotés	2010
1283	VSS 2000/339	Grundlagen für eine differenzierte Bemessung von Verkehrsanlagen	2008
1282	VSS 2004/715	Massnahmenplanung im Erhaltungsmanagement von Fahrbahnen: Zusatzkosten infolge Vor- und Aufschub von Erhaltungsmassnahmen	2010
1281	SVI 2004/002	Systematische Wirkungsanalysen von kleinen und mittleren Verkehrsvorhaben	2009
1280	ASTRA 2004/016	Auswirkungen von fahrzeuginternen Informationssystemen auf das Fahrverhalten und die Verkehrssicherheit Verkehrspsychologischer Teilbericht	2010
1279	VSS 2005/301	Leistungsfähigkeit zweistreifiger Kreisel	2009
1278	ASTRA 2004/016	Auswirkungen von fahrzeuginternen Informationssystemen auf das Fahrverhalten und die Verkehrssicherheit - Verkehrstechnischer Teilbericht	2009
1277	SVI 2007/005	Multimodale Verkehrsqualitätsstufen für den Strassenverkehr - Vorstudie	2010
1276	VSS 2006/201	Überprüfung der schweizerischen Ganglinien	2008
1275	ASTRA 2006/016	Dynamic Urban Origin - Destination Matrix - Estimation Methodology	2009
1274	SVI 2004/088	Einsatz von Simulationswerkzeugen in der Güterverkehrs- und Transportplanung	2009
1273	ASTRA 2008/006	UNTERHALT 2000 - Massnahme M17, FORSCHUNG: Dauerhafte Materialien und Verfahren SYNTHESE - BERICHT zum Gesamtprojekt "Dauerhafte Beläge" mit den Einzelnen Forschungsprojekten: - ASTRA 200/419: Verhaltensbilanz der Beläge auf Nationalstrassen - ASTRA 2000/420: Dauerhafte Komponenten auf der Basis erfolgreicher Strecken - ASTRA 2000/421: Durabilité des enrobés - ASTRA 2000/422: Dauerhafte Beläge, Rundlaufversuch - ASTRA 2000/423: Griffigkeit der Beläge auf Autobahnen, Vergleich zwischen den Messergebnissen von SRM und SCRIM - ASTRA 2008/005: Vergleichsstrecken mit unterschiedlichen oberen Tragschichten auf einer Nationalstrasse	2008
1272	VSS 2007/304	Verkehrsregelungssysteme - behinderte und ältere Menschen an Lichtsignalanlagen	2010
1271	VSS 2004/201	Unterhalt von Lärmschirmen	2009
1270	VSS 2005/502	Interaktion Strasse Hangstabilität: Monitoring und Rückwärtsrechnung	2009
1269	VSS 2005/201	Evaluation von Fahrzeugrückhaltesystemen im Mittelstreifen von Autobahnen	2009
1268	ASTRA 2005/007	PM10-Emissionsfaktoren von Abriebspartikeln des Strassenverkehrs (APART)	2009
1267	VSS 2007/902	MDAinSVT Einsatz modellbasierter Datentransfernormen (INTERLIS) in der Strassenverkehrstelematik	2009

Bericht-Nr.	Projekt Nr.	Titel	Jahr
1266	VSS 2000/343	Unfall- und Unfallkostenraten im Strassenverkehr	2009
1265	VSS 2005/701	Zusammenhang zwischen dielektrischen Eigenschaften und Zustandsmerkmalen von bitumenhaltigen Fahrbahnbelägen (Pilotuntersuchung)	2009
1264	SVI 2004/004	Verkehrspolitische Entscheidfindung in der Verkehrsplanung	2009
1263	VSS 2001/503	Phénomène du dégel des sols gélifs dans les infrastructures des voies de communication et les pergélisols alpins	2006
1262	VSS 2003/503	Lärmverhalten von Deckschichten im Vergleich zu Gussasphalt mit strukturierter Oberfläche	2009
1261	ASTRA 2004/018	Pilotstudie zur Evaluation einer mobilen Grossversuchsanlage für beschleunigte Verkehrslastsimulation auf Strassenbelägen	2009
1260	FGU 2005/001	Testeinsatz der Methodik "Indirekte Vorauserkundung von wasserführenden Zonen mittels Temperaturdaten anhand der Messdaten des Lötschberg-Basistunnels	2009
1259	VSS 2004/710	Massnahmenplanung im Erhaltungsmanagement von Fahrbahnen - Synthesebericht	2008
1258	VSS 2005/802	Kaphaltestellen Anforderungen und Auswirkungen	2009
1257	SVI 2004/057	Wie Strassenraumbilder den Verkehr beeinflussen Der Durchfahrtswiderstand als Arbeitsinstrument bei der städtebaulichen Gestaltung von Strassenräumen	2009
1256	VSS 2006/903	Qualitätsanforderungen an die digitale Videobild-Bearbeitung zur Verkehrsüberwachung	2009
1255	VSS 2006/901	Neue Methoden zur Erkennung und Durchsetzung der zulässigen Höchstgeschwindigkeit	2009
1254	VSS 2006/502	Drains verticaux préfabriqués thermiques pour la consolidation in-situ des sols	2009
1253	VSS 2001/203	Rétention des polluants des eaux de chausées selon le système "infilitrations sur les talus". Vérification in situ et optimisation	2009
1252	SVI 2003/001	Nettoverkehr von verkehrsintensiven Einrichtungen (VE)	2009
1251	ASTRA 2002/405	Incidence des granulats arrondis ou partiellement arrondis sur les propriétés d'ahérence des bétons bitumineux	2008
1250	VSS 2005/202	Strassenabwasser Filterschacht	2007
1249	FGU 2003/004	Einflussfaktoren auf den Brandwiderstand von Betonkonstruktionen	2009
1248	VSS 2000/433	Dynamische Eindringtiefe zur Beurteilung von Gussasphalt	2008
1247	VSS 2000/348	Anforderungen an die strassenseitige Ausrüstung bei der Umwidmung von Standstreifen	2009
1246	VSS 2004/713	Massnahmenplanung im Erhaltungsmanagement von Fahrbahnen: Bedeutung Oberflächenzustand und Tragfähigkeit sowie gegenseitige Beziehung für Gebrauchs-	2009

Bericht-Nr.	Projekt Nr.	Titel	Jahr
		und Substanzwert	
1245	VSS 2004/701	Verfahren zur Bestimmung des Erhaltungsbedarfs in kommunalen Strassennetzen	2009
1244	VSS 2004/714	Massnahmenplanung im Erhaltungsmanagement von Fahrbahnen - Gesamtnutzen und Nutzen-Kosten-Verhältnis von standardisierten Erhaltungsmassnahmen	2008
1243	VSS 2000/463	Kosten des betrieblichen Unterhalts von Strassenanlagen	2008
1242	VSS 2005/451	Recycling von Ausbauasphalt in Heissmischgut	2007
1241	ASTRA 2001/052	Erhöhung der Aussagekraft des LCPC Spurbildungstests	2009
1240	ASTRA 2002/010	L'acceptabilité du péage de congestion : Résultats et analyse de l'enquête en Suisse	2009
1239	VSS 2000/450	Bemessungsgrundlagen für das Bewehren mit Geokunststoffen	2009
1238	VSS 2005/303	Verkehrssicherheit an Tagesbaustellen und bei Anschlüssen im Baustellenbereich von Hochleistungsstrassen	2008
1237	VSS 2007/903	Grundlagen für eCall in der Schweiz	2009
1236	ASTRA 2008/008_07	Analytische Gegenüberstellung der Strategie- und Tätigkeitsschwerpunkte ASTRA-AIPCR	2008
1235	VSS 2004/711	Forschungspaket Massnahmenplanung im EM von Fahrbahnen - Standardisierte Erhaltungsmassnahmen	2008
1234	VSS 2006/504	Expérimentation in situ du nouveau drainomètre européen	2008
1233	ASTRA 2000/420	Unterhalt 2000 Forschungsprojekt FP2 Dauerhafte Komponenten bitumenhaltiger Belagsschichten	2009
651	AGB 2006/006_OBF	Instandsetzung und Monitoring von AAR-geschädigten Stützmauern und Brücken	2013
650	AGB 2005/010	Korrosionsbeständigkeit von nichtrostenden Betonstählen	2012
649	AGB 2008/012	Anforderungen an den Karbonatisierungswiderstand von Betonen	2012
648	AGB 2005/023 + AGB 2006/003	Validierung der AAR-Prüfungen für Neubau und Instandsetzung	2011
647	AGB 2004/010	Quality Control and Monitoring of electrically isolated post- tensioning tendons in bridges	2011
646	AGB 2005/018	Interactin sol-structure : ponts à culées intégrales	2010
645	AGB 2005/021	Grundlagen für die Verwendung von Recyclingbeton aus Betongranulat	2010
644	AGB 2005/004	Hochleistungsfähiger Faserfeinkornbeton zur Effizienzsteigerung bei der Erhaltung von	2010

Bericht-Nr.	Projekt Nr.	Titel	Jahr
		Kunstbauten aus Stahlbeton	
643	AGB 2005/014	Akustische Überwachung einer stark geschädigten Spannbetonbrücke und Zustandserfassung beim Abbruch	2010
642	AGB 2002/006	Verbund von Spanngliedern	2009
641	AGB 2007/007	Empfehlungen zur Qualitätskontrolle von Beton mit Luftpermeabilitätsmessungen	2009
640	AGB 2003/011	Nouvelle méthode de vérification des ponts mixtes à âme pleine	2010
639	AGB 2008/003	RiskNow-Falling Rocks Excel-basiertes Werkzeug zur Risikoermittlung bei Steinschlagschutzgalerien	2010
638	AGB2003/003	Ursachen der Rissbildung in Stahlbetonbauwerken aus Hochleistungsbeton und neue Wege zu deren Vermeidung	2008
637	AGB 2005/009	Détermination de la présence de chlorures à l'aide du Géoradar	2009
636	AGB 2002/028	Dimensionnement et vérification des dalles de roulement de ponts routiers	2009
635	AGB 2004/002	Applicabilité de l'enrobé drainant sur les ouvrages d'art du réseau des routes nationales	2008
634	AGB 2002/007	Untersuchungen zur Potenzialfeldmessung an Stahlbetonbauten	2008
633	AGB 2002/014	Oberflächenschutzsysteme für Betontragwerke	2008
632	AGB 2008/201	Sicherheit des Verkehrssystem Strasse und dessen Kunstbauten Testregion - Methoden zur Risikobeurteilung Schlussbericht	2010
631	AGB 2000/555	Applications structurales du Béton Fibré à Ultra-hautes Performances aux ponts	2008
630	AGB 2002/016	Korrosionsinhibitoren für die Instandsetzung chloridverseuchter Stahlbetonbauten	2010
629	AGB 2003/001 + AGB 2005/019	Integrale Brücken - Sachstandsbericht	2008
628	AGB 2005/026	Massnahmen gegen chlorid-induzierte Korrosion und zur Erhöhung der Dauerhaftigkeit	2008
627	AGB 2002/002	Eigenschaften von normalbreiten und überbreiten Fahrbahnübergängen aus Polymerbitumen nach starker Verkehrsbelastung	2008
626	AGB 2005/110	Sicherheit des Verkehrssystems Strasse und dessen Kunstbauten: Baustellensicherheit bei Kunstbauten	2009
625	AGB 2005/109	Sicherheit des Verkehrssystems Strasse und dessen Kunstbauten: Effektivität und Effizienz von Massnahmen bei Kunstbauten	2009
624	AGB 2005/108	Sicherheit des Verkehrssystems / Strasse und dessen Kunstbauten / Risikobeurteilung für Kunstbauten	2010
623	AGB 2005/107	Sicherheit des Verkehrssystems Strasse und dessen Kunstbauten: Tragsicherheit der bestehenden Kunstbauten	2009

Bericht-Nr.	Projekt Nr.	Titel	Jahr
622	AGB 2005/106	Rechtliche Aspekte eines risiko- und effizienzbasierten Sicherheitskonzepts	2009
621	AGB 2005/105	Sicherheit des Verkehrssystems Strasse und dessen Kunstbauten Szenarien der Gefahrenentwicklung	2009
620	AGB 2005/104	Sicherheit des Verkehrssystems Strasse und dessen Kunstbauten: Effektivität und Effizienz von Massnahmen	2009
619	AGB 2005/103	Sicherheit des Verkehrssystems / Strasse und dessen Kunstbauten / Ermittlung des Netzrisikos	2010
618	AGB 2005/102	Sicherheit des Verkehrssystems Strasse und dessen Kunstbauten: Methodik zur vergleichenden Risikobeurteilung	2009
617	AGB 2005/100	Sicherheit des Verkehrssystems Strasse und dessen Kunstbauten Synthesebericht	2010
616	AGB 2002/020	Beurteilung von Risiken und Kriterien zur Festlegung akzeptierter Risiken in Folge aussergewöhnlicher Einwirkungen bei Kunstbauten	2009